AUBURN UNIVERSITY

SAMUEL GINN
COLLEGE OF ENGINEERING

Research Report

TORSIONAL RESISTANCE OF DRILLED SHAFT FOUNDATIONS

Submitted to

The Auburn University Highway Research Center

Prepared by

Victor Aguilar, J. Michael Stallings, J. Brian Anderson, and Andrzej Nowak

OCTOBER 2018

Highway Research Center
Harbert Engineering Center
Auburn, Alabama 36849

www.eng.auburn.edu/research/centers/hrc.html

1. Report No.	2. Government Accession No.	3. Recipient Catalog No.
4. Title and Subtitle Torsional Resistance of Drilled Shaft Foundations		5. Report Date October 2018 6. Performing Organization Code
7. Author(s) Aguilar V., Stallings J. M., Anderson J. B., and Nowak A.		8. Performing Organization Report No.
9. Performing Organization Name and Address Highway Research Center Department of Civil Engineering 238 Harbert Engineering Center Auburn, AL 36849		10. Work Unit No. (TRAIS) 11. Contract or Grant No.
12. Sponsoring Agency Name and Address Highway Research Center Department of Civil Engineering 238 Harbert Engineering Center Auburn, AL 36849		13. Type of Report and Period Covered 14. Sponsoring Agency Code
15. Supplementary Notes		

16. Abstract

Drilled shaft foundations are commonly selected by public transportation agencies to support mast-arm traffic sign and signal pole structures. Those inverted L-shaped structures are subjected to lateral and torsional loading simultaneously during wind. Although drilled shafts are widely used, there is no standard to help engineers to design for torsional loading. Furthermore, the resistance mechanism is not well understood, and the existing design methods have been validated against limited experimental data.

This report presents an up-to-date literature review regarding torsional resistance of drilled shafts. Several methods for calculating the torsional resistance were compared in a statistical manner against available test data. Cohesive, cohesionless and mixed layered soils were included in the analysis. It is not clear which is the best method to predict the torsional capacity of drilled shafts. α and β methods are recommended for ALDOT.

The response under an eccentrically applied lateral load of a mast-arm assembly supported by a short drilled shaft was simulated using ABAQUS/Standard for FEM analysis. Two loading conditions and five eccentricities were considered. The results of the analyses suggest that the torsional resistance is enhanced when combined loading is applied. The eccentricity of the lateral loads decreases the overturning resistance in sand. No significant reduction in the overturning resistance was observed for the clay soil. The interaction between torque and overturning resistance is not considered in the reliability analysis.

Based on the reliability analysis performed in this research, a factor of safety of 1.10 for cohesionless soils and a factor of safety of 1.30 for cohesive soils are recommended. These factors of safety are large enough to obtain a reliability index within the range 1.2 to 2.0, which is considered an adequate range for this kind of foundation and its consequences of failure. Recommendations for layered soils are also made.

17. Key Words	18. Distribution Statement		
Drilled shaft foundations, torsional resistance, reliability.	No restrictions		
19. Security Classification (of this report) Unclassified	**20. Security Classification (of this page)** Unclassified	**21. No. of Pages** 124	**22. Price** None.

Research Report

TORSIONAL RESISTANCE OF DRILLED SHAFT FOUNDATIONS

Submitted to

The Auburn University Highway Research Center

Prepared by

Victor Aguilar
J. Michael Stallings
J. Brian Anderson
Andrzej Nowak

OCTOBER 2018

DISCLAIMERS

The contents of this report reflect the views of the authors who are responsible for the facts and accuracy of the data presented herein. The contents do not necessarily reflect the official views or policies of Alabama DOT, Auburn University, or the Highway Research Center. This report does not constitute a standard, specification, or regulation. Comments contained in this paper related to specific testing equipment and materials should not be considered an endorsement of any commercial product or service; no such endorsement is intended or implied.

NOT INTENDED FOR CONSTRUCTION, BIDDING, OR PERMIT PURPOSES

J. Michael Stallings

J. Brian Anderson

Andrzej Nowak

Research Supervisors

ACKNOWLEDGEMENTS

This project was sponsored by Highway Research Center at Auburn University, which is gratefully acknowledged. Guidance and help from Alabama DOT are also very much appreciated.

ABSTRACT

Drilled shaft foundations are commonly selected by public transportation agencies to support mast-arm traffic sign and signal pole structures. Those inverted L-shaped structures are subjected to lateral and torsional loading simultaneously during wind. Although drilled shafts are widely used, there is no standard to help engineers to design for torsional loading. Furthermore, the resistance mechanism is not well understood, and the existing design methods have been validated against limited experimental data.

This report presents an up-to-date literature review regarding torsional resistance of drilled shafts. Several methods for calculating the torsional resistance were compared in a statistical manner against available test data. Cohesive, cohesionless and mixed layered soils were included in the analysis. It is not clear which is the best method to predict the torsional capacity of drilled shafts. α and β methods are recommended for ALDOT.

The response under an eccentrically applied lateral load of a mast-arm assembly supported by a short drilled shaft was simulated using ABAQUS/Standard for FEM analysis. Two loading conditions and five eccentricities were considered. The results of the analyses suggest that the torsional resistance is enhanced when combined loading is applied. The eccentricity of the lateral loads decreases the overturning resistance in sand. No significant reduction in the overturning resistance was observed for the clay soil. The interaction between torque and overturning resistance is not considered in the reliability analysis.

Based on the reliability analysis performed in this research, a factor of safety of 1.10 for cohesionless soils and a factor of safety of 1.30 for cohesive soils are recommended. These factors of safety are large enough to obtain a reliability index within the range 1.2 to 2.0, which is considered an adequate range for this kind of foundation and its consequences of failure. Recommendations for layered soils are also made.

TABLE OF CONTENTS

LIST OF TABLES

LIST OF FIGURES

Chapter 1

INTRODUCTION

1.1 Background

Drilled shaft foundations are commonly selected by public transportation agencies to support mast-arm traffic signals and highway signs, and Alabama Department of Transportation (ALDOT) is not an exception. Mast-arm structures are subjected to lateral and torsional loading simultaneously during wind. Even though drilled shafts are widely used for a number of geotechnical applications, there is not a standard to help engineers to design for torsional loading. The resistance mechanism is not well understood, and the existing design methods have been validated against only limited experimental data.

Section 718 of the *Alabama Standard Specifications for Highway Construction* (ALDOT 2018), titled Structures for Traffic Control Devices and Highway Lighting requires that the foundation design be sufficient to provide a minimum factor of safety of 2.0 against overturning and torsion induced displacement. The requirement related to torsional displacement has resulted in the increased size of drilled shaft foundations and in some cases the need for wings to provide the specified resistance to torsional displacement. Larger than normal foundation diameters with wings are necessary in loose saturated soils. The standard foundation for this type structure is shown in Figure 1-1(a), and a special foundation with wings is shown in Figure 1-1(b). The increased foundation diameters and wings create conflicts with utilities, and overall add significant costs to the foundations. Unfortunately, the conditions that demand an increased diameter and wings are often not discovered until the project is under construction and changes are very expensive.

The traditional design procedure for a drilled shaft subjected to lateral and torsional loading simultaneously treats the lateral and torsional load separately; nevertheless, since both loads are capable of generating shear stresses at the interface shaft-soil, a coupling effect could be expected (lateral-torsional interaction).

This research reviewed several methods for calculating torsional resistance available in the literature. The design methods that appear most appropriate for use by ALDOT are identified, and factors of safety are recommended for different geotechnical conditions based on reliability analysis. The interaction between lateral and torsional loading is addressed by summarizing the research published on this matter and through numerical modeling.

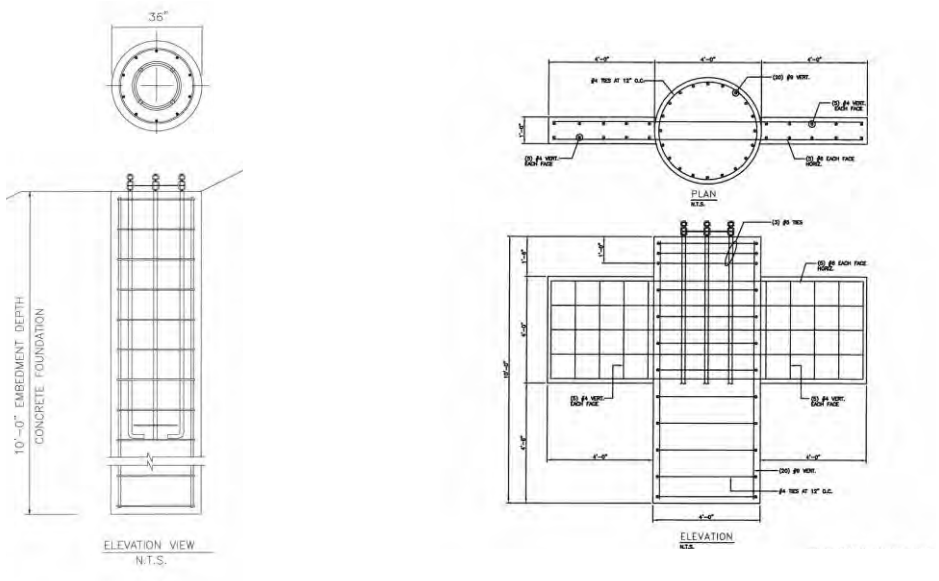

(a) (b)

Figure 1-1: Drilled shaft foundation for a signal mast-arm pole, (a) Standard foundation, (b) Special foundation with wings for torsional resistance (Courtesy of ALDOT)

1.2 Objectives

The goal of this research project is to determine whether the current factor of safety for designing drilled shaft foundations for torsional loading specified by ALDOT (FS = 2.0) is too high. Literature review, comparison to other design codes and practices, with consideration for qualitative input from ALDOT, and reliability analyses provide the quantitative and qualitative basis for selecting new factors of safety.

Following specific steps facilitate the achievement of this goal:

1) Review the published literature that is pertinent to the analysis and design of drilled shafts for torsional loading.
2) Review the state of practice regarding the torsional design of drilled shafts including estimation of geotechnical properties, analytical solutions, and design methods.
3) Assess the accuracy of a selected group of design methods statistically and compare to experimental results available in the literature.
4) Develop resistance reliability models by identifying the most important soil strength parameters, and characterize them statistically based on published literature and Monte Carlo simulations.
5) Contribute to the understanding of the interaction between overturning resistance and torsional loading by performing finite element simulations.
6) Define an appropriate range of target reliability index for drilled shaft foundations supporting traffic signs and pole signals by reviewing typical practice in safety management in geotechnical

designs, previous experience in reliability based design codes, considering the consequences of failure, and considering qualitative input from ALDOT.

7) Assess current wind load provisions for calculating the wind pressure used to design drilled shafts, and the available statistical information on wind load, in order to select an appropriate wind load model for reliability analysis.

8) Define the limit state and perform a reliability analysis to recommend factors of safety for design purposes.

1.3 Outline of the Report

Chapter 2 presents a comprehensive review of the state of the art regarding analysis methods used to calculate the torsional capacity of drilled shafts. Typical behavior and a range of all identified geotechnical parameters involved are also included. Chapter 3 summarizes the state of the practice by describing past and current requirements in AASHTO specifications for structural supports for highway signs, luminaries and traffic signals (AASHTO 2009, AASHTO 2015), including wind provisions, Alabama DOT current practice and other DOTs' specifications. Chapter 4 provides a comparison between analytical predictions and experimental results available in the literature. The aim is to judge the accuracy of each method used to estimate torsional resistance. Chapter 5 presents the recent research on the effect of an applied torque on the overturning resistance of a drilled shaft, a phenomenon that is called lateral-torsional interaction. Chapter 6 identifies and characterizes statistically major parameters involved in determining the torsional resistance. Chapter 7 describes to the reliability analysis and the selection of a factor of safety appropriate to the uncertainties and the selected target reliability index. Chapter 8 summarizes the findings and conclusions of this work.

Chapter 2

LITERATURE REVIEW

Driven piles, jacked piles, and drilled shafts are commonly used as the foundation system for a wide variety of structures. Those are frequently subjected to torsional loading due to eccentricity in various lateral loads such as wind, earthquake, wave, or impact loads. Drilled shaft foundations are commonly selected by public transportation agencies, such as ALDOT, to support mast-arm traffic sign and signal pole structures along highway alignments, and to support bridge column loads (Li et al. 2017). Drilled shafts are widely used, but there is not a standard to help to engineers to design them for torsional loading. Besides, the resistance mechanism is not well understood, and the existing design methods have been validated against only limited experimental data.

In general, a mast-arm assembly needs to be designed to safely carry large torsion, and lateral loads developed during a hurricane (high wind velocity), in addition to the axial load and the moment due to the eccentric dead weight of the structure (Thiyyakkandi et al. 2016). A pile/shaft can be loaded to failure more easily by torsional loading than by compressive loading (Zhang and Kong 2006). In fact, torsional loads can often control the design length of the foundation, particularly in storm-prone regions that experience significant wind speeds (Li et al. 2017). This can result in an increased size of drilled shaft foundations and in some cases the need for wings on the foundations to provide the specified resistance to torsional displacement. Larger than normal foundation diameters with wings could be necessary in loose saturated soils. The increased foundation diameters and wings create conflicts with utilities, and overall add significant costs to the foundations. Unfortunately, the conditions that demand an increased diameter and wings are often not discovered until the project is under construction and changes are very expensive.

In contrast to the extensive research on the analysis of piles under axial and lateral loads, the analysis of piles under torsional loading has received less attention (Chen, Kong, and Zhang 2016). Some torsional loading tests are available in the literature. Those physical models described in the literature may be categorized into three types: 1) 1g-scaled models 2) n-g centrifuge loading tests 3) full-scale 1g loading tests.

Li et al. (2017) summarize significant studies that have been conducted on the prediction of the response of foundation elements subjected to torsion. Analytical and numerical models have been developed using boundary element methods (Poulos 1975; Basack and Sen 2014), discrete element analyses (Chow 1985), nonlinear spring models (Georgiadis 1987; Georgiadis and Saflekou 1990), and closed-form analytical solutions (Randolph 1981; Hache and Valsangkar 1988; Guo and Randolph 1996; Guo, Chow, and Randolph 2007; L. Zhang 2010). Also, Doherty and Deeks (2003) studied the elastic response of circular footing embedded in non-homogenous half-space response under vertical, horizontal, moment and torsional loading. Şahin (2011)

developed a mathematical model and their numerical implementation for design of reinforced concrete piles loaded at all 6-DOF at the head. Nevertheless, superposition was used to combine the effects, and thus all effects are independent of each other. Chen, Kong, and Zhang (2016) proposed an analytical method to analyze the torsional behavior of freestanding pile groups with rigid caps starting from previous analytical solutions. Most of above solutions assume linear elastic soil behavior and/or simplified layout.

In addition to the analytical methods to find the rotation response based on an applied torque, there are several options to compute the torsional resistance. Some design guidance for predicting the torsional capacity of drilled shafts foundations is provided by public agencies (VDOT, FDOT, IDOT, CDOT). It is generally assumed that the torsional unit skin friction (also called unit shear resistance) is equal to the axial unit skin friction based on the Mohr-Coulomb friction law, which is predicted using various direct and indirect methods available in the literature (Thiyyakkandi et al. 2016; Hu et al. 2006). However, these design approaches do not provide any guidance on the amount of rotation that may be anticipated upon reaching the ultimate resistance (Nusairat et al. 2004).

Nusairat et al. (2004) evaluated the accuracy of selected design methods for torsional capacity of drilled shafts by comparing predictions with measured torsional resistance in tests reported in the literature. The authors recognized a lack of relevant test data. Nevertheless, Florida Structures Design Office Method (FL SDO) and Florida District 7 Method (FL D7) were tentatively recommended for the torsional design of drilled shafts in cohesionless and cohesive soils, respectively. Also, Nusairat et al. (2004) noted that the Colorado DOT method (CDOT) tends to overpredict the torsional resistance.

Thiyyakkandi et al. (2016) performed three torsional load tests at full-scale in layered soil. Five methods to predict torsional capacity were compared, and the authors concluded that β method (sand) in combination with α method (clay) predicted the torsional resistance quite well; the difference was only ±10%–14%. Hu et al. (2006) found the torsional resistance of drilled shafts in sand characterized by β method predicted within 20%.

Li et al. (2017) compared β method and the Brown et al. (2010) method against the results from full-scale torsional load test performed by Thiyyakkandi et al. (2016) and its own study. The β method showed a bias factor (predicted-to-measured ratio) λ=1.15 and a coefficient of variation (standard deviation divided by mean) COV=0.05, while Brown et al. (2010) resulted in unconservative predictions (λ=0.86) with higher variability (COV=0.196). Li et al. (2017) also studied the performance of α method comparing against 21 1g-scaled tests and one full-scale test on plastic soils (clays). The α method predictions showed a bias factor λ=1.14 and a COV=0.198.

Zhang and Kong (2006) investigated the torsional behavior of a well-instrumented pile jacked into loose and dense sand. The torsional load transfer was studied, showing that β-values

decrease with depth, rather than remaining constant, as would be assumed in several conventional analysis methods. Torsional load transfer in drilled shaft foundations was only investigated on two full-scale test on predominantly cohesive soil by Li et al. (2017).

2.1 Soil Strength and Design Parameters

Strength is the ability of a material of carrying stress, in geotechnical engineering; usually, the focus is shear stress. The shear strength of a soil is often represented in the Mohr-Coulomb stress plane as

$$\tau = c + \sigma' \tan\phi \qquad (2.1)$$

where τ is the shear strength; c is the soil cohesion, σ' is the effective normal stress; and ϕ is the angle of internal friction.

Soil strength behavior is appropriately discussed regarding cohesionless and cohesion soils under drained and undrained conditions. When saturated coarse-grained soils (sand and gravel) are loaded slowly, volume changes occur, resulting in excess pore pressure that dissipates rapidly, due to high permeability. This is called drained loading. On the other hand, when fine-grained soils (silts and clays) are loaded, they generate excess pore pressure that remains entrapped inside the pores because these soils have very low permeability. And this is called undrained loading. Both drained and undrained conditions can be investigated in laboratory tests. Based on experimental results the shear strength for drained loading condition is $\tau = \sigma' \tan\phi$, while the shear strength for undrained loading condition is $\tau = c = s_u$, where s_u is called undrained shear strength.

For designing drilled shaft foundations to support mast-arm traffic sign and signal pole structures, the usual assumptions are that cohesionless soil layers can be defined by a friction angle and cohesive layers by an undrained shear strength. Therefore, in this document the terms cohesionless soil, sand, and fully drained loading are used indistinctly. Similarly, cohesive soil, clay, and undrained loading are also used as synonyms. The reader should realize that sand or clay are not necessarily referring to soil classification, instead it refers to the soil behavior under loading.

Geotechnical design parameters are required to perform predictions. Those parameters should be assigned based on in-situ and laboratory testing. However, usually for short piles supporting traffic signals this information is limited. A standard penetration test (SPT) or perhaps a cone penetration test (CPT) is the only test available for the designer. Therefore, the engineer may consider using correlations available in the literature (i.e., Kulhawy and Mayne 1990; Bowles 1996; Kramer 1996; Das 2010) or pick parameters from experience and available regional information.

Some correlations are compared, and ALDOT recommended values are addressed in this chapter. A full list of ALDOT recommended geotechnical parameters can be found in Appendix C.

2.1.1 Correlations for Cohesionless Soils

2.1.1.1 Unit Weight

Puzley (2011), the design guide used by Illinois DOT, recommends the following expression for estimating the unit weight of a granular soil based on an SPT (N),

$$\gamma = 0.095N^{0.095} \text{ (kcf)} \tag{2.2}$$

when CPT is available, a unit weight ranging from 111pcf to 121pcf can be estimated based on the Soil Behavior Type index (SBT) from tables. Alternatively, Robertson and Cabal (2010) proposed the following expression

$$\frac{\gamma}{\gamma_w} = 0.27\left(\log R_f\right) + 0.36\left[\log\left(\frac{q_c}{P_a}\right)\right] + 1.236 \tag{2.3}$$

where γ is the moist unit weight of soil; γ_w is the unit weight of water in the same units as γ; R_f = F_s/q_c is the friction ratio as a percentage; where F_s is the sleeve friction; q_c is the cone penetration tip resistance; and P_a is the atmospheric pressure in the same units as q_c.

2.1.1.2 Internal Friction Angle

Two popular correlations based on the N value from a Standard penetration test (SPT) to estimate the friction angle ($\varnothing$) are as follows,

Peck, Hanson, and Thornburn (1974) recommended

$$\phi = 53.88 - 27.60e^{-0.0147N} \tag{2.4}$$

and Kulhawy and Mayne (1990) recommended

$$\phi = \arctan\left(\frac{N_{60}}{12.2 + 20.3\left(\frac{\sigma'_o}{p_a}\right)}\right)^{0.34} \qquad (2.5)$$

where N_{60} is the blow-count from the SPT corrected to a 60% energy efficiency; σ'_0 is the vertical pressure; and P_a the atmospheric pressure in the same units that σ'_0.

Other recommendations are presented in the form of charts, see Figure 2-1.

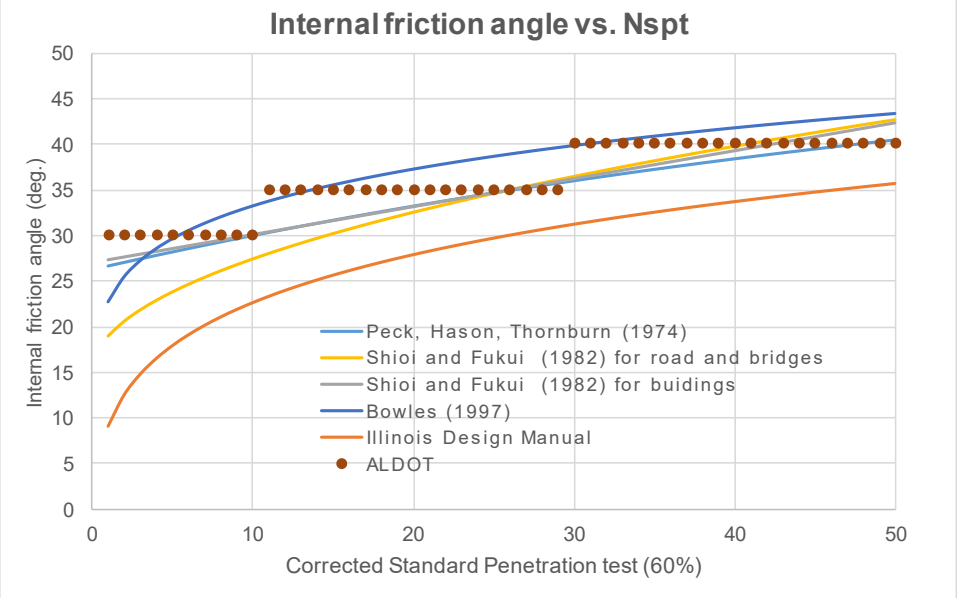

Figure 2-1: Internal friction angle vs. standard penetration test from several sources

An expression based on the CPT test was proposed by Kulhawy and Mayne (1990)

$$\phi = \arctan\left[0.1 + 0.38\log\left(\frac{q_c}{\sigma'_o}\right)\right] \qquad (2.6)$$

where q_c is the cone penetration tip resistance, and σ'_0 is the vertical pressure in the same units as q_c.

If the relative density is available, the Figure 2-2 can be useful.

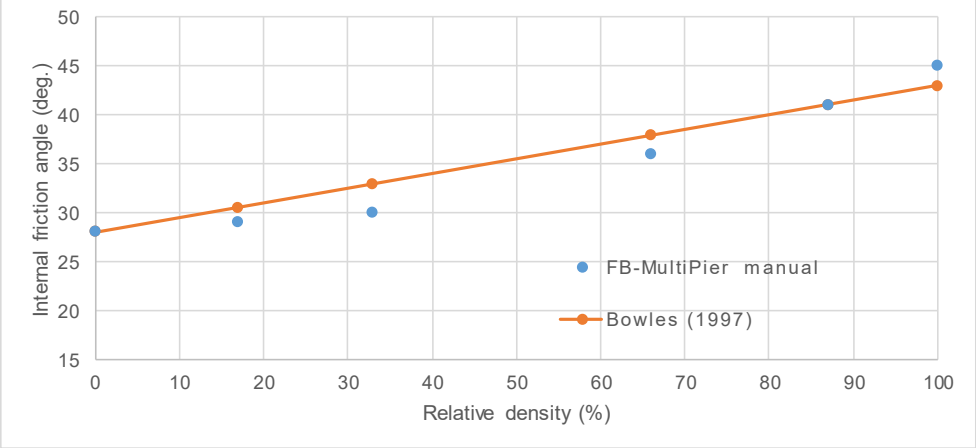

Figure 2-2: Internal friction angle vs. relative density from several sources

2.1.2 Correlations for Cohesive Soils

2.1.2.1 Unit Weight

Puzley (2011), the design guide used by Illinois DOT, recommends the following expression for estimating the unit weight of a cohesive soil (γ)

$$\gamma = 0.1215 q_u^{0.095} \text{ (kcf)} \tag{2.7}$$

where q_u is the unconfined compressive strength in ksf. When CPT is available, a unit weight ranging from 111pcf to 121pcf can be estimated based on the Soil Behavior Type index (SBT) from tables.

2.1.2.2 Cohesion

Two expressions for estimating the undrained shear strength, s_u (or the unconfined compressive strength, q_u) based on a SPT are recommended by Kulhawy and Mayne (1990).

First,

$$\frac{q_u}{p_a} = 0.58 N_{60}^{0.72} \tag{2.8}$$

where $q_u = 2s_u$; p_a is the atmospheric pressure; and N_{60} is the blow-count from the SPT corrected to a 60% energy efficiency.

And second,

$$\frac{s_u}{p_a} = 0.08N \tag{2.9}$$

where p_a is the atmospheric pressure; and N is the blow-count from the SPT.

Based on CPT results, the cohesion can be estimated from

$$s_u = \frac{q_c - \sigma_o}{N_k} \tag{2.10}$$

where σ_o is the vertical pressure; and N_k is a bearing capacity factor, approximately 18.3 for all cones (Das 2010).

Other recommendations are presented in the form of a chart in Figure 2-3.

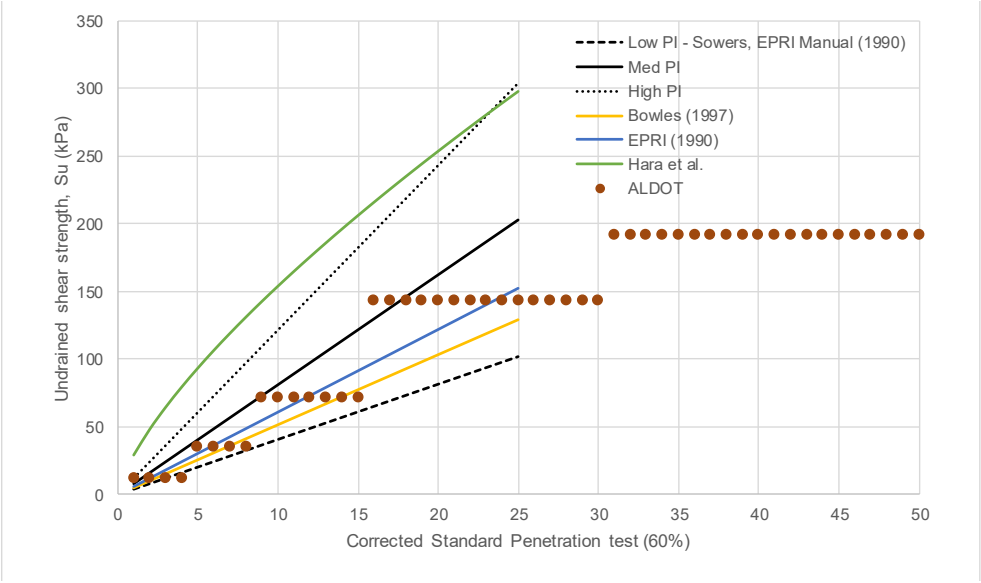

Figure 2-3: Undrained shear strength vs. standard penetration test from several sources

2.1.3 Comments

There are several issues in selecting geotechnical properties. On one side, most of the correlations based on the standard penetration test do not account for the hammer energy used. It is commonly assumed that N_{60} should be used for those correlations. Nevertheless, several practitioners do not correct the SPT defending that not all of the boring logs have energy calibrations available; neglecting the corrections adds an additional factor of safety to the number as classification tests are not performed, and sometimes the visuals could be different from what is described. On the other hand, correlations based on SPT have an unknown variability that is presumably very high.

In general, geotechnical engineers approximate reasonably well the unit weight and tend to be overly-conservative at selecting internal friction angles. However, when selecting an undrained shear strength based on SPT, it is well known that a value chosen from correlations can be far off from reality.

ALDOT recommendations on geotechnical parameters were compared with other sources working with N_{60}. Those recommended values can be considered in a middle range. Nevertheless, in practice, the selection of geotechnical parameters is based on uncorrected SPT boring logs. Properties based on uncorrected SPT values do not allow comparison.

2.2 Typical Behavior and Failure Criteria

Figure 2-4 shows typical torque-twist angle responses during torsional load tests of drilled shafts, (a) and (b), and jacked piles (c). It can be seen the torque increases non-linearly until reaching the fully mobilized capacity. The unload curves in Figure 2-4(a) do not show elastic recovery.

Three failure criteria were used in previous research:

1) The failure has occurred when the rate of shear stress increase is zero with additional rotation. This may correspond to large twist angles, which could be difficult to achieve in load tests. Li et al. (2017) used a hyperbolic curve fit technique to extrapolate the torque-rotation behavior beyond the measurements and to estimate the torsional resistance.

2) FDOT uses 15 deg twist angle as a failure criterion for traffic sign supports based on serviceability requirements (Hu et al. 2006). None of the reviewed load tests have reached 15 deg twist angle.

3) Zhang and Kong (2006) proposed an objective failure criterion. The pile-head twist angle at failure can be expressed as the sum of the elastic torsional deformation of the pile/shaft and the toe twist angle.

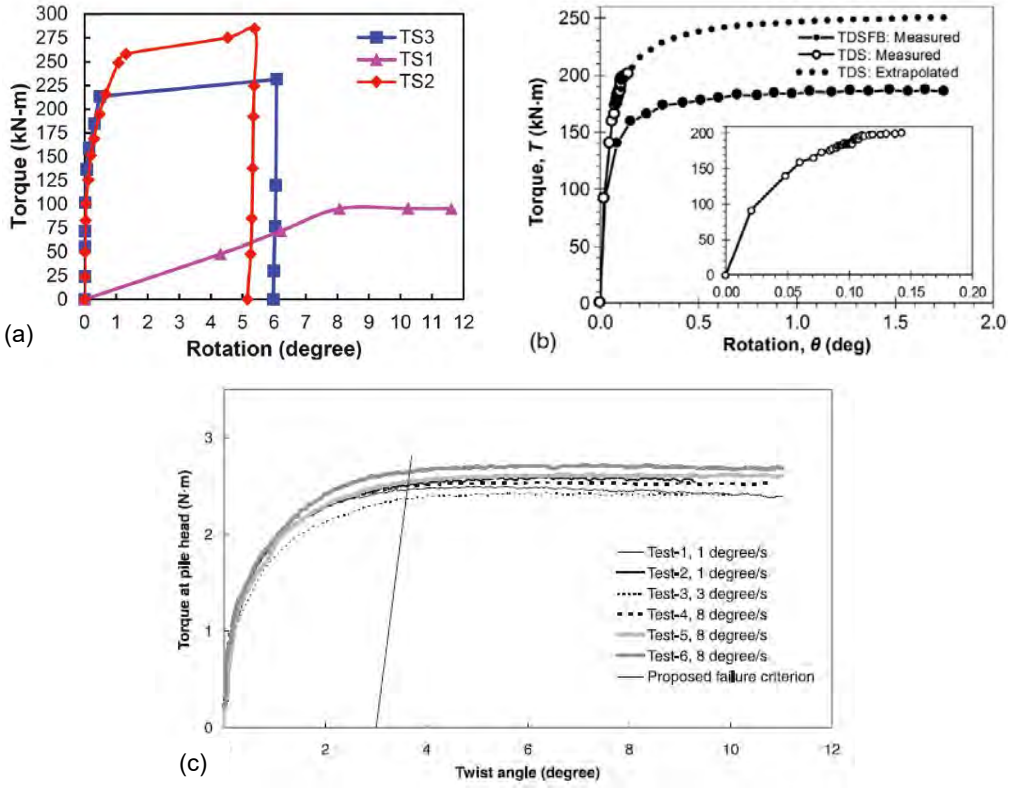

Figure 2-4: Typical torque-rotation angle response,
(a) Thiyyakkandi et al. 2016; (b) Li et al., 2017; and (c) Zhang and Kong (2006)

2.3 Analytical Solutions for Torque-Twist Response

Consider a homogenous-layered soil condition (Figure 2-5). Hache and Valsangkar (1988) described the governing equations and the solutions for this case.

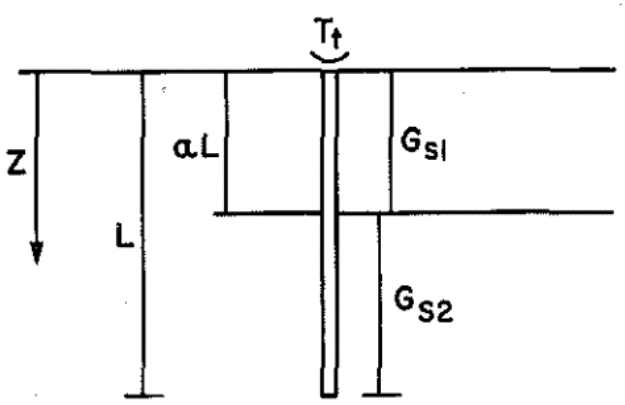

Figure 2-5: Pile in two-layered soil with homogeneous layers (Hache and Valsangkar 1988)

The governing differential equations are:

$$\frac{\partial^2 \phi}{\partial z^2} - \eta \lambda_2^{'2} \phi = 0 \qquad \text{for} \qquad 0 \le z \le \alpha L$$

$$\frac{\partial^2 \phi}{\partial z^2} - \lambda_2^{'2} \phi = 0 \qquad \text{for} \qquad \alpha L \le z \le L \qquad (2.11)$$

where,

$\phi =$ Rotation of the shaft as a function of the depth from the soil surface.

$$\lambda_2^{'} = \sqrt{\frac{4\pi r_0^2 G_{s2}}{(GJ)_p}}$$

$$\eta = \frac{G_{s1}}{G_{s2}}$$

$(GJ)_p =$ Pile shear stiffness

$r_0 =$ Radius of the pile

$z =$ Depth from the soil surface

$L =$ Length of the pile

$\alpha L =$ Thickness of the upper layer

The solutions are:

$\phi = C_1 e^{-\sqrt{\eta}\lambda_2^{'} z} + C_2 e^{-\sqrt{\eta}\lambda_2^{'} z}$, for $0 \le z \le \alpha L$

$\phi = C_3 e^{-\lambda_2^{'} z} + C_2 e^{\lambda_2^{'} z}$, for $\alpha L \le z \le L$ (2.12)

where C_1, C_2, C_3, C_4 are calculated from the boundary conditions and continuity restraints.

The solution for a two-layered soil where the shear modulus is linearly varying with depth can also be found in Hache and Valsangkar (1988). There is a set of solutions for similar problems. The most common ones are summarized as follows.

Poulos (1975) proposed a solution for cohesive uniform soil and a soil in which shear modulus and pile-soil adhesion increase linearly with depth.

$$\phi_h = \frac{T_h}{G_s d^3} \frac{I_\phi}{F_\phi} \qquad (2.13)$$

where *d* is the pile diameter; *L* is the pile embedded length; T_h is the torque applied at the pile head; $\varnothing_h$ is the pile head rotation; G_s is the shear modulus of the soil; I_ϕ is an elastic influence factor; and F_ϕ represents the relative reduction in pile-head stiffness due to partial slip between pile and soil.

Randolph (1981) provided a solution for homogeneous soil and a soil where the stiffness is proportional to depth.

$$\frac{T_h}{Gd^3\phi_h} = \frac{\frac{2}{3} + \pi\frac{L}{d}\frac{\tanh(\mu L)}{\mu L}}{1 + \frac{64}{3\pi\lambda}\frac{L}{d}\frac{\tanh(\mu L)}{\mu L}} \tag{2.14}$$

where,

$$\mu L = \frac{L}{d}\sqrt{\frac{32}{\lambda}}$$

$$\lambda = \frac{32\left(GJ\right)_p}{\pi d^4 G_s}$$

where *d* is the pile diameter; *L* is the pile embedded length; T_h is the torque applied at the pile head; $\varnothing_h$ is the pile head rotation; λ is the stiffness ratio of the pile relative to the soil; G_s is the shear modulus of the soil; and $(GJ)_p$ is the torsional rigidity if the pile.

Hache and Valsangkar (1988) presented non-dimensional solutions and charts for torsional response influence factors at the top of a pile. The twist at the pile due to an applied torque is then calculated as follows:

$$\phi_h = \frac{T_h L}{\left(GJ\right)_p} I_\phi \tag{2.15}$$

where *L* is the pile embedded length; T_h is the torque applied at the pile head; $\varnothing_h$ is the pile head rotation; $(GJ)_p$ is the torsional rigidity if the pile.; I_ϕ is the torsional response influence factor.

All of the solutions above assumed elastic behavior of the soil. Solutions that are more complex are coded into software, but in general, are considered difficult for practical applications. A more detailed list can be found in Nuisarat (2004). Zhang (2010) developed an algorithm that provided reasonable prediction compared against Paulos (1975) database (cohesive soils only).

2.4 Review of Methods for Nominal Torsional Resistance

In practice, methods to estimate the nominal torsional resistance are commonly used. These methods are based on the estimation of the skin friction between the pile and the soil. It is assumed that the nominal torsional resistance (T_n) of a drilled shaft can be presented as the sum of two contributions

$$T_n = T_s + T_t \tag{2.16}$$

where T_s is the side resistance, and T_t *is* the toe resistance. This section includes the derivations.

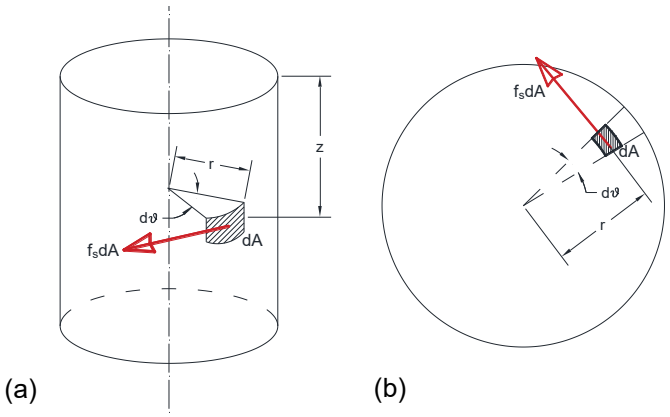

Figure 2-6: Differential element location: (a) at the side of the shaft; and (b) at the toe of the shaft

Side Resistance. Consider the Figure 2-6(a). Taking an area differential element at the side of the shaft, *dA*, the infinitesimal torsional contribution of the differential element can be written as

$$dT_s = r\left(f_s dA\right) = r\left(f_s r d\theta dz\right) = r^2 f_s d\theta dz$$

where f_s is the unit shear resistance; and r is the pile radius. Since r is constant, the integral results in

$$T_s = r^2 \iint_{\theta\, z} f_s(z) d\theta dz$$

integrating between $0 \le \theta \le 2\pi$ and $0 \le z \le L$ the side contribution to the torsional resistance is

$$T_s = \frac{1}{2}\pi D^2 \int_0^L f_s(z)\,dz \tag{2.17}$$

Toe Resistance. Similarly, using r and θ as variables now, the contribution of a differential element located at the toe of the shaft, see Figure 2-6(b), can be written as follows

$$dT_t = r\left(f_s dA\right) = r\left(f_s r dr d\theta\right) = r^2 f_s dr d\theta$$

the unit shear resistance (f_s) is assumed constant at the toe. Therefore the integral to solve is

$$T_t = r\left(f_s dA\right) = f_s \int_\theta \int_r r^2 dr d\theta$$

integrating between $0 \le \theta \le 2\pi$ and $0 \le r \le D/2$, where D is the pile diameter, the toe contribution to torsional resistance is

$$T_t = \frac{1}{12}\pi D^3 f_s \tag{2.18}$$

A linear variation from the center of the toe to the edge has also been used for defining the unit shear resistance in previous research (Li et al. 2017). Several methods are available in the literature for estimating the unit shear resistance (f_s). A selected group of methods is described in this section.

2.4.1 α method – Cohesive Soils

The α method proposed by O'Neill and Reese (1999) is based on the adhesion factor, α, which is an empirical factor used to correlate the results of full-scale load tests with the material property or characteristic of the cohesive soil. The adhesion factor is usually related to s_u and is derived from the results of full-scale pile and drilled shaft load tests. Use of this approach presumes that the measured value of s_u is correct, and that all shaft behavior resulting from construction and loading can be lumped into a single parameter. Neither assumption is strictly correct, but the approach is used due to its simplicity (AASHTO 2012).

The unit shear resistance can be taken as

$$f_s = \alpha s_u \tag{2.19}$$

where s_u is the undrained shear strength of the soil; and the adhesion coefficient α is

α = 0 for a length of 5 ft (1.52 m) at head of the shaft

α = 0 for a length of D just above shaft toe

$$\alpha = 0.55 \; for \frac{s_u}{p_a} \leq 1.5$$

$$\alpha = 0.55 - 0.1\left(\frac{s_u}{p_a} - 1.5\right) for \; 1.5 \leq \frac{s_u}{p_a} \leq 2.5$$

2.4.2 Colorado DOT – Cohesive Soils

Colorado DOT design method (Stuedlein et al. 2016) neglects the contribution of the top *1.5D*, and the skin contribution to the torsional resistance can be calculated same as before

$$T_s = \frac{1}{2}\pi D^2 \left(L - 1.5D\right) f_s \tag{2.20}$$

for the toe contribution, Equation (2.18) can be used with the unit shear resistance at the toe depth

$$T_t = \frac{1}{12}\pi D^3 f_s$$

where the unit shear resistance is estimated as $f_s = s_u$.

2.4.3 Florida DOT – Cohesive

FDOT specifications (FDOT 2012) does not include provision for cohesive soils, but Drilled Shaft v2.0.5 in FDOT website suggests neglecting the top 0.46 m (1.5 ft) for the side contribution, so

$$T_s = \frac{1}{2}\pi D^2 \left(L - 0.46m\right) f_s \tag{2.21}$$

Equation (2.18) is used for estimating the toe resistance

$$T_t = \frac{1}{12}\pi D^3 f_s$$

and the unit shear resistance calculated with an adhesion factor of 0.55, so

$$f_s = 0.55 s_u$$

2.4.4 β method – Cohesionless Soils

O'Neill and Reese (1999) proposed a method to determine the side resistance for uncemented soils in that it is independent of the soil friction angle or the SPT blow count. According to their findings, the friction angle approaches a common value due to high shearing strains in the sand caused by stress relief during drilling. This method is commonly referred as the β method and can be found in the latest version of AASHTO (2012). It was originally developed to determine the side resistance contribution to the axial capacity of drilled shaft; however, it is commonly used for determining the torsional capacity, as well.

The unit shear resistance of drilled shafts in cohesionless soils by the β method is taken as

$$f_s = \beta\sigma_v^{'} \le 28MPa \text{ for } 0.25 \le \beta \le 1.2 \tag{2.22}$$

where σ_v' is effective vertical earth pressure; and β is defined in two parts

$$\beta = 1.5 - 0.245\sqrt{z}\text{ , for } N_{60} \geq 15 \quad (2.23)$$

$$\beta = \frac{N_{60}}{15}\left(1.5 - 0.245\sqrt{z}\right)\text{, for } N_{60} < 15 \quad (2.24)$$

where *z* is the depth coordinate in meters.

β method has been used by others considering β and σ_v' are functions of the depth *z*, but also in an approximate fashion using the β and σ_v' values at mid-depth of soil layers. The approximation tends to predict a higher capacity.

2.4.5 Colorado DOT – Cohesionless Soils

According to Colorado DOT method (Stuedlein et al. 2016) for cohesionless soil, the side and toe contributions can be estimated as follows

$$T_s = \frac{1}{2}\pi D^2 L\, f_s \quad (2.25)$$

$$T_t = \frac{1}{3} DW \tan\delta \quad (2.26)$$

where the unit shear resistance should be estimated based on a coefficient of lateral earth pressure (*K)*, the effective overburden pressure (σ_v'), and the soil-concrete friction angle (δ), using

$$f_s = K\sigma_v^{'} \tan\delta \quad (2.27)$$

where the coefficient of lateral earth pressure is given by

$$K = \frac{2L}{3D}\left(1 - \sin\phi^{'}\right) \quad (2.28)$$

where *D* is the drilled shaft diameter; *L* is the pile embedded length; and $\emptyset$ is the soil internal friction angle.

2.4.6 Florida DOT – Cohesionless Soils

Florida DOT specifications (FDOT 2017) presents a simplified method based on β method valid for cohesionless soils. The side contribution is calculated same as before

$$T_s = \frac{1}{2}\pi D^2 L\, f_s$$

where

$$f_s = \sigma_{vz}^{'} \omega_{fdot} \tag{2.29}$$

where σ_{vz}' is the effective vertical earth pressure; ω_{fdot} is a load transfer ratio where the allowable shaft rotation may exceed 10 degrees. ω_{fdot} =1.5 for granular soils where uncorrected SPT N_{values} are 15 or greater. ω_{fdot} =1.5 N_{value}/15 for uncorrected N_{values} greater than or equal to 5 and less than 15.

Since N_{values} without correction cannot be compared, the corrected SPT value at a 60% energy efficiency is used throughout this report for N_{values}.

FDOT (2012, 2017) does not give any guidance for toe resistance. Nevertheless, in Drilled Shaft v2.0.5 (FDOT 2016) the toe contribution is calculated as

$$T_t = \frac{1}{3} DW \tan\phi \tag{2.30}$$

where *D* is the drilled shaft diameter; *W* is the pile weight; and $\emptyset$ is the soil internal friction angle.

2.4.7 Florida DOT Structure Design Office – Cohesionless Soils

The Florida DOT Structure Design Office method is described by Tawfiq (2000), Hu (2003), and Stuedlein et al. (2016). The side and toe resistances are defined in the same form as before

$$T_s = \frac{1}{2}\pi D^2 L\, f_s$$

$$T_t = \frac{1}{3} DW \tan\delta \tag{2.31}$$

where *D* is the drilled shaft diameter; *W* is the pile weight; and δ is the soil-concrete interface friction angle. The unit shear resistance is defined as

$$f_s = K_0 \sigma_{vz}^{'} \tan\delta \tag{2.32}$$

where K_0 is coefficient of lateral earth pressure at rest; σ_{vz}' is the effective vertical earth pressure; and δ is the soil-concrete interface friction angle. For this method, as with the previous one, the friction angle at the soil-concrete interface (δ) can be considered equal to the internal friction angle of the soil (Tawfiq 2000).

2.4.8 Florida District 7 – cϕ soils

In reality, most often the soils are not purely cohesionless or pure cohesive. The Florida District 7 method is the only method that allows taking into consideration a contribution from the undrained shear strength and the soil-concrete friction in the calculation of unit shear resistance. This method is described by Tawfiq (2000), Hu (2003), and Stuedlein et al. (2016). The torsional resistance is estimated as follows

$$T_s = \frac{1}{2}\pi D^2 \left(L - 1.5m\right) f_s \tag{2.33}$$

$$T_t = \frac{4}{9} D\left(W + N\right)\tan\delta \tag{2.34}$$

similar to the α method, FDOT, and CDOT methods the resistance from the ground surface to a depth of 1.5 m (5 ft) is neglected (Brown et al. 2010). This method considers the axial load applied to the shaft in the toe resistance.

The unit shear resistance is defined as

$$f_s = \alpha s_u + K\sigma_{vz}^{'} \tan\delta \tag{2.35}$$

where α is the adhesion factor as proposed by the α method; σ_{vz}' is the effective vertical earth pressure; δ is the soil-concrete interface friction angle; and *K* is coefficient of lateral earth pressure ranging from K_0 to 1.75. Values of *K* close to K_0 are generally recommended (Hu 2003).

Chapter 3

CURRENT DESIGN PRACTICE

3.1 AASHTO Specifications

AASHTO specifications for highway signs, luminaires, and traffic signals were studied (AASHTO 2009, 2015). AASHTO (2009) is based on the Allowable Stress Design (ASD) philosophy, while AASHTO (2015) uses a Load and Resistance Factors Design (LRFD) philosophy. Both documents establish that shaft embedment shall be sufficient to provide suitable vertical and lateral load capacities and acceptable displacement. AASHTO (2015) suggests using the method cited in Section 10 of the AASHTO LRFD Bridge Design Specifications (AASHTO 2012) to determining the lateral resistance; those are *p-y* analysis and strain wedge theory. In lieu of more detailed procedures, Broms' approximate procedure (Broms 1964a, 1964b) for the estimation of embedment as outlined in the AASHTO (2009, 2015) commentary may be used. Broms suggested an undercapacity factor of 0.7 and an overload factor of 2 to 3, which corresponds to a global factor of safety between 2.86 and 4.29. AASHTO (2009, 2015) do not provide recommendations or guidance to estimate the torsional resistance of drilled shaft foundations.

AASHTO (2009) specifications are based on a basic wind speed taken from the 3-s gust wind speed maps presented in the document. A mean recurrence interval (MRI) of 50-yr is used as a base. Importance factors are used to adjust to wind pressures with 10-,25-, or 100-yr MRI. 50-yr MRI is recommended for overhead sign structures, luminaries support structures, traffic signal structures, and 10-yr for roadside sign structure. Nevertheless, if a luminaire support structure is less than 50 ft in height a traffic signal supports may be designed for a 25-yr MRI, where location and safety considerations permit and when approved by the owner. An alternate method for wind pressure is included in Appendix C of AASHTO (2009). This method is based on maps for fastest-mile wind speed for different MRI. The fastest-mile speed is then amplified by 1.30 to adjust for 3-s gust. As before, for traffic signs supports structures can be designed for 25 yrs if the owner approves.

AASHTO (2015) says wind load shall be based on the pressure of the wind acting horizontally on the supports, signs, luminaries, traffic signs, and other attachments computed in accordance with a series of maps, using the appropriate mean recurrence interval (MRI) of basic wind speed. The owner, in this case ALDOT, can specify the ADT and risk category, or directly specify the MRI. The selection of the MRI accounts for the consequences of failure and importance factors are not used. Supports that cannot fall across the travelway during a failure are assigned a low-risk category, and the appropriate MRI is 300 yrs. While all supports that could stop a lifeline travelway during a failure are assigned a high-risk category, hence the MRI is 1700 yrs. If a support can lay cross the travelway during a failure, creating a hazard for travelers, then the appropriate

MRI is 300 yrs if ADT < 100; 700 yrs if 100 < ADT < 10,000; and 1700 yrs if ADT > 10,000. For service limit states an MRI of 10 yrs should be used.

The latest version, AASHTO (2015) does not include the simplified calculation of wind load based on the fastest-mile speed.

3.2 Alabama Department of Transportation

Alabama Standard Specifications for Highway Construction (ALDOT 2002, 2006, 2008, 2012, 2018), and special provisions (ALDOT 2013, 2014) regarding Section 718 are reviewed in this section in reference to drilled shaft design.

ALDOT (2002) establish that geotechnical borings and, when applicable, passive pressure versus depth graphs will be shown on the plans along with notes to indicate which borings are to represent which foundation elements. Otherwise, the contractor shall obtain all required geotechnical data to complete the required design. This requirement of plotting the passive earth pressure versus depth is no longer present in ALDOT (2006) or successive editions. However, charts titled Ultimate Passive Earth Pressure vs. Depth were found in the example projects provided by ALDOT to this research. ALDOT current practice is to determine the lateral resistance for the foundation from a *p-y* analysis by using LPILE (Reese et al. 2004) or similar software. The torsional resistance is estimated from skin friction methods (α and β methods).

ALDOT (2002, 2006, 2008 and 2012) use AASHTO (1994) as design requirement reference. Special provision of Section 718 (ALDOT 2013) establishes all structures shall be designed in accordance with the requirements given in AASHTO (2009). ALDOT (2018) maintains AASHTO (2009) as the design requirement.

In all editions of *Alabama Standard Specifications for Highway Construction* (ALDOT 2002, 2006, 2008, 2012, 2018) the minimum wind speed is 100 mph for Mobile and Baldwin Counties and 80 mph elsewhere in the State. These wind speeds are meant to be the fastest-mile wind speed, not to be confused with the 3s-gust wind speed. Wind load is calculated based on the procedure described in AASHTO (2009) Appendix C, called alternate method for wind pressures.

The Applied Technology Council publishes a website where the wind speed can be obtained for a location of interested (http://windspeed.atcouncil.org/). By using this resource, a comparison between wind speeds for Montgomery and Mobile were performed. The goal is to compare the current ALDOT specification with the requirements in AASHTO (2009 and 2015).

Table 3-1: Basic Wind speed for different risk levels at two locations

Mean Recurrence Interval (MRI)	Montgomery (mph)	Mobile (mph)	Comment
10 yrs	76	81	Used for service limit state
25 yrs	84	99	Traffic signal structures less than 15-ft height may be designed for 25-yr design life, where locations and safety considerations permit and when approved by the owner. (AASHTO 2009)
50 yrs	90	110	Recommended wind speed for traffic signal structures (AASHTO 2009)
100 yrs	96	124	
ALDOT current practice	1.30x80 = 104	1.30x100 = 130	(ALDOT 2002, 2006, 2008, 2012, 2018)
300 yrs	106	142	Basic wind speed recommended for supports in low-risk category (AASHTO 2015)
700 yrs	116	154	
1700 yrs	120	163	Basic wind speed recommended for supports in high-risk category (AASHTO 2015)

Table 3-1 shows that current ALDOT practice corresponds to an MRI between 100 yrs and 300 yrs. Therefore, the basic wind speed is lower than the minimum recommended by AASHTO (2015), still higher than the wind speed recommended by AASHTO (2009). Nevertheless, In addition to differences in the basic wind speed, three different models to estimate the wind pressure overlap in today's practice:

1) AASHTO (2009), Chapter 3
2) AASHTO (2009), Appendix C, ALDOT current practice
3) AASHTO (2015)

Based on the wind speed reported in Table 3-1 wind pressure was calculated by those three methods for an 18-ft height traffic signal and the same two locations. 25-yrs design life was considered. Results are presented in Table 3-2 and details are given in Appendix D. AASHTO (2009) allows for an increase of a 33% on the allowable stress when wind load is present in the load combination. ALDOT current practice allows for a 40% increase in the allowable stress. In both cases, the simplified procedure in Appendix C of AASHTO (2009) resulted in higher wind pressures than the obtained by AASHTO (2009) Chapter 3 method. Also, one can see that ALDOT current practice is lower than AASHTO (2015) wind pressure for 300-yr MRI (low-risk traffic signals).

Table 3-2: Wind pressure for different specifications

Spec.	MRI	Montgomery (psf)	Mobile (psf)	Comment
AASHTO (2009)	25 yrs	21.8/1.33 = 16.4	28.8/1.33 = 21.7	33% increase in allowable stress was applied.
AASHTO (2009) - Appendix C	25 yrs	33.2/1.40 = 23.7	51.9/1.40 = 37.1	ALDOT current practice. 40% increase in allowable stress was applied.
AASHTO (2015)	10 yrs	15.1	17.1	Service limit state
	300 yrs	29.4	52.7	Low-risk category
	700 yrs	35.2	62.0	
	1700 yrs	37.6	69.4	High-risk category

Regarding geotechnical resistance, all editions of *Alabama Standard Specifications for Highway Construction* (ALDOT 2002, 2006, 2008, 2012, 2018) require that the shaft design shall be sufficient to provide a minimum factor of safety of 2.0 against overturning. However, when the design is based on *p-y* analysis, the condition of acceptance of a given design is a displacement less than 0.5 in. at the ground surface under the wind load. This is not part of any specification, but rather a common practice of designers.

In the special provision of section 718 (ALDOT 2014), the requirement says design shall be sufficient to provide a minimum factor of safety of 2.0 against overturning and torsion induced displacement. This is the first time the torsional design is required for drilled shafts supports for traffic signals in *Alabama Standard Specifications for Highway Construction*, and it is maintained in the most recent edition (ALDOT 2018).

Alabama DOT typical design for traffic signal foundations is a drilled shaft with 3-ft diameter, 10-ft length. Common dimensions for the inverted L-support are 17-ft height and 40-45 ft arm length.

3.3 Other DOTs

The state of Colorado allows the use of either Brom's method or *p-y* analysis for designing against overturning. A factor of safety of 2.0 is required. Colorado DOT developed their own method for calculating the torsional capacity of drilled shafts. It is used with a factor of safety of 1.25 or 1.50, depending on the type of detail used for construction.

The state of Florida published a manual: *FDOT Modifications to Standard Specifications for Structural Supports for Highway Signs, Luminaires and Traffic Signals* (FDOT 2012). A safety factor against overturning of 2.0 is recommended when using Broms' method. FDOT (2012) provides a simplified method for calculating torsional capacity. A MathCAD file (FDOT 2016) that can be used for designing shafts in a single uniform layer of soil is available on the FDOT website. A modification of Broms' method for clay soils is incorporated into the MathCAD routine. FDOT (2017) follows LRFD philosophy.

The State of Illinois published a design guide that is available for engineers (Puzley 2011), and a design example is provided. An extended version of Broms' method is used in multilayer soil systems. ILDOT recommend a skin friction approach (α and β) to calculate the torsional resistance.

The State of Oregon recommends Broms' method be used with a factor of safety of 2.15 for lateral loads. It is assumed that this approach also will provide adequate resistance for applied torsional loads.

In the State of Virginia, Broms' method or *p-y* analysis can be used for overturning. Torsional resistance can be evaluated as specified by the nominal axial compression resistance of single drilled shafts, in other words, skin friction based approaches such as $\alpha\beta$. The total horizontal deflection shall be limited to 0.75 in. at the ground level, and the tip of the pile deflection must not exceed 0.25 in.

Table 3-3 summarizes the current practice of several DOTs for the design of drilled shaft foundation for traffic signals and highway signs.

Table 3-3: Current practice for traffic signal support foundation design

Specification	Overturning	Torsion	Overturning	Torsion	Comments
	Method	*Method*	*FS*	*FS*	
AASHTO (2015)	Broms	-	2.86 - 4.29	-	Currently LRFD
Alabama	*p-y*	$\alpha\beta$	2.0 or displacement limit	2.00	Typical dimensions D=3ft L=10ft
Colorado	Broms, *p-y*	CDOT	2.00	1.25 - 1.50	Typical dimensions D=3ft L=14-18ft
Florida (FDOT 2016)	Modified Broms	FDOT	2.00	1.0 Mast-arm 1.3 Overhead	Version 2017 is LRFD
Illinois	ILDOT	$\alpha\beta$	2.86	1.13	
Oregon	Broms	NA	2.15	NA	
Virginia	Broms, *p-y*	$\alpha\beta$	2.25 or displacements limit	1.30	

Chapter 4

PERFORMANCE OF DESIGN METHODS

4.1 Experimental Research Available

Available experimental information is described in this section. Torsional loading tests on drilled shafts of physical models described in the literature may be categorized into three types:

1) 1g-scaled models (Poulos 1975, Li et al. 2017)
2) n-g centrifuge loading tests (Herrera 2001; Hu 2003)
3) 1g- full-scale loading tests (Li et al. 2017; Thiyyakkandi et al. 2016; Tawfiq 2000)

The 1g-scaled tests ran by Poulos (1975) correspond to specimens of plastic soils (clays). The n-g centrifuge tests done by Herrera (2001) and Hu (2003) correspond to tests on cohesionless soil (sand). The available 1g-full scale tests were performed on layered soils. Details of specimens and predictions are included in Appendix A.

4.2 Comparison

Li et al. (2017) present torsional resistance measured from 1g-scaled and full-scale tests compared with α method predictions. Hu (2003) reports shear stresses measured from centrifuge tests versus those predicted by β method in sand models. These data and predictions are used to perform a statistical analysis to study the performance of α and β methods, in cohesive and cohesionless soils, respectively, see Figure 4-1(a) and Figure 4-1(b).

Four full-scale torsional tests, performed in layered mixed soils are used to compare the methods described in Chapter 2: α and β, Colorado Department of Transportation (CDOT), Florida Department of transportation (FDOT), FDOT district 7 (FL D7), and FDOT Structural Design Office (FL SDO). For this purpose, α and β methods were used in combination with the toe contribution proposed by Colorado Department of Transportation (CDOT) method. Florida Structural Design Office (FL SDO) method was used in conjunction with α method, adding the toe resistance using Equation (2.18) with α = 0.55, see Figure 4-1(c).

The accuracy of the selected methods considered in this paper was compared using graphics, statistical measurements, and normal probability plots. Outliers were excluded from the analysis. Points with absolute standard residual greater than 2 were considered outliers. Three data points were eliminated from the Hu (2003) database, and one from Li et al. (2017) database.

4.2.1 Graphical Comparison

As a first step to explore the outcomes, measured vs. predicted values are plotted in Figure 4-1. α method predictions show good performance, having just a few points of unconservative predictions. β method shear stress predictions are conservative, but scattering is observed. For layered mixed soils, $\alpha\beta$ and CDOT predictions are the closest to the measured values. FDOT method seems unconservative, and FLD7 and FL SDO provided overly-conservative predictions.

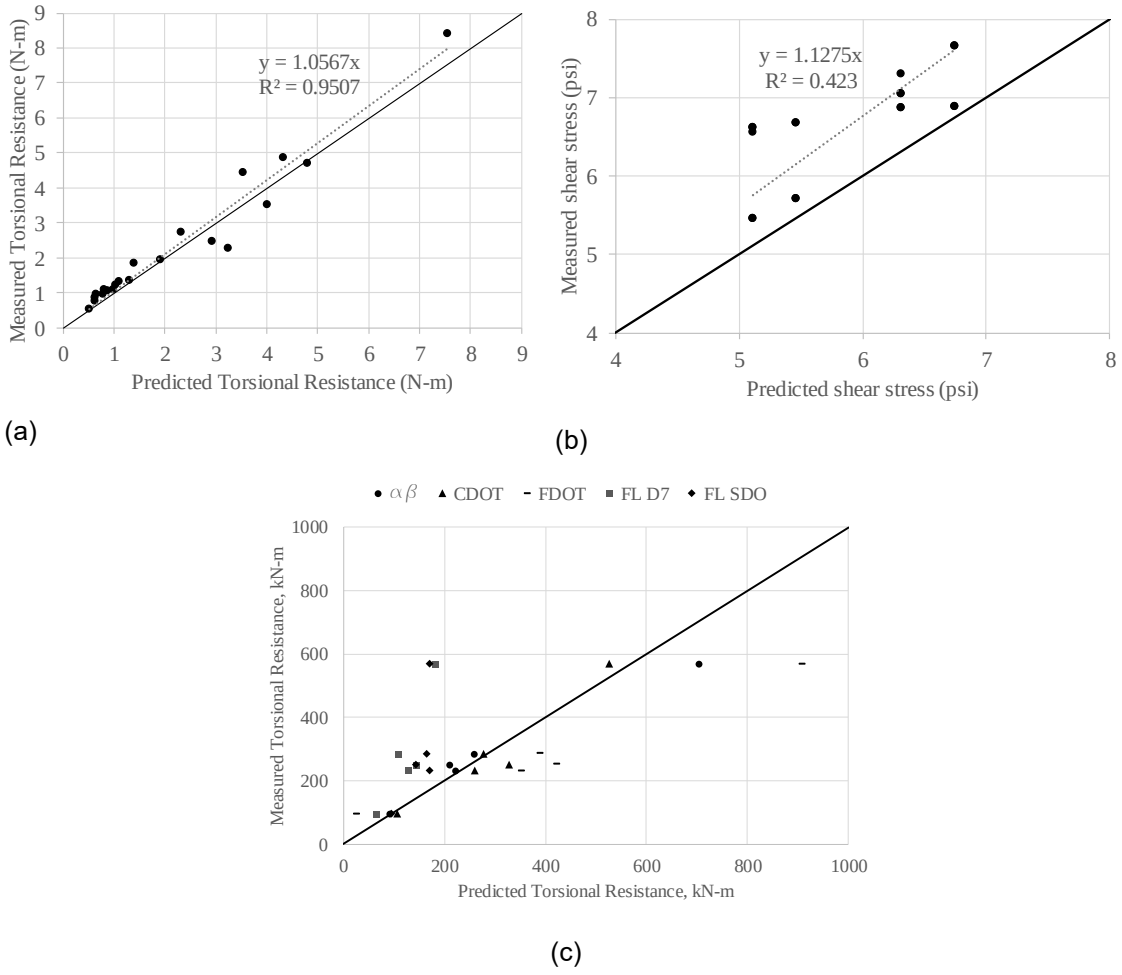

Figure 4-1: Measured vs. predicted resistance: (a) α method performance; (b) β method performance; and (c) all methods performance

4.2.2 Statistical Comparison

The calculated statistical parameters for the measured-to-predicted ratio (T_m/T_p) are summarized in Table 4-1 and Table 4-2. Also, the average of the absolute error is included as a percentage. Table 4-1 corresponds to the application of α and β to cohesive and cohesionless soils, respectively. Table 4-2 presents the statistical information calculated based on four full-scale load tests on layered mixed soils. $\alpha\beta$ and CDOT methods provided the lowest COV and a limited average error. FDOT average is greater than 1.0, but the 5th percentile is low. FL D7 and FL SDO results are overly-conservative, and COV is high.

Table 4-1: statistical parameter calculated for α and β methods. Clay and sand, respectively.

Method	μ	P_5	STD	COV	E (%)
α method	1.16	0.86	0.20	0.17	18
β method	1.14	1.02	0.09	0.08	11

Table 4-2: statistical parameter calculated for all methods. Layered mixed soils.

Method	μ	P_5	STD	COV	E (%)
$\alpha\beta$	1.04	0.86	0.14	0.14	12
CDOT	0.93	0.79	0.12	0.13	13
FDOT	1.30	0.60	1.44	1.11	58
FL D7	2.16	1.55	0.68	0.31	50
FL SDO	1.83	1.08	0.89	0.48	36

4.2.3 Normal Probability Paper Comparison

To study the normality and the lower tail of the distributions, the cumulative distribution functions (CDF) of the measured-to-predicted ratio *(T_m/T_p)* were plotted on normal probability paper, according to the procedure described in Nowak and Collins (2013), see Figure 4-2. The horizontal axis represents the measured-to-predicted ratio *(T_m/T_p)*. The vertical axis is the corresponding probability that a data value is less than or equal to the value in the horizontal axis.

The CDF of the T_m/T_p ratio of both methods seems normally distributed with a reasonable variability. A closer look at the lower tail of the distributions (for reliability analysis) indicates that α method can be modeled as normally distributed with λ= 1.18 and COV = 0.19, while the β method should be modeled with λ= 1.09 and COV = 0.03, see Figure 4-2.

Figure 4-3 shows the CDF of the T_m/T_p ratio of the methods described in the previous section used in layered mixed soils. The largest T_m/T_p ratio is for a test in a particular soil profile that contains a very loose sand layer at the top. The three Florida methods do not recognize any resistance from this layer, making those predictions overly-conservative. If this point is omitted from the analysis, the reader can notice that a larger variability is observed in the results from FL DOT and FL DS7, but the predictions are conservative. FL DOT predictions are biased since the corrected N_{value} was used rather than uncorrected N_{value}. It is hard to draw a conclusion about this method.

α, β, and CDOT methods are considered as the best fit for this database, with an average T_m/T_p ratio close to 1.0 and low COV. A similar conclusion was reached by other researchers regarding α and β methods (Li et al. 2017; Thiyyakkandi et al. 2016). CDOT presents an average less than 1.0. Thus, the capacity was overpredicted, which agrees with the findings of Nusairat et al. (2004).

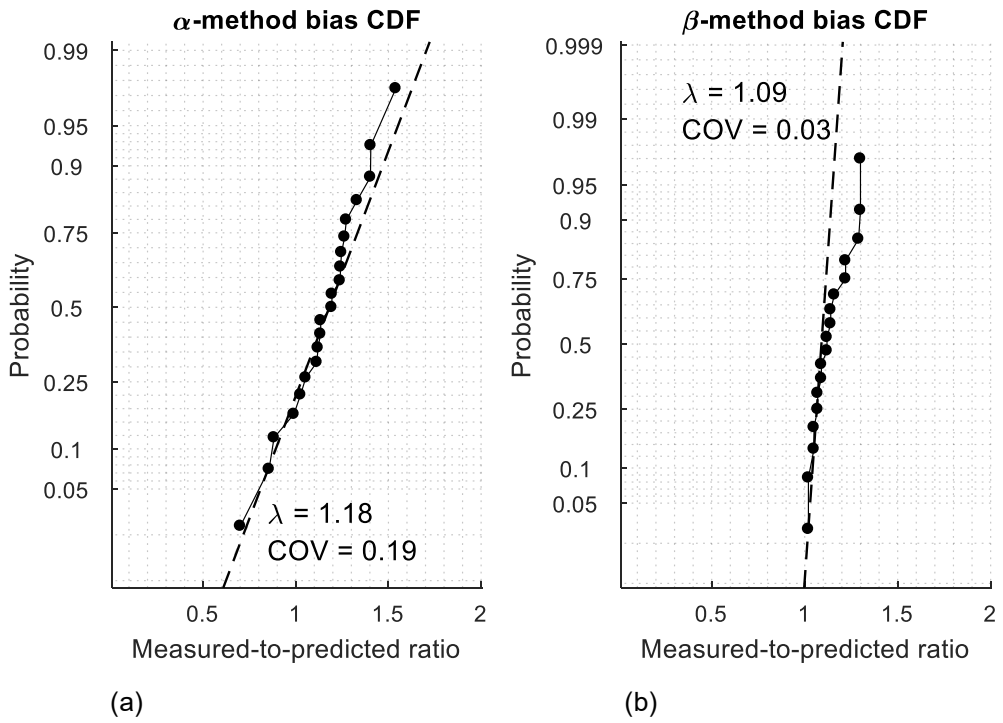

Figure 4-2: T_m/T_p ratio CDF for α method (a) and for β method (b)

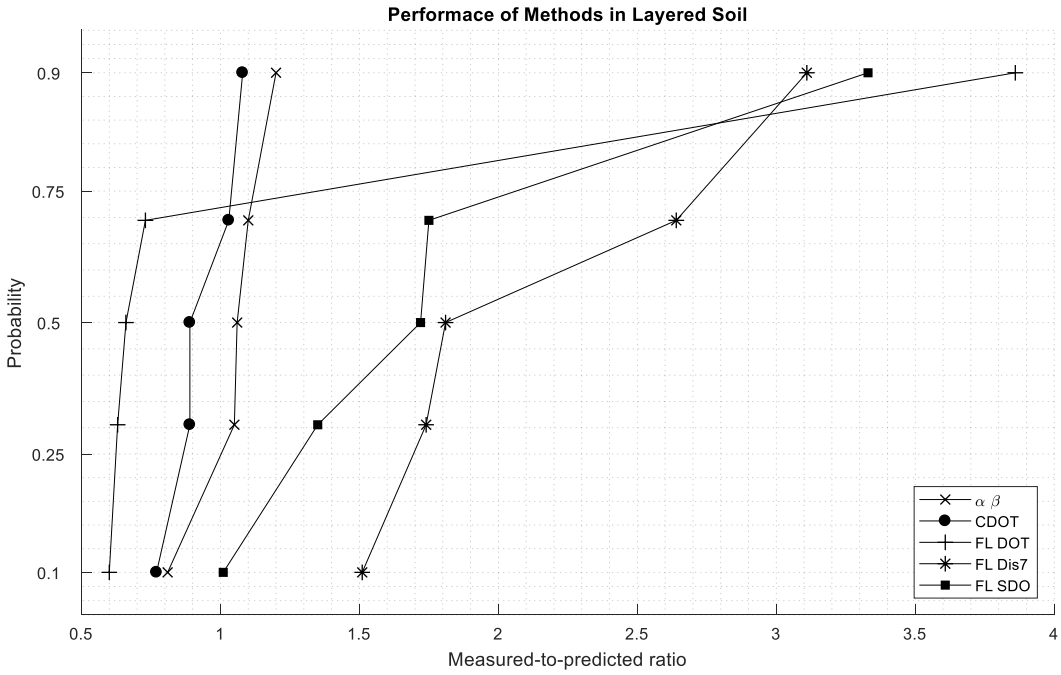

Figure 4-3: T_m/T_p ratio CDF for predictions on mixed layered soils

4.3 Discussion

A common conservatism built into the methods reviewed is to neglect the contribution of the top 0.46m or 1.52m if clayey or c-ϕ soil. The resistance from the ground surface to the depth of seasonal moisture change (usually taken as 1.52m) is neglected due to the potential loss of shaft resistance as soil expands and contracts induced by wetting and drying or freezing and thawing near the ground surface (Brown et al. 2010).

The axial loads applied to the foundation in the estimation of the toe resistance is usually neglected. Often, the toe contribution to the torsional resistance can be omitted entirely, considering the uncertainty in the effective contact between the shaft base and the underlying soil (Hu et al. 2006). For the full-scale tests in the database available, the toe contribution to the total torsional resistance varies between 4 and 13%, and from 2 to 11% according to predictions from $\alpha\beta$ and CDOT, respectively.

The prediction using α and β methods can be considered appropriate overall, on average. Nevertheless, the torsional load transfer plots shown in Figure 4-4 indicates that the unit shear resistance prediction differs significantly from the measured values. Therefore, the good agreement observed between the torsional capacity measured and predicted is a result of compensating errors in the integration along the length of the shaft.

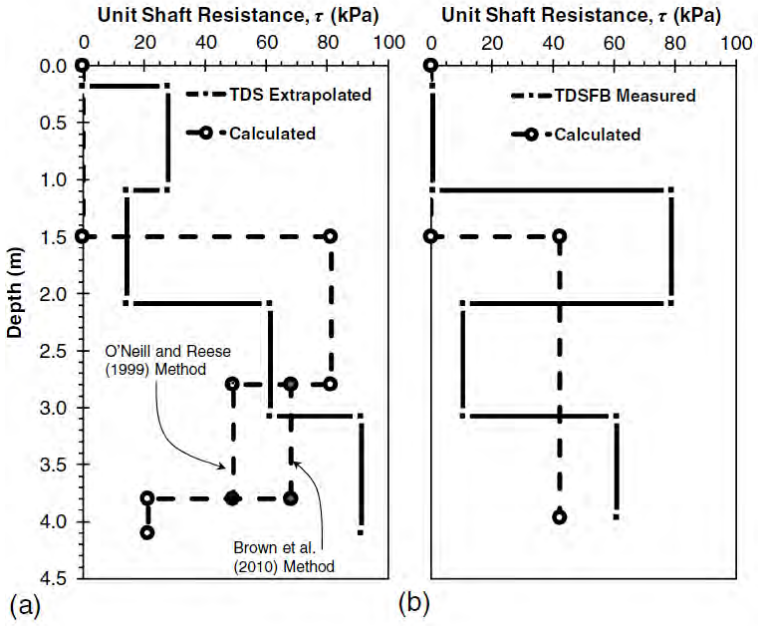

Figure 4-4: Torsional load transfer study (Li et al. 2017)

Based on the limited experimental information available, $\alpha\beta$ and CDOT methods appear to be good alternatives to predict the torsional capacity of drilled shafts. Although the methods can

be used with judgment in the interim, there is a need for the development of improved design methods. Such methods would benefit from additional full-scale loading tests similar to those conducted in Thiyyakkandi et al. (2016) and Li et al. (2017).

4.4 Comparison of α and β, and CDOT methods

The results of the comparison have shown that $\alpha\beta$ method and CDOT method are the most accurate approximations within the group of method included in this analysis. So, it is of interest to compare them within a broader range of geotechnical parameters.

On cohesive soils, CDOT assumes an α-value of 1.0, regardless the undrained shear strength of the soil. Therefore, CDOT method prediction, in general, will be greater that α method by a factor of 1.82 to 2.22.

On cohesionless soils, the comparison is not evident. Consider a shaft diameter D=0.91 m and embedment lengths of 3D, 5D, and 7D. Also, assume different soil conditions based on an SPT value from 1 to 40. Thus, the unit weight and friction angle can be defined as:

$$\gamma = 14.92N^{0.095} \leq 20.5\frac{kN}{m^3} \tag{4.1}$$

$$\phi = 53.88 - 27.60e^{-0.0147N} \leq 50^{\circ} \tag{4.2}$$

The side contribution to the torsional capacity was calculated according to the two methods, for dry and saturated conditions, and the results are plotted in Figure 4-5. One can observe important differences between them. Agreement was found for *L/D* = 3 with shaft in poor soil. Figure 4-6 compares the unit shear resistance profile predicted by $\alpha\beta$ and CDOT methods for the full-scale load tests available. Although the predicted torsional capacities are similar, Figure 4-6 shows how different these two approaches are. TS1 and TS2 unit shear resistance profiles can be considered comparable, but considerable differences are observed for TS3, TH2, TDS and TDSFB tests. Measured and extrapolated values are also drawn for TDS and TDSFB. Neither method provided a satisfactory approximation of the unit shear resistance.

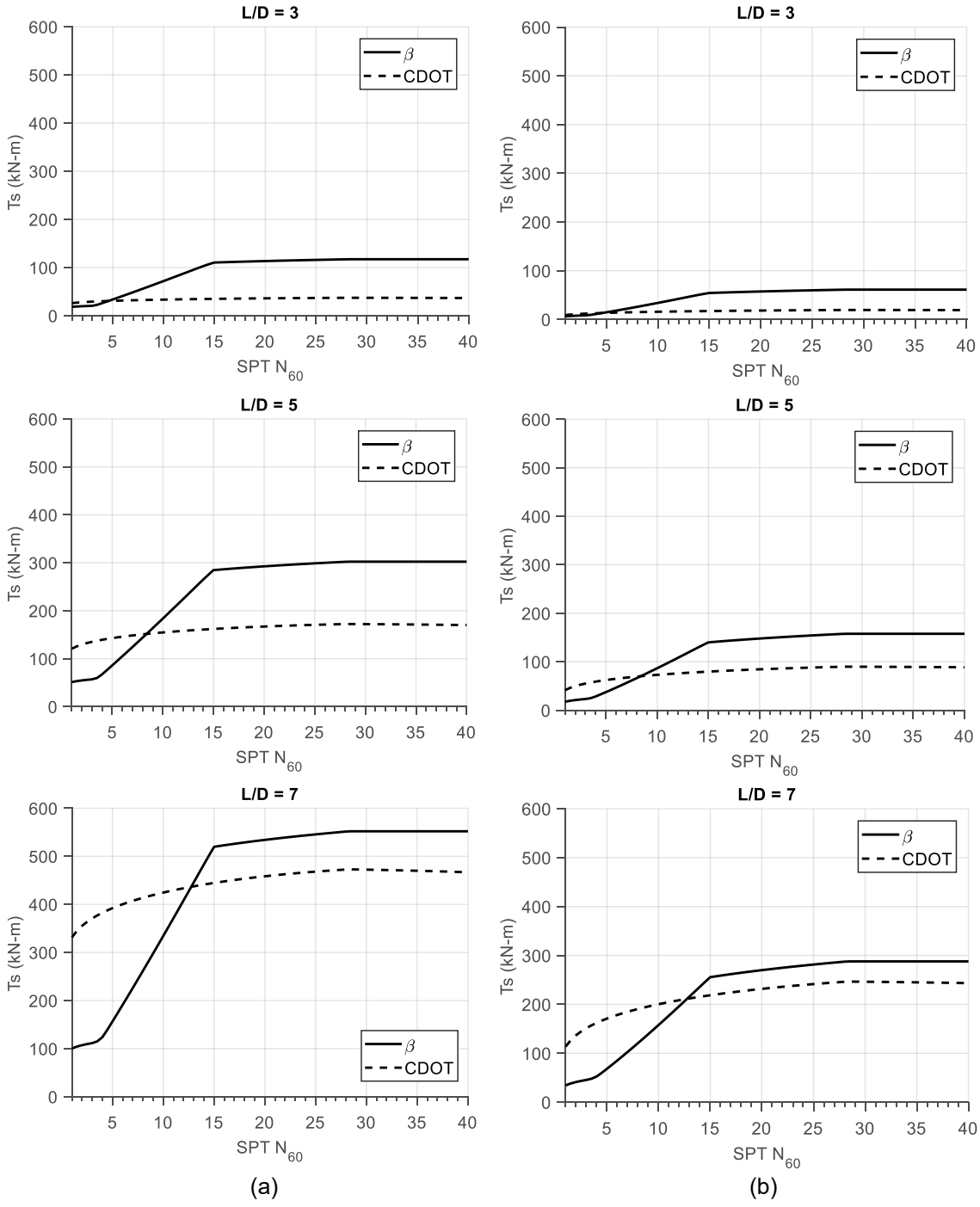

Figure 4-5: Torsional resistance from β and CDOT methods in uniform layers of sand, (a) dry condition, and (b) saturated condition

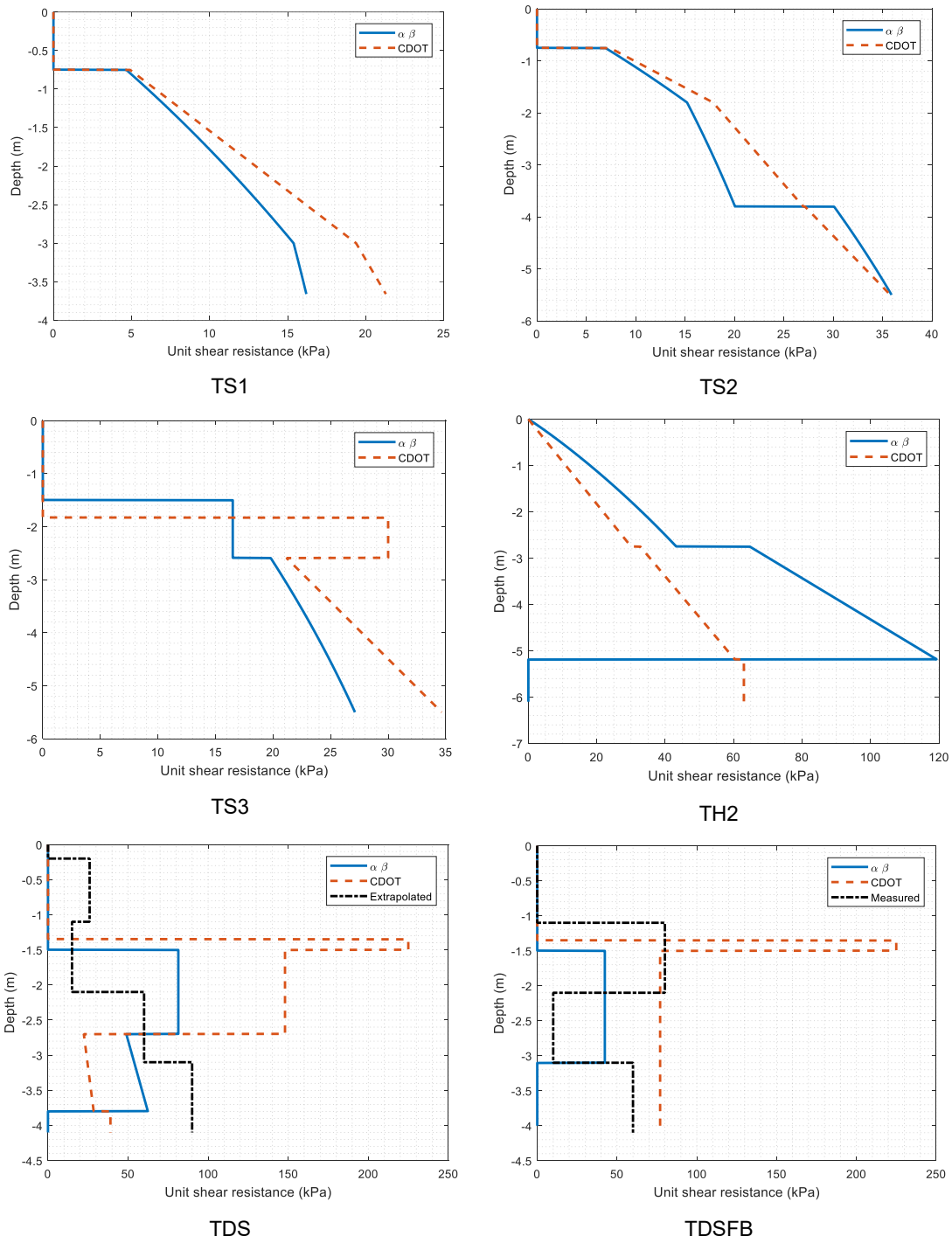

Figure 4-6: Unit shear resistance profile for full-scale tests according to α and β, and CDOT

Chapter 5

LATERAL AND TORSIONAL INTERACTION

5.1 Lateral-Torsional Interaction

The traditional design procedure for a drilled shaft subjected to lateral and torsional loading simultaneously begins with calculating the lateral capacity of the shaft using the Broms (1964a, 1964b) solution, p–y analysis approach, or continuum analysis. The lateral load analysis determines the required shaft diameter and the minimum embedment depth. Next, the torsional capacity of the foundation with the minimum embedment depth is compared with the design torque. If the design torque exceeds the estimated torsional capacity, the embedment depth is increased. Safety factors (ASD) or resistance factors (LRFD) may be applied, depending on the nature of the structure and the consequence of failure. It is evident that the current approach treats the lateral and torsional load separately, with no consideration of coupling or reduction of resistance due to the combination of loading (Thiyyakkandi et al. 2016). The underlying assumption is a linear elastic behavior of the soil, a hypothesis that is usually false for geotechnical problems. Since both, lateral and torsional loading generate shear stresses at the interface shaft-soil, a coupling effect could be expected.

Tawfiq (2000) reported that the torsional resistance of a drilled shaft was influenced by the lateral load. Specifically, the lateral displacement of the shaft caused by the lateral loading influences the torsional resistance. Similarly, centrifuge studies of scaled models (Herrera 2001; Hu 2003; McVay et al. 2003; Hu et al. 2006) of drilled shafts supporting high mast-arm or cantilever signal structures, showed that the torsional resistance of the shaft was influenced slightly by lateral load when thin slurry cake layers formed in wet shaft construction prior to concreting. Whereas the lateral capacity was significantly decreased by the applied torsion (Thiyyakkandi et al. 2016). Laterally loaded drilled shafts subject to torque can undergo a significant reduction in lateral resistance, as great as 50% (Hu et al. 2006).

The research effort made by Tawfiq (2000); Herrera (2001); Hu (2003); McVay et al (2003) at University of Florida has resulted in a method to design drilled shafts considering a couple loading. The method is based on a lateral-torsional-modifier that depends on the load eccentricity and the length-over-diameter ratio (L/D). A description can be found in Hu et al. (2006) and a MatCAD implementation is presented in (Hu 2003)

To provide support to the centrifuge test findings, three full-scale load tests were performed to study the interaction in the field (Thiyyakkandi et al. 2016). One of them failed in a combined lateral-torsional mode, while the other two shafts failed in a pure torsional mode. The horizontal load eccentricity of those tests was over 10 m. Thus, a pure torsional failure was very likely.

Centrifuge modeling is a powerful tool in geotechnical engineering. However, several complications can lead to a misrepresentation of the stress state of the prototype (field). One of the most common drawbacks is the particle size not scaled as every other dimension is. Furthermore, the lateral-torsional interaction has not been studied for cohesive soils. Those reasons could explain why the research results on this matter have not yet been applied into design guidance by any public agency.

There is a lack of knowledge in this area, and further research is needed. Similar experimental experiences with moderate eccentricities would be beneficial and are strongly recommended. In this work, the interaction will be studied from a numerical point of view. The goal of this numerical study is to explore the different failure modes described previously and to assess how the eccentricity of the load affects the torque-rotation and the force-displacement responses of a typical drilled shaft foundation. Lateral and torsional responses are calculated using the finite element methods with ABAQUS/Standard (Hibbitt, Karlsson, and Sorensen 2001), which is a general-purpose finite element method (FEM) software that employs implicit integration scheme. Many examples of the use of this software in the geotechnical field can be found in the literature.

5.2 Previous Physical Modeling Results

The results of 91 centrifuge tests are reported by Hu et al. (2006). 54 of the tests were conducted in dry sand, and 37 in saturated sands. Figure 5-1(a) shows one example of the models used. The tests varied the lateral load-to-torque ratios, shaft embedment depths *(L/D)*, and relative densities *(D_r)*. Figures 5-1(b) and 5-1(b) show the lateral load versus deflection (at ground level) results, for medium dense (D_r = 53%) and dense (D_r = 66%) sands, at three different embedment lengths (*L/D* = 3, 5, and 7). In the case of loading on the pole (i.e., no torque), the tests suggest that the deeper the shaft, the greater the shaft's initial stiffness and the higher the shafts lateral resistance. Also the load versus deflection of the top of the shaft with the load applied at the middle of the mast-arm (4.25 m from pole) and at the arm tip (6 m from the pole) are included in Figure 5-1. Evident from the plots is that moving the load further along the mast-arm significantly diminishes the lateral resistance of a drilled shaft. Moreover, the reduction appears to be independent of soil properties, but rather a function of the torque to lateral load ratio (Hu et al. 2006).

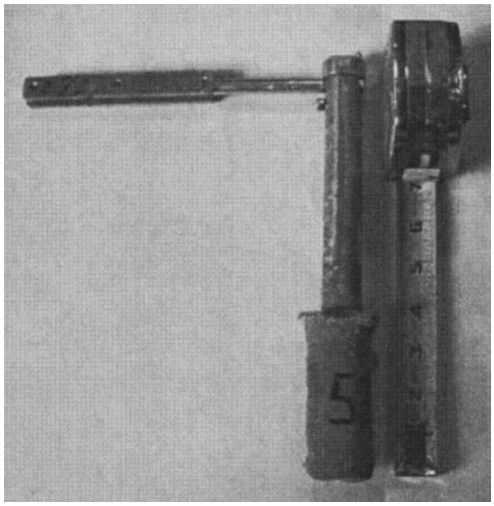

(a)

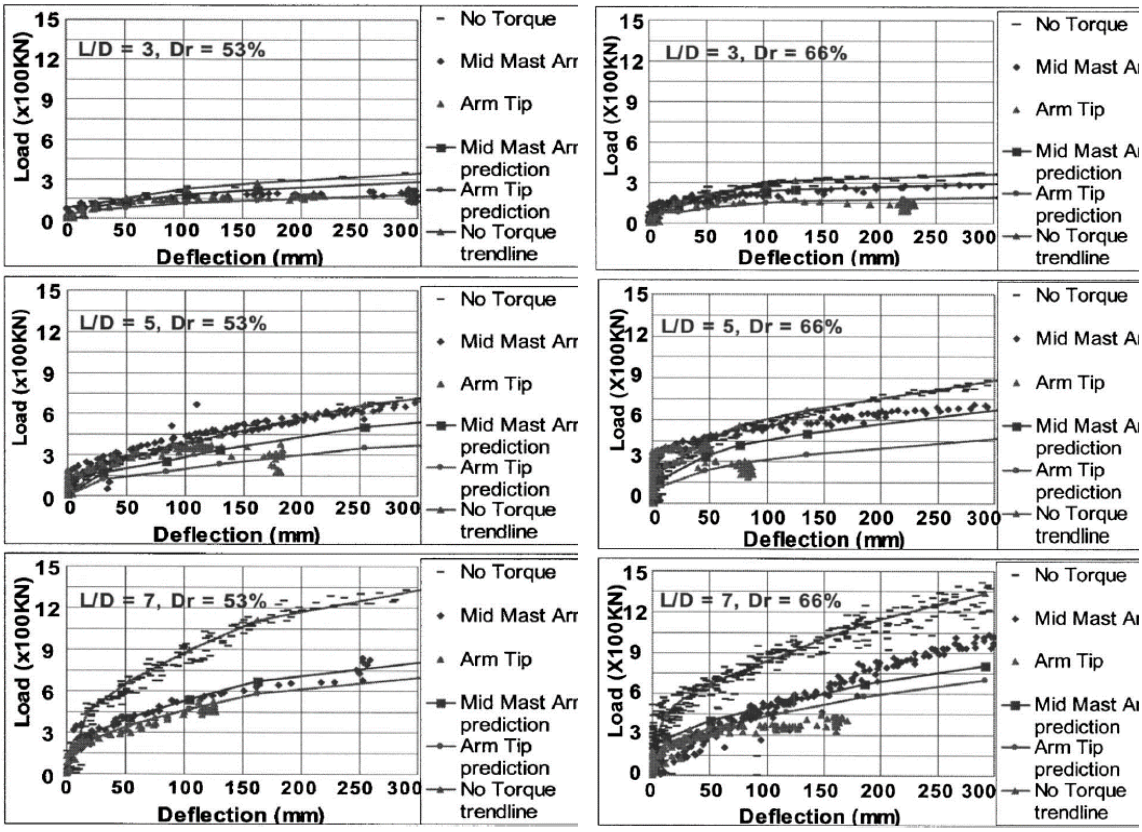

(b) (c)

Figure 5-1: Centrifuge tests results, (a) model example (b) dry medium dense sand, (c) dry sands (Hu et al. 2006)

Three full-scale tests to investigate the coupled load behavior of drilled shafts are reported in Thiyyakkandi et al. (2016). One of them (test TS1) showed a combined lateral-torsional mode of failure; however, because of instrumentation problems the displacement is not reported. The other

two tests showed a pure torsional failure mode. The reduction in lateral resistance from the centrifuge tests and the one full-scale test relevant are summarized in Figure 5-2.

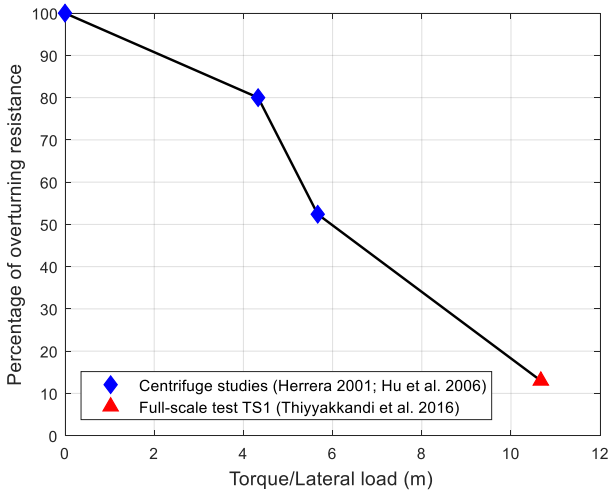

Figure 5-2: Reduction of the overturning resistance due to applied torque (L/D = 3)

Then, the hypothesis is that when applying an eccentric load to a mast-arm assembly, three failure modes could be possible: Overturning failure, torsional failure, or a combination of the two.

Figure 5-3 and Figure 5-4 show the lateral force capacity of a drilled shaft with the following dimensions: D = 0.91 m (3 ft) and L = 3.05 m (10 ft). The drilled shaft is supporting a mast-arm structure with a vertical eccentricity of e = 8.23 m (27 ft). The dimensions used are based on a City of Auburn Ornamental Traffic Sign Pole. The lateral load capacity of the shaft is the minimum value of the lateral load resistance associated with an overturning failure (red line) and the torsional resistance divided by the horizontal eccentricity of the load (blue line). The interaction diagrams were generated for several soil conditions based on Alabama Department of Transportation (ALDOT) soil ranges and properties recommendations. Resistances were calculated based on the Broms (1964a, 1964b) and α or β method (O'Neill and Reese 1999) models for overturning and torsional resistance, respectively. No factor of safety was applied, Hu (2003) lateral capacity reduction values (similar to those in Figure 5-2) were applied for all cases. Although the reduction in overturning capacity due to the presence of torque has been studied only in cohesionless soil, in this exercise, it is assumed in the reduction applies to clay soils, as well.

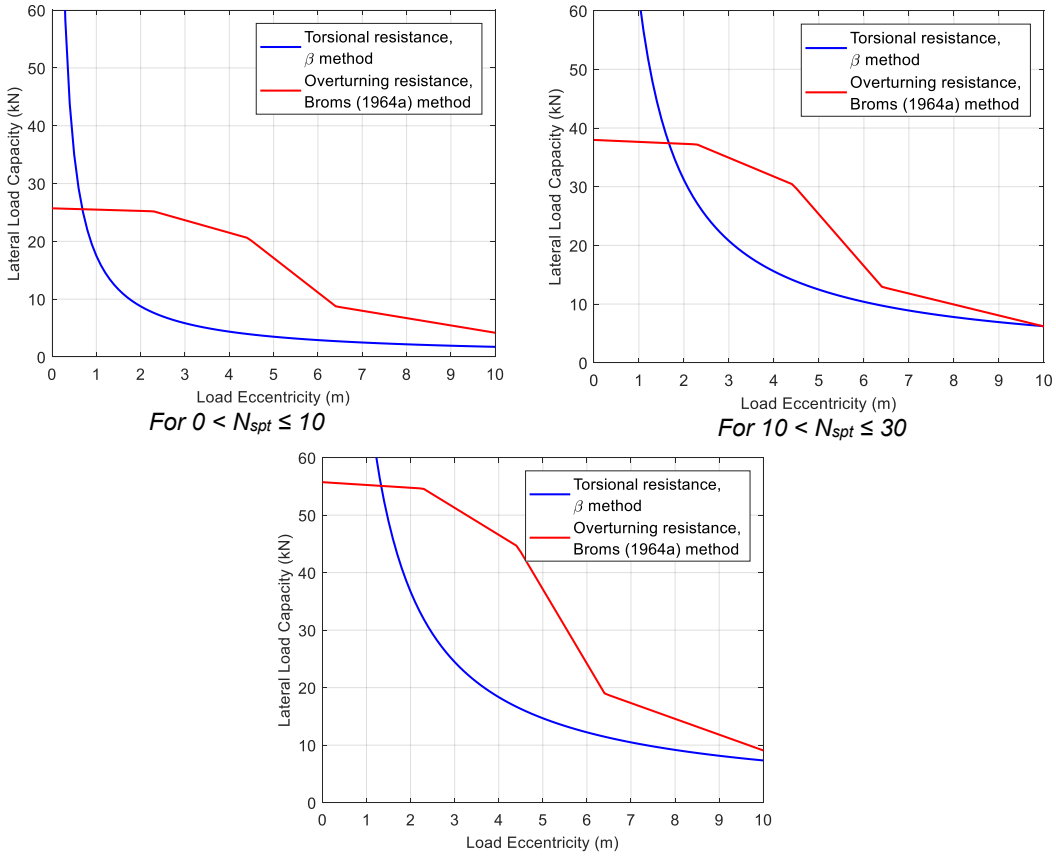

Figure 5-3: Lateral capacity of a drilled shaft in cohesionless soil under combined loading

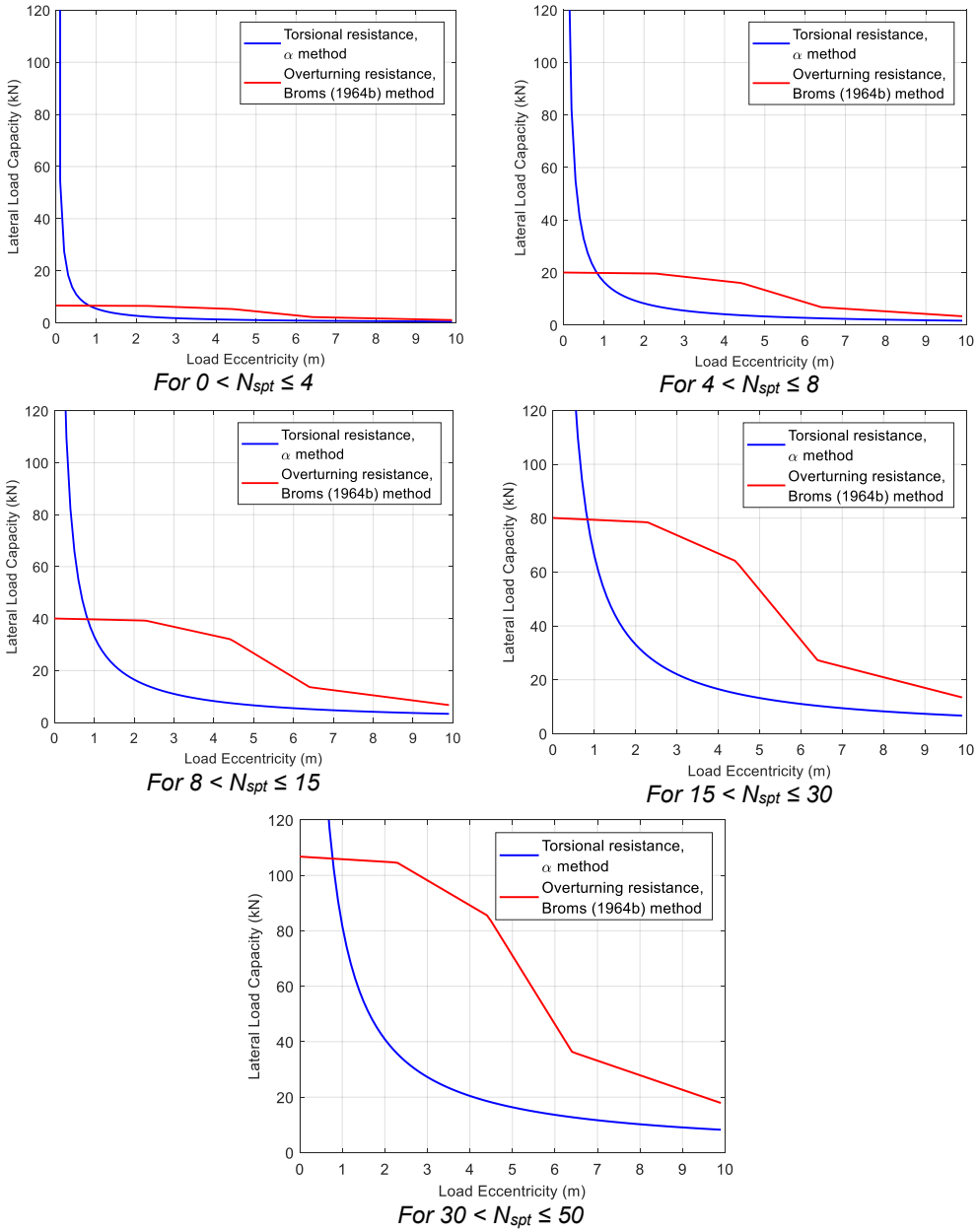

Figure 5-4: Lateral capacity of a drilled shaft in cohesive soil under combined loading

First, for the cases shown in Figures 5-3 and 5-4, the torsional resistance controls except for small load eccentricities. Second, the case where the overturning resistance (red line) is below the torsional resistance (blue line) is plausible if we take into consideration the uncertainties involved in this geotechnical problem. This would mean that an overturning failure could happen in combination to a torsional failure for large eccentricities. Based on the gap between the red and the blue lines, one can see that this case is less likely to happen in clay soils (Figure 5-4). Numerical models were developed to study this phenomenon.

5.3 Numerical Model Description

Based on ALDOT usual practice a 0.90-m diameter, 3.0-m length drilled shaft supporting a 5.30-m height signal for different mast-arm length was used as a case of study. Later, the effect of increasing the signal height to 10.6 m was investigated. Five load eccentricities were considered: 1 m, 2.5 m, 4 m, 6 m, and 8 m.

Several finite element models were created in order to study the effect of the load eccentricity on the overall response. Those can be grouped into two models types: 1) Models to analyze a drained loading condition (sand), and 2) models to analyze an undrained loading condition (clay). In all cases, the initial excess pore pressure is considered zero since it is assumed the loading will happen after all excess pore pressure is dissipated. The water table is assumed at the ground level and initial pore pressure and initial stress condition are calculated accordingly. In this analysis, the coefficient of lateral earth pressure at rest is assumed to be 0.5.

Mohr-Coulomb plasticity and Drucker-Prager/Cap plasticity models were selected to simulate the behavior of the cohesionless and cohesive soils, respectively. For the concrete drilled shaft a linear elastic model was used.

The simulations are ran until equilibrium of the finite element model cannot be achieved, or until the displacement or the rotation at the ground surface reach a limiting value. The failure criteria defined by FDOT (Hu et al. 2006) of 0.30m displacement and 15 deg rotation was considered.

General scheme and boundary conditions are shown in Figure 5-5. Material constitutive models and properties are described in sections 5.5 and 5.6.

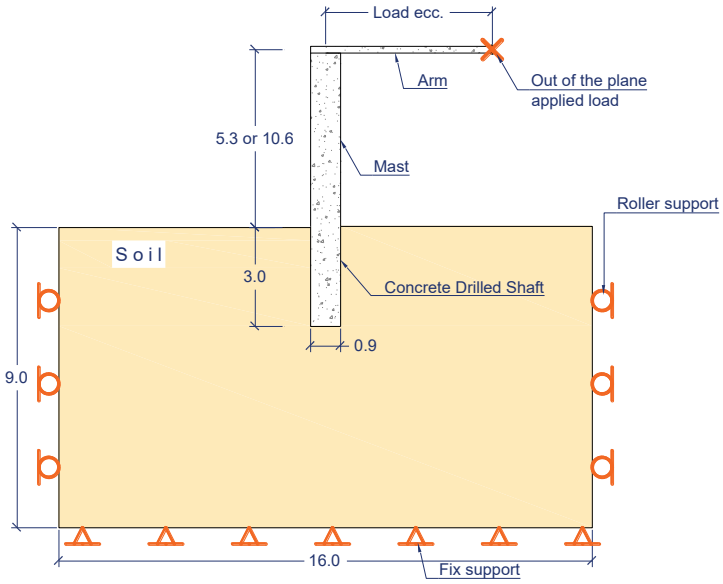

Figure 5-5: Problem geometry description (units: meters)

Figure 5-6 shows a 3D view of the model. Mesh and general geometry can be observed. All results of displacements and rotations were measured at the pile head, which is 50cm above the ground level. The Reference Point (RP-1) is constrained rigidly to the pile head. So that the relative positions of the pile head and the reference point (RP-1) remain constant throughout the analysis. The load was applied at the reference point, and the eccentricity of the load was generated by changing its location.

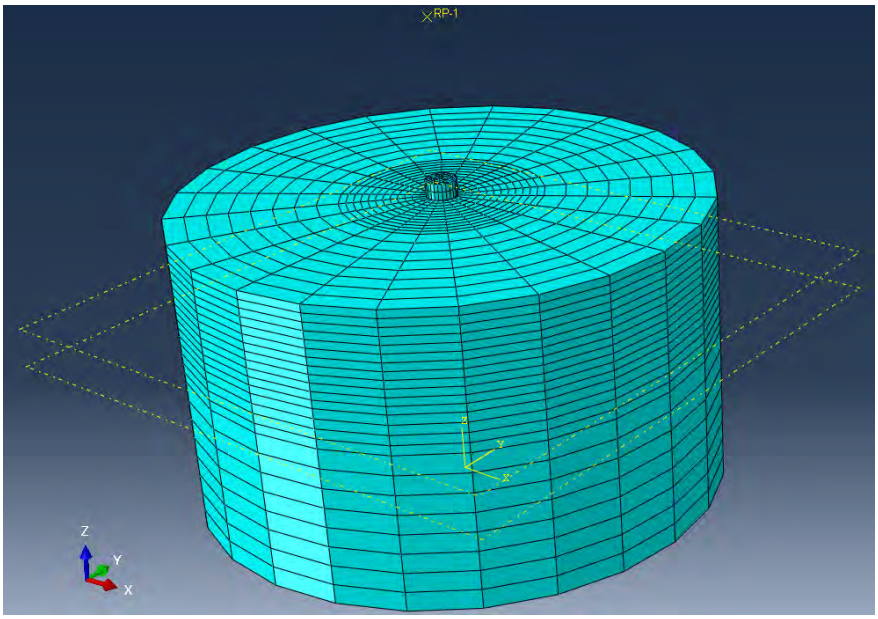

Figure 5-6: 3D view of finite element model

5.4 Numerical Simulation Procedure

Soils are pressure dependent materials since their strength is a function of the stress state. Therefore, the modeling needs to be performed step by step. First, stresses and void ratio were initialized. Then, the self-weight of the soil and shaft were applied as body forces. The analysis is solved under the geostatic type solver. Geostatic command makes sure that the initial stress conditions in any element within the soil falls within the initial yield surface of the constitutive model. The loading is then applied at the reference point.

The static general analysis was used for the drained loading conditions since the pore pressure change is not of interest. The high permeability of the sand allows the excess pore pressure to dissipate rapidly without having an effect on the effective stress. On the other hand, clays have very low permeability. Therefore, the excess pore pressure is developed during loading. Coupled consolidation analysis was performed for undrained loading condition to include this effect on the effective stress. Since the plastic flow rule is not associated with the constitutive model selected for clays, the unsymmetrical solver of ABAQUS was used.

The geometry is created based on hexahedral elements. Eight-node linear brick elements were used to model the drilled shaft. The same kind of finite element was used to simulate the soil when a drained situation was simulated (sand). Eight-node linear brick pore stress/fluid element was used for coupled consolidation simulations. Reduced integration was selected in all cases. All simulations were run with full output precision to avoid errors from numerical approximations. Also, the artificial energy was compared to the total energy of the system as a measure of the error in the simulation.

The mesh created to represent the soil surrounding the drilled shaft is a cylinder and is 16-m radius, and 9-m height. The dimensions were selected based on preliminary models, so that the boundaries do not affect the solution. No mesh convergence studies were performed. Nevertheless, the mesh was created finer in the vicinity of the shaft since stress concentration is expected at that location. In addition, shape and size metric limits recommended by ABAQUS were followed (see Table 5-1).

Table 5-1: Meshing description and metrics

Drilled shaft no. of elements	840
10 < Angle on quad faces < 160	Min = 63.76 Max = 131.04
Aspect ratio <10	Average = 2.72 Max = 4.05
Soil no. of elements	12,240
10 < Angle on quad faces < 160	Min = 63.76 Max = 131.91
Aspect ratio <10	Average = 3.61 Max = 9.76

The interaction between pile and soil was modeled by a frictional surface with a shear stress limit calculated from the α and β method, for undrained and drained condition, respectively. The pile is assumed to be in perfect contact with the soil at the beginning of the analysis.

5.5 Constitutive Models

Since the concrete shaft has much greater stiffness than the soil, and the shaft can be considered short (L/D<10), a mainly rigid body behavior can be expected. Thus, a linear elastic model seems suitable for representing the concrete drilled shaft. Elastic-perfectly plastic Mohr-Coulomb constitutive model is used to represent cohesionless soil behavior. Its use is commonly accepted for design applications in the geotechnical engineering area to simulate material response under essentially monotonic loading. For cohesive soil, Drucker-Prager/Cap plasticity model gave better results than Mohr-Coulomb. A brief description of each constitutive model is provided next. More details can be found in Hibbitt, Karlsson, and Sorensen (2001), and Helwany (2007)

5.5.1 Linear Elastic Model

In a linear elastic material, change in stress ($\delta\sigma$) can be directly related to the change in strain ($\delta\varepsilon^{el}$) through the elastic stiffness matrix ($\mathbf{D}^{el}$) as follows

$$\delta\boldsymbol{\sigma} = \mathbf{D}^{el}\delta\boldsymbol{\varepsilon}^{el} \tag{5.1}$$

where the elastic stiffness matrix ($\mathbf{D}^{el}$) is defined as a function of two parameters: modulus of elasticity (*E*) and Poisson's ratio (υ). $\mathbf{D}^{el}$ can be written as follows, see Equation (5.2), for the 3-dimensional state of stress and isotropic material (notice that engineering shear strain shall be used to be consistent with this matrix).

$$\mathbf{D}^{el} = \frac{E}{(1+\upsilon)(1-2\upsilon)}\begin{bmatrix} 1-\upsilon & \upsilon & \upsilon & 0 & 0 & 0 \\ \upsilon & 1-\upsilon & \upsilon & 0 & 0 & 0 \\ \upsilon & \upsilon & 1-\upsilon & 0 & 0 & 0 \\ 0 & 0 & 0 & \frac{1}{2}(1-2\upsilon) & 0 & 0 \\ 0 & 0 & 0 & 0 & \frac{1}{2}(1-2\upsilon) & 0 \\ 0 & 0 & 0 & 0 & 0 & \frac{1}{2}(1-2\upsilon) \end{bmatrix} \tag{5.2}$$

5.5.2 Mohr-Coulomb Plasticity Model

In general, elastic-perfectly plastic models assume that the strain can be divided into elastic and plastic parts as follows

$$\delta\boldsymbol{\varepsilon} = \delta\boldsymbol{\varepsilon}^{e} + \delta\boldsymbol{\varepsilon}^{p} \tag{5.3}$$

Elasticity. As in the linear elastic model, in the elastic regime, the change in stress can be directly related to the change in strain through $\mathbf{D}^{el}$, see Equation (5.1) and Equation (5.2).

Plasticity. When plastic strain occurs the change in stress is related to the change in strain through the stiffness tensor **D**, see Equation (5.4).

$$\delta\boldsymbol{\sigma} = \mathbf{D}\delta\boldsymbol{\varepsilon} \tag{5.4}$$

where **D** is define as a correction of $\mathbf{D}^{el}$ based on three components: **g**, **f**, *H*.

$$\mathbf{D} = \mathbf{D}^{el} - \frac{\mathbf{D}^{el}\,\mathbf{g}\,\mathbf{f}\,\mathbf{D}^{el}}{H + \mathbf{f}\,\mathbf{D}^{el}\,\mathbf{g}} \tag{5.5}$$

where **f** is the first derivative of the yield function, **g** is the first derivative of the plastic potential, both with respect to the stress tensor, and *H* is the hardening modulus. Those are define below.

Yield function. The boundary of the elastic region is called a yield surface and is mathematically described by a yield function *(F)* of the stress tensor

$$F\left(\boldsymbol{\sigma}\right) = 0 \tag{5.6}$$

the Mohr-Coulomb criterion assumes that yield occurs when the shear stress on any point in a material reaches a value that depends linearly on the normal stress in the same plane. The failure envelope for this model corresponds to a Mohr-Coulomb criterion (shear yield function) with tension cut-off (tension yield function). In terms of principal stresses (σ_1 and σ_3), the shear yield function is given by Equation (5.7) while the tension cut-off is modeled using the Rankine surface, see details in ABAQUS (2010).

$$F = \frac{1}{2}\left(\sigma_1 - \sigma_3\right) + \frac{1}{2}\left(\sigma_1 + \sigma_3\right)\sin\phi - c\cos\phi = 0 \tag{5.7}$$

where $\emptyset$ is the friction angle, and *c* is the cohesion.

Plastic potential. The potential function describes the direction of plastic strain. For the shear yield surface, the plastic flow is chosen as a hyperbolic function in the meridional stress plane and the smooth elliptic function proposed by Menetrey and William (1995). While for the tension cut-off yield surface, a modification of the same potential function results in a nearly associative flow (see details in Hibbitt, Karlsson, and Sorensen 2001).

Hardening/softening. Isotropic cohesion hardening is assumed for the hardening behavior of the Mohr-Coulomb yield surface. Rankine surface for tensile failure allows defining hardening of the tension cut-off as a function of the tensile equivalent plastic strain. This analysis does not consider hardening or softening using the Mohr-Coulomb model.

5.5.3 Modified Drucker-Prager/Cap Plasticity Model

The Drucker-Prager/Cap plasticity model has been widely used in finite element analysis programs for a variety of geotechnical engineering application. It is capable of considering the effect of stress history, stress path, dilatancy, and the effect of the intermediate principal stress (Helwany 2007). The strain decomposition and the elastic behavior is the same as the one described for Mohr-Coulomb model.

Yield function. The Drucker-Prager failure surface is given by

$$F_{shear} = t - p\tan\beta - d = 0 \tag{5.8}$$

where β is the friction angle and *d* is the cohesion of the soil. Notice that this form in *p-t* stress plane, it definition can be seen in ABAQUS (2010). The cap yielding and the transition surface are given as

$$F_{cap} = \sqrt{\left(p - p_a\right)^2 + \left(\frac{Rt}{1+\alpha-\frac{\alpha}{\cos\beta}}\right)^2} - R\left(d + p_a\tan\beta\right) = 0 \tag{5.9}$$

$$F_{transition} = \sqrt{\left(p - p_a\right)^2 + \left[t - \left(1-\frac{\alpha}{\cos\beta}\right)\left(d + p_a\tan\beta\right)\right]^2} - \alpha\left(d + p_a\tan\beta\right) = 0 \tag{5.10}$$

where *R* is a material parameter that controls the shape of the cap; α is a number used to define a smooth transition between shear failure and cap; and p_a is the evolution parameter that controls the hardening.

Plastic potential. Associated plastic flow rule is used in the cap region. For the shear failure and transition surface, a non-associated flow rule is assumed. The plastic potential is described by an elliptical function.

Hardening/softening law. Hardening behavior is described by a function relating the mean effective yield stress and the volumetric plastic strain. It is obtained from isotropic consolidation test.

5.6 Calibration of Constitutive Models

The combined loading effect is studied in two soil conditions: 1) a uniform layer of loose sand, and 2) a uniform layer of stiff weathered clay. This section details how the material properties were selected (calibrated) for analysis.

As a first step, strength parameters were estimated based on ALDOT recommended properties for *p-y* analysis, and elastic properties were selected from literature recommendations. Equations for shear modulus *(G)* based on in-situ testing can be found in the literature. A fundamental relationship from the theory of elasticity is used to relate modulus of elasticity *(E)*, Poisson's ratio (ν), and shear modulus *(G)*, see Equation (5.11).

$$G = \frac{E}{3(1-2\nu)} \tag{5.11}$$

Once the elastic parameters were selected, analysis was performed for the pure lateral load case. It was found that the direct use of the values in Tables 5-2 and 5-3 resulted in very stiff responses. It is known that the shear modulus and the modulus of elasticity reduce as the shear strain increases. Therefore, the lateral responses from the widely accepted *p-y* analysis were used for calibrating the ABAQUS FEM models. O'Neill *p-y* curve was selected for sand soils, and saturated soft clay *p-y* curves for clay soils. The software FB-MultiPier (Jae H. Chung 2017) was used for performing the *p-y* analysis. It is nonlinear finite element for beam type elements developed by the Bridge Software Institute.

Modulus of elasticity and strength parameters were adjusted for calibrating the ABAQUS FEM models.

Hardening behavior was assumed based on literature examples.

5.6.1 Concrete Properties

The concrete was modeled as a linear elastic material. Two parameters are needed to characterize this material: modulus of elasticity *(E)*, and Poisson's ratio (ν). The modulus of elasticity can be estimated with the following ACI 318 (ACI Committee 2014) equation:

$$E_{concrete} = 4700\sqrt{f_c'} \tag{5.12}$$

where f_c' is the 28-day compressive strength (in MPa). A typical value of 28 MPa is specified. A Poisson's ratio of 0.20 was used.

5.6.2 Cohesionless Soil (Sand) Properties

Mohr-Coulomb plasticity model is used to represent sand. Six properties are required to define a Mohr-Coulomb material: modulus of elasticity *(E)*, Poisson's ratio (ν), cohesion *(c)*, friction angle *(ϕ)*, dilation angle *(ψ),* and tension cut-off *(σ_t)*.

A drained strength set of properties are selected for the analysis in cohesionless soil. In-situ testing performed by Thiyyakkandi et al. (2016) on sands that fall in the range selected are used as input values for correlations founded in the literature. For the cohesionless soil, the shear modulus is estimated based on correlations based on SPT (N_{60}) and CPT (q_c) found in Wood (2003). Imai and Tonouchi (1982) recommends

$$G_{\max} = 15560 N_{60}^{0.68} \text{ [kPa]} \tag{5.13}$$

and Rix and Stokoe (1991) recommends

$$G_{\max} = 1634 \left(q_c\right)^{0.25} \left(\sigma_v'\right)^{0.375} \text{[kPa]} \tag{5.14}$$

Once a shear modulus is selected, the modulus of elasticity can be calculated with an assumed a Poisson's ratio. Table 5-2 summarizes the model parameters and provide the assumed values and sources used to select those values.

Table 5-2: Mohr-Coulomb model parameters for a cohesionless soil (loose sand)

In-situ tests[1]	**Drained strength parameters**[2]	**Gmax**[3] (kPa)	**Gmax**[4] (kPa)	**Gmax**[5] (kPa)	**Emax**[6] (kPa)
SPT N_{60} = 5 CPT q_c = 2,900 kPa	ϕ = 30 γ = 17.3 kN/m^3	46,500	40,700	44,000	52,800

Notes:
[1]from Thiyyakkandi et al. (2016)
[2]ALDOT recommendation Appendix C
[3]from Imai and Tonouchi (1982)
[4]from Rix and Stokoe (1991)
[5]Selected value for maximum shear modulus
[6]Selected value for maximum elastic modulus from Equation (5-11) assuming ν=0.30

5.6.3 Cohesive Soil (Clay) Properties

Modified Drucker-Prager/Cap plasticity model is used for modeling the clay soil. Eight properties are required to define a Drucker-Prager/Cap material: modulus of elasticity *(E)*, Poisson's ratio (υ), cohesion *(d)*, friction angle *(β)*, initial cap position *(ε_{vol}^{pl}),* cap eccentricity *(R),* transition surface radius (α), and flow stress (*K*).

Undrained strength properties are selected for the cohesive soil case. Wood (2003) provided several equations to estimate shear modulus based on undrained shear strength *(s_u)*. Weiler (1988) defines shear modulus as

$$G_{\max} = 700\, s_u \tag{5.15}$$

this correlation is valid for normally consolidated clay (ORC=1) with a plasticity index (PI) between 20 to 25.

Once a shear modulus is selected, the modulus of elasticity can be calculated with and assumed a Poisson's ratio. Table 5-3 summarizes the model parameters and provide the assumed values and sources used to select those values

Table 5-3: Ducker Prager Cap-plasticity model parameter for a cohesive soil (stiff weathered clay)

Lab tests[1]	**Undrained strength parameters**[2]	**G_{max}**[3] (kPa)	**E_{max}**[4] (kPa)	**d**[5] (kPa)
ORC = 1 PI = 20-25	s_u = 72 kPa γ = 18.8 kN/m^3	50,400	60,480	124.7

Notes:
[1]Selected parameters for stiff weather clay
[2]ALDOT recommendation Appendix C
[3]from Weiler (1988)
[4]Selected value for maximum elastic modulus from Equation (5-11) assuming υ=0.30
[5]Cohesion in p-t stress plane

The hardening was defined by a straight line passing through two points: (0, 35kPa) and (0.0464, 1034kPa), where the first coordinate is the plastic volumetric strain, and the second is the mean effective stress. This curve was taken from an example in Helwany (2007).

Since the analyses for clays include the fluid influence, in addition to the strength parameters, permeability is required. A permeability of k=10^{-7}m/s at a void ratio of e=1.20 was assumed.

5.6.4 Concrete-Soil Interface Properties

The constitutive model for interfaces is defined by a Mohr-Coulomb shear strength criterion. In ABAQUS, a friction coefficient and a maximum shear stress are needed to fully define the interface. The friction angle was selected so the torsional response is not overly stiff, and the maximum shear stress was taken from the α and β methods.

For the sand, the friction coefficient was selected as 0.30, and maximum shear stress is selected from β method. While for the clay soil, the friction coefficient was selected as 0.35 and the maximum shear stress calculated from the α method. Interface properties selected are shown in Table 5-4.

Table 5-4: Interface properties

Property	Sand	Clay
Friction coefficient	0.30	0.35
Max Shear Stress	24 kPa	20 kPa

5.6.5 Calibrated Properties

Figure 5-7 and Figure 5-8 compare the results from FB-Multipier (*p-y*) and ABAQUS (FEM) models. The calibrated properties based on matching *p-y* analysis results are also provided. Notice that the calibrated modulus of elasticity is 12 to 15 times lower than the maximum value computed in the previous section, which is reasonable.

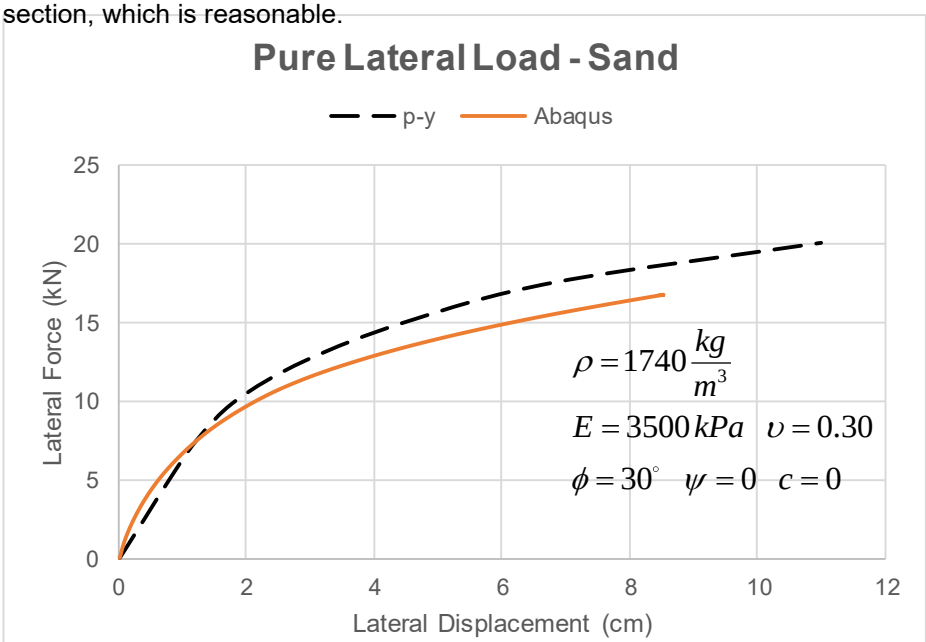

Figure 5-7: Calibration and calibrated properties for sand

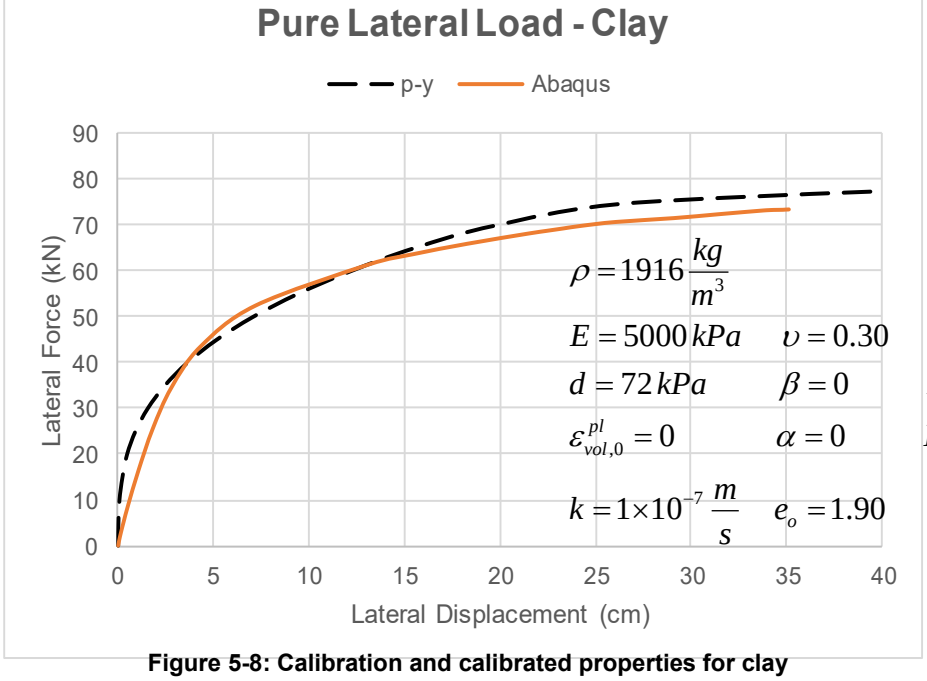

Figure 5-8: Calibration and calibrated properties for clay

5.7 Simulation Results

Results obtained from numerical modeling are presented and described in this section. Figure 5-9 and 5-11 show a comparison of the responses for eccentricities: 1 m, 2.5 m, 4 m, 6 m, and 8 m, for a load height of 5.3 m, and for simulations in sand and in clay, respectively. Figure 5-10 and 5-12 show the comparison when the load height is increased to 10.6 m, for sand and clay soil, respectively.

The models were run until the convergence was no longer possible. In models for clay, large displacements were obtained, so the overturning failure load is taken as the load when the displacement of the pile head reaches 30 cm. On the other hand, a 15 deg rotation angle is consider a torsional failure, nevertheless those model that were not able to describe the rotation until that limit reached a cap value, which was consider as torsional resistance at failure.

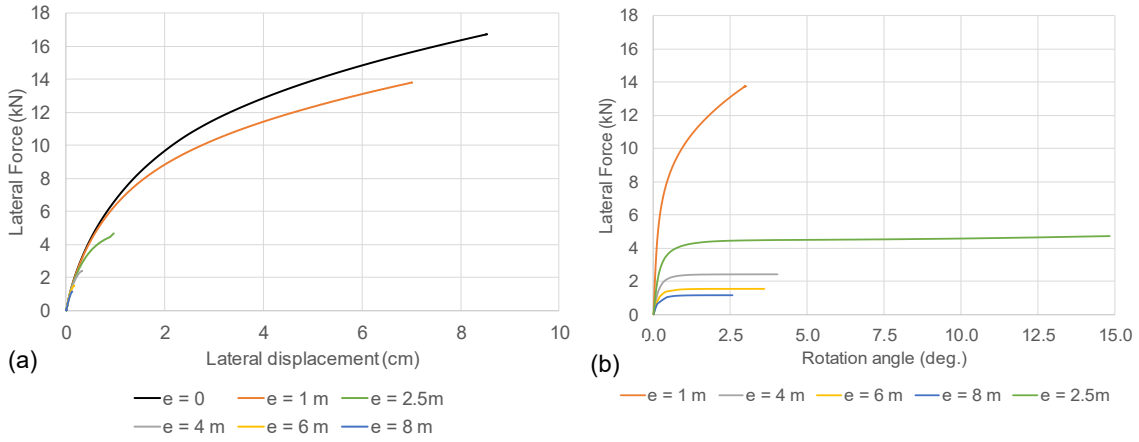

Figure 5-9: Lateral (a) and rotational (b) response of drilled shaft in sand with load height 5.3 m

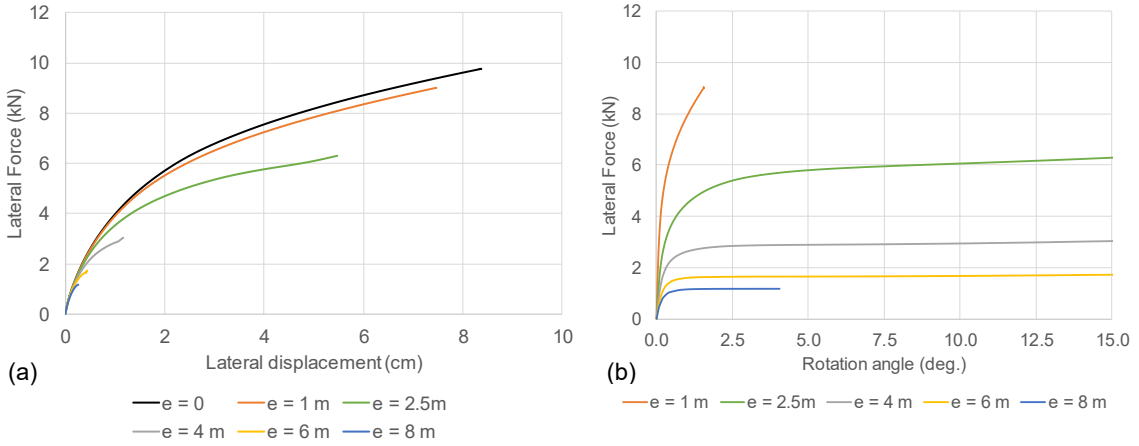

Figure 5-10: Lateral (a) and rotational (b) response of drilled shaft in sand with load height 10.6 m

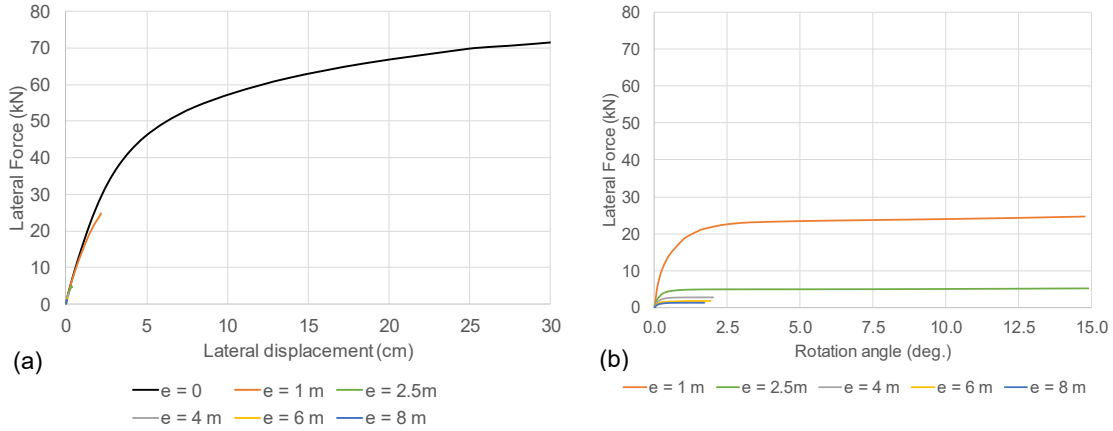

Figure 5-11: Lateral (a) and rotational (b) response of drilled shaft in clay with load height 5.3 m

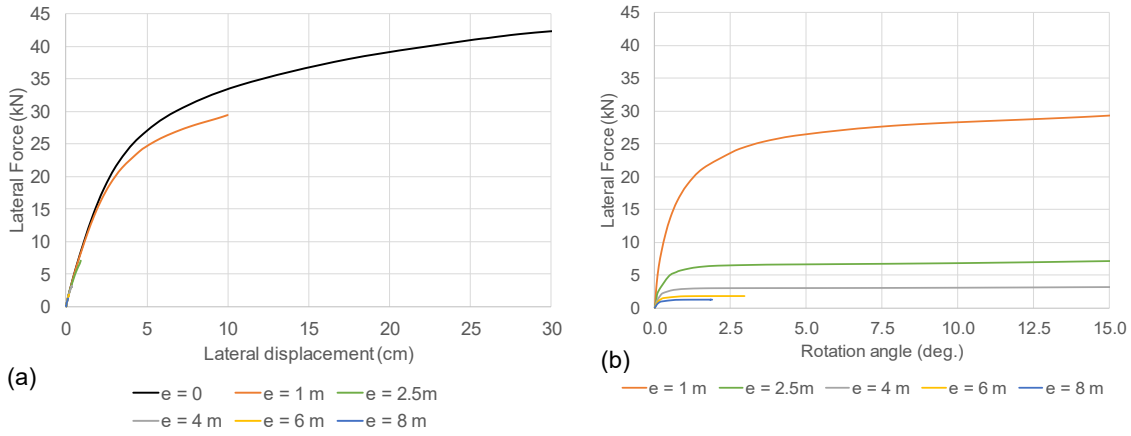

Figure 5-12: Lateral (a) and rotational (b) response of drilled shaft in clay with load height 10.6 m

The results can be grouped into two types:

1) Those that do not reach a cap in the rotational response, instead their failure can be described as an overturning type failure.
2) Those that reach a cap in the rotational response and then keep rotating almost freely until reaching 15 deg. This failure is understood as a torsional failure.

The premature analysis end can be attributed to the formulation of the interface elements in ABAQUS. All analysis that stopped before reaching 15 deg rotation angle involved large eccentricities. Therefore, there were large shear stresses and strains developed at the interface from the very beginning of the analysis.

In the analyses where the response was obtained for large rotation, the post torsional failure behavior was captured. Figures from 5-13 to 5-16 present lateral force and the corresponding displacement and rotation for each case, torque-rotation responses are included. The following behavior is observed. First, lateral displacement and rotation occur. Then, the shaft

reaches a cap in the rotational response and rotates almost freely, without increasing the force (a drastic change in slope of the lateral response is seen). Then, the rotational response hardens, and the shaft starts displacing laterally again with stiffness similar to the case of a pure lateral load. Initially the applied force is perpendicular to the mast-arm (simulating the wind force). As the foundation rotates the wind direction does not change, so the torque decreases so that at a rotation of 90 deg the torque is zero, see Figure 5-15(c). Concomitant with the rotation response, the shaft keeps displacing laterally until the convergence is no longer possible (overturning failure). This failure mode can be called “lateral-torsional failure”, where large rotation occurs first (torsional failure), and then the shaft carries more load and displaces until the overturning failure occurs. The eventual overturning failure has important practical implications, but the large rotation angles requires may not be possible to achieve in a single storm event. Based on Figure 5-14, the most vulnerable structures are those in loose sand where the horizontal eccentricity is significantly less than the vertical height.

The load eccentricity has an influence on the shaft response, both rotational and lateral. The force that the shaft is able to carry before a torsional failure occurs increases with the decrease in load eccentricity. On the other hand, the overturning resistance decreases when the load is applied with a small eccentricity, but for moderate eccentricity, this is not necessarily the case. For large eccentricities, the models were not able to give the full lateral response; therefore, no conclusion can be drawn about it.

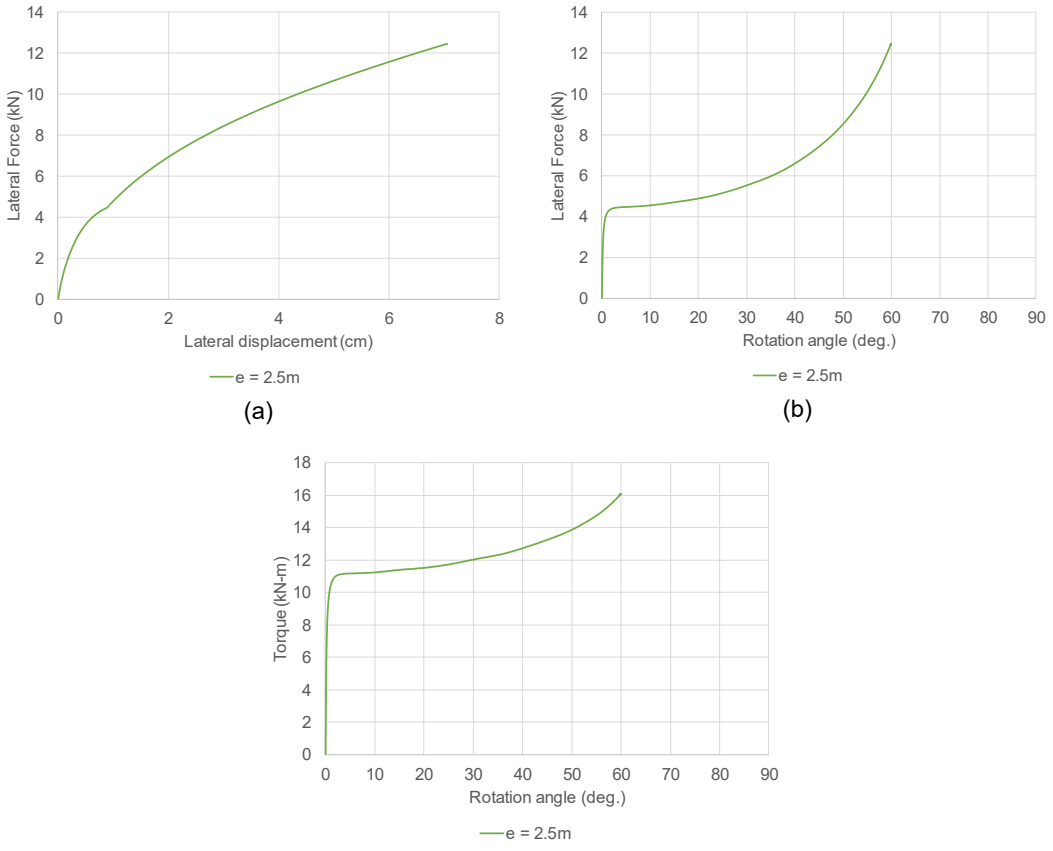

Figure 5-13: Full responses drilled shaft in sand with load height 5.3 m, (a) force vs. displacement; (b) force vs. rotation; and (c) torque vs. rotation

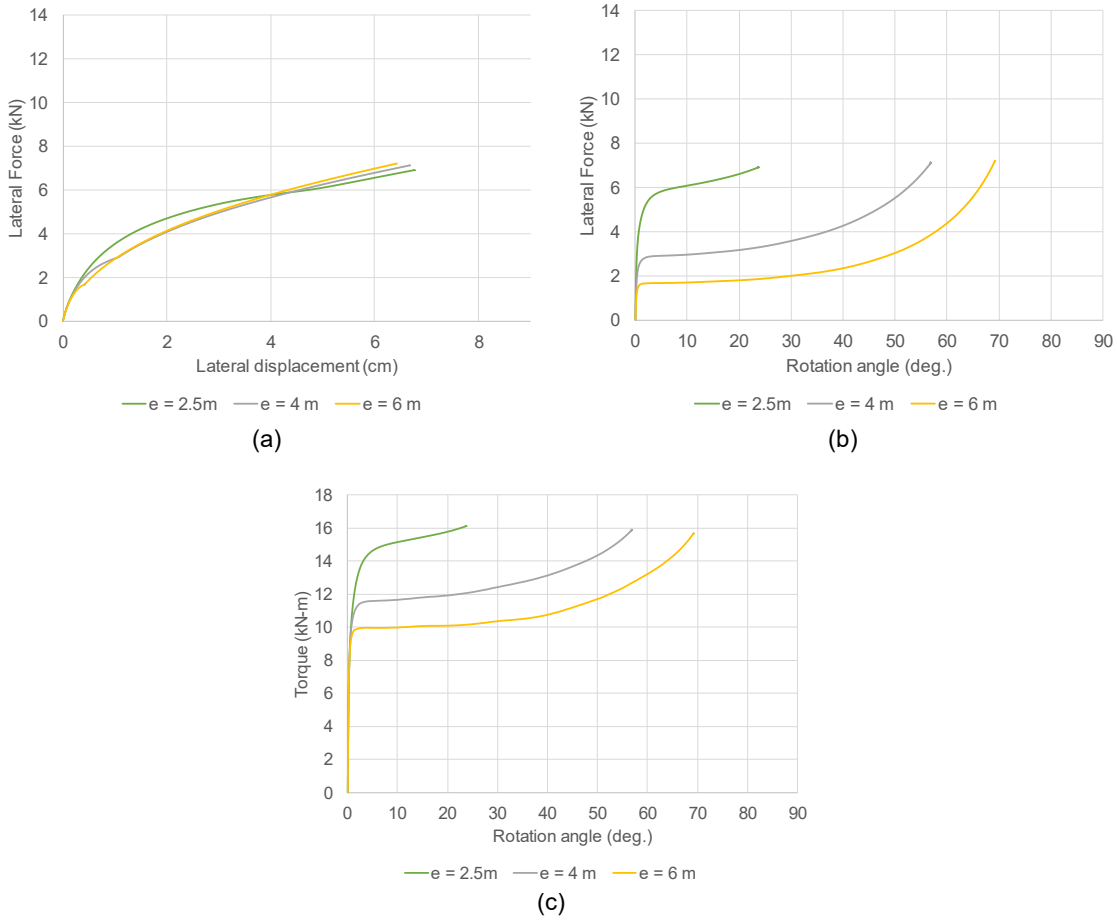

Figure 5-14: Full responses drilled shaft in sand with load height 10.6 m, (a) force vs. displacement, (b) force vs. rotation, and (c) torque vs. rotation

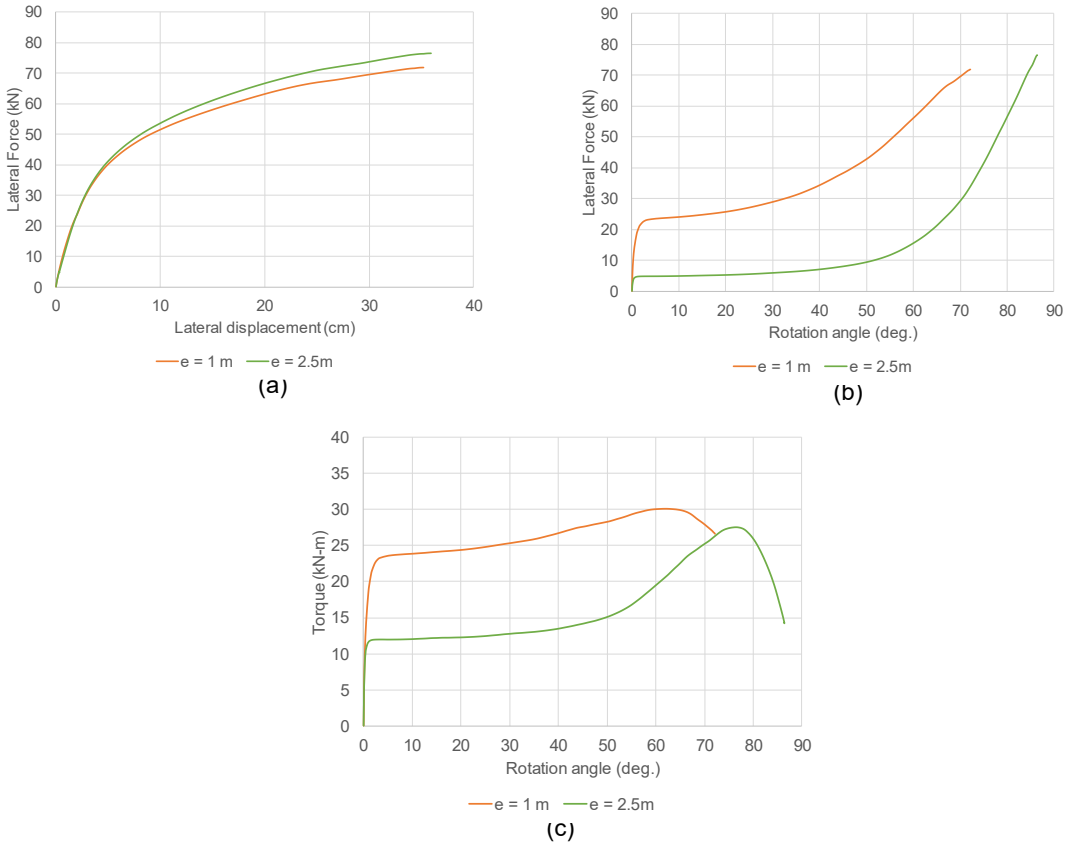

Figure 5-15: Full responses drilled shaft in clay with load height 5.3 m, (a) force vs. displacement, (b) force vs. rotation, and (c) torque vs. rotation

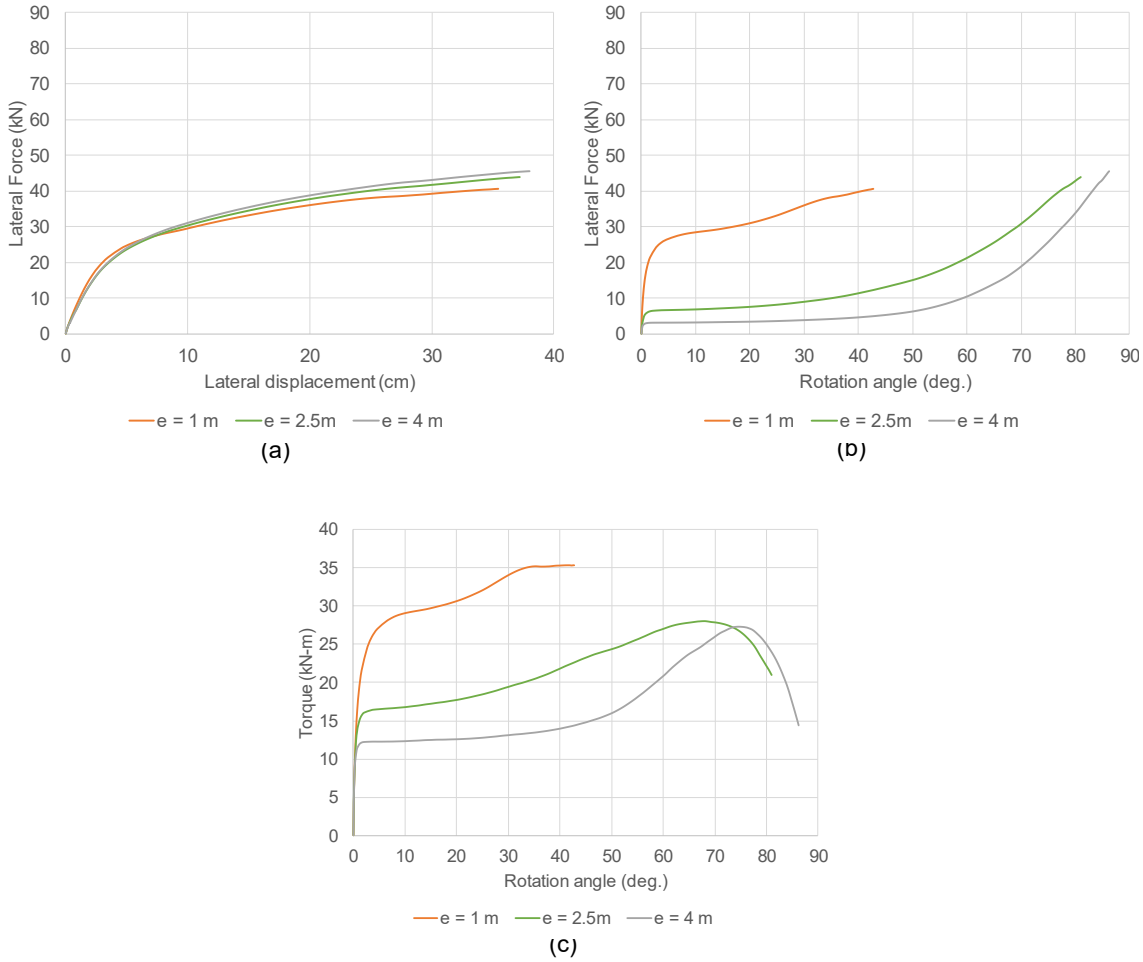

Figure 5-16: Full responses drilled shaft in clay with load height 10.6 m, (a) force vs. displacement, (b) force vs. rotation, and (c) torque vs. rotation

5.8 Comparison to Traditional Design

The results considering combined loading are compared to traditional design practice. Consider a shaft with an overturning resistance equal to the force determined from FEM at 30 cm, or when the model did not reach such a displacement, the overturning resistance is considered as the maximum force before the analysis stopped. Consider also the torsional resistance as the cap in the rotational response for the load eccentricity of 8 m. Using these resistances, design charts can be drawn (Figure 5-17). The initial cap is the overturning resistance, and the hyperbolic part is the torsional resistance divided by the load eccentricity. Thus, the dashed line represents the failure envelope that would be used in usual design practice. The markers included in the Figure 5-17 are the lateral forces at failure determined from FEM analyses shown in Figures from 5-9 to 5-12 that include applied torque and lateral load. It can be seen that for moderate eccentricities when torsional failure controls; the failure load is higher than expected by traditional design practice. Overturning failure for traditional design practice is indicated by the plateau of the dashed line in Figure 5-17. When the overturning failure occurred under combined loading, it happened at a lower load than traditional design practice would predict (sand only).

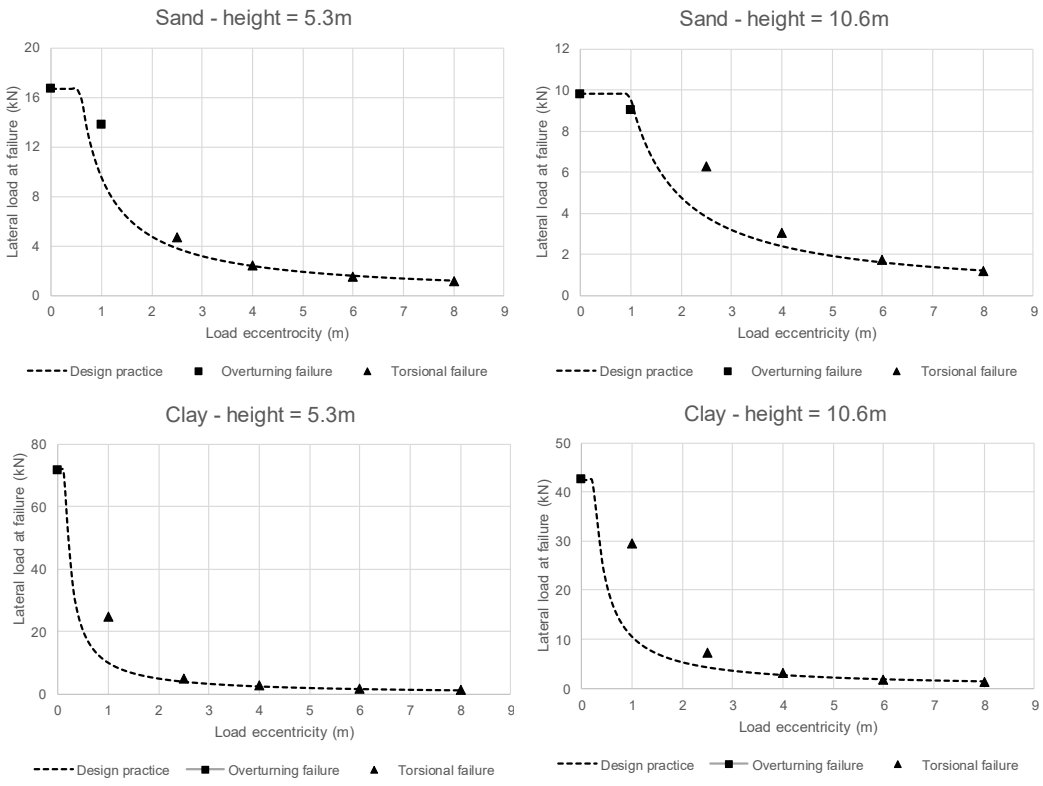

Figure 5-17: FEM results vs. typical design practice

When the load height increases the overturning resistance to lateral load decreases significantly. The torsional resistance does not change much. Based on this numerical study, the influence of the height of the load application is recognized in the reduction in the lateral load resistance due to the presence of torque (or load eccentricity). Figure 5-18 and 5-19 shows the failure loads as a fraction of the overturning resistance *(P_o)* for load height of 5.3 m and 10.6 m, respectively. Figure 5-18 shows that the height of the applied load influences the reduction of the load resistance. When the failure load is plotted as a function of the ratio eccentricity-to-height (Figure 5-19) the difference between the plots for different heights are small.

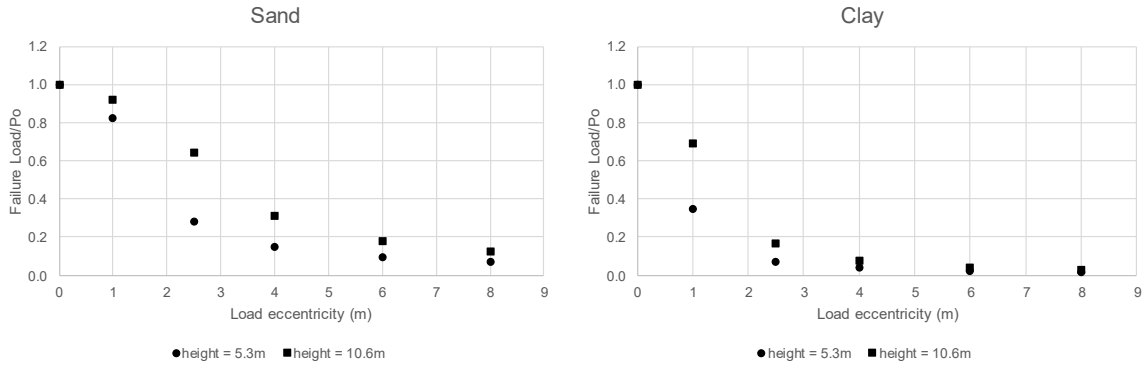

Figure 5-18: Failure load as a function of the load eccentricity

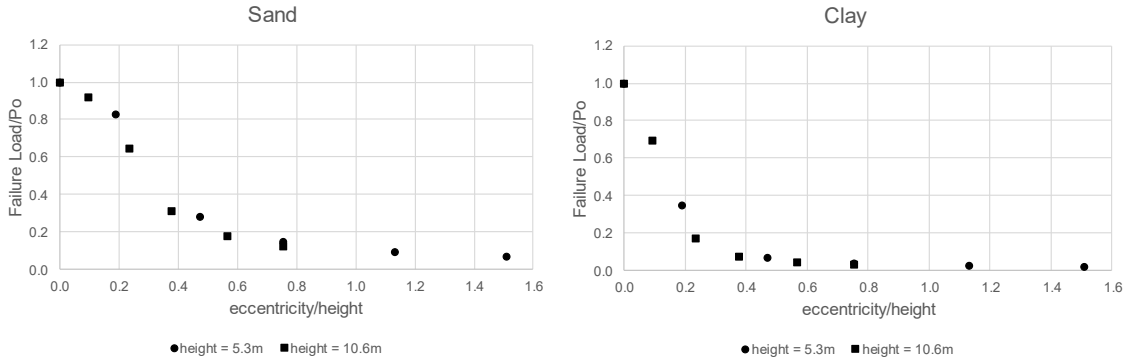

Figure 5-19: Failure load as a function of the ratio load height to load eccentricity

The overturning failure loads, defined as before, considering the post-torsional failure response, are plotted relative to the pure lateral loading case in Figure 5-20. For comparison purposes, the results from previous experimental research are included. For sand, when the load height is 5.3 m, the reduction in overturning capacity is close to the values reported in Thiyyakkandi et al. (2016). Their experiments were run with a load height of 6.1 m. For a load height of 10.6m, the reduction for 1 m and 4 m eccentricity coincide with the curve presented in Thiyyakkandi et al. (2016). For larger eccentricities, the trend is significantly different. Results from clays models

(undrained type loading) showed a neglectable reduction for 1 m-eccentricity, and reduction is not seen for larger load eccentricities in these analyses. Notice that a soil model that includes softening could have resulted in a reduction of the overturning capacity. More research should be done in this area.

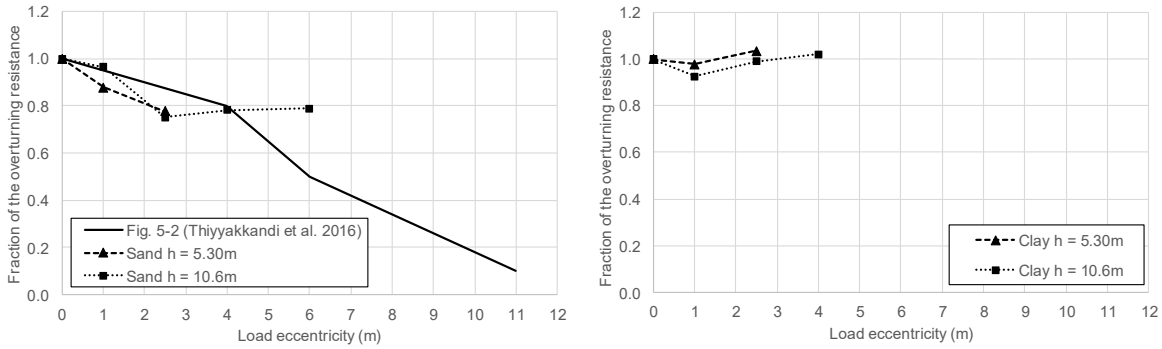

Figure 5-20: Overturning resistance reduction as a function of the load eccentricity

The need for including the lateral-torsional interaction in design practice and in this research project was discussed in a meeting with ALDOT personnel. Considering that, the previous research has not been conclusive, and Florida Department of Transportation has not included these effects in its design requirements, ALDOT has decided not to apply lateral-torsional interaction in their design practice.

The results shown in Figures 5-17 indicate that based on the finite element analyses performed, the failure was always torsional driven first, for large eccentricities. Figure 5-20 shows that for those analyses where the combined lateral-torsional failure mode was found, the reduction in overturning resistance is not as significant as previous research has reported. For 6 m eccentricity, this research found a 20% reduction versus a 50% reduction reported by Herrera (2001) and Hu (2006) based on scaled centrifuge models, see Figure 5-1(a). Figure 5-20 suggests that the need for a design procedure that integrates couple loading could be beneficial for eccentricities less than 6 m. Figure 5-20 shows that the reduction in overturning resistance due to eccentric loading is less than 25%. Therefore, this research team considers that there is still not enough evidence to incorporate lateral-torsional interaction into ALDOT design practice. A comprehensive review of the safety associated with overturning design is recommended. More research, experimental and numerical, is required in order to recommend a design method that includes the effect of combined loading and quantify its importance.

Chapter 6

MAJOR PARAMETERS AND STATISTICAL CHARACTERIZATION

The goal of this section is to identify the relevance of the parameters in the resistance model. This task will be done by performing a sensitivity analysis from a deterministic point of view, and then, a statistical characterization will be done.

6.1 Deterministic Sensitivity Analysis

A deterministic sensitivity analysis was conducted to study the influence of the different parameters involved in calculating the torsional capacity considering the equations for α and β methods. The methodology followed is explained in Aguilar et al. (2016) . All parameters except one were kept fixed at their medium value (i.e., an intermediate point between the maximum and minimum), and the others were varied in a selected range. The range of each parameter involved in the resistance model was assumed from values recommended by ALDOT. For the α method, cohesion (s_u) and geometry *(L/D)* are needed, while for the β method the unit weight (γ) and the geometry *(L/D)* of the pile are the parameters required for calculation.

Figure 6-1 illustrates the results of this analysis, in which the variation of each parameter is drawn against the variation caused in the value of torsional capacity with respect to the value of the torsional capacity obtained by fixing all parameters at their medium value (medium torsional capacity). The parameter variation scale is established in such a way that 0% corresponds to the minimum value of the parameter, 50% to the medium value, and 100% to the maximum value in the range. In Figure 6-1, a horizontal line would mean the parameter has no effect on the torsional capacity. The slope of the line increases with the increasing effect of the parameter.

Therefore, for the α method cohesion and geometry are equally important, while in the β method the geometry is more important than the unit weight of the soil.

The quality of the estimation of the cohesion of the soil (undrained shear strength) based on an SPT is very poor as was discussed in section 2.1. Since cohesion is very important for the torsional capacity prediction, it is recommended that additional testing such as vane shear strength testing be used when cohesive soil controls the design.

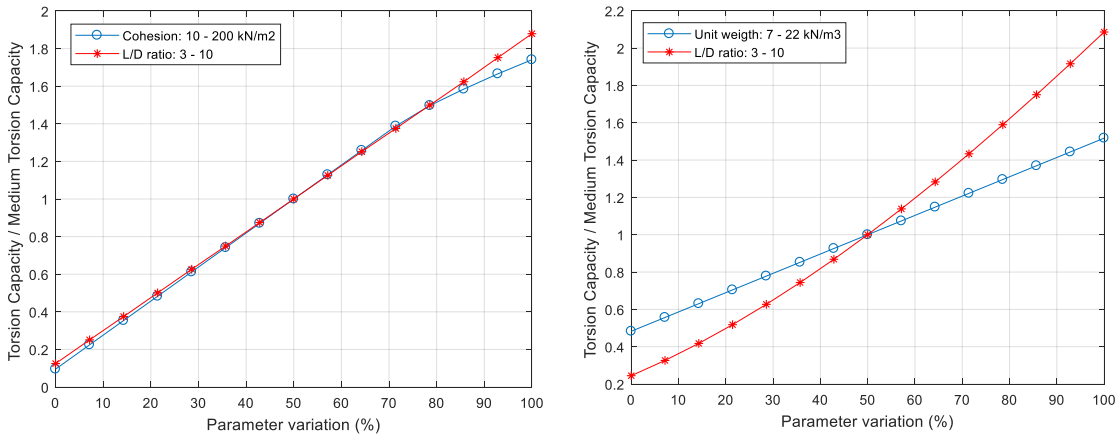

Figure 6-1: Deterministic sensitivity analysis for α and β methods

6.2 Statistical Characterization

Measurement in different soils has suggested considerable variability in soil properties, not only from site to site and stratum to stratum, but even within an apparently homogenous deposit at a single site (Baecher and Christian 2005). Several sources have reported coefficients of variation (COV) as a measurement of the uncertainties in soil design parameters associated with laboratory testing, in-situ testing, and correlations. Duncan (2000), Baecher and Christian (2005) and Huber (2013) have gathered several sources, and the most relevant for this analysis are summarized in following tables. Table 6-1 contains COV associated with geotechnical parameters when measured from laboratory tests. Table 6-2 corresponds to COV of field tests SPT, CPT, and VST. Table 6-3 splits the source of variability into equipment, procedure, and random noise for several common in-situ tests and lists recommended COV for analysis. Table 6-4 contains recommended COV when the undrained shear strength is obtained from different field tests.

Table 6-1: COV of different soil properties

Soil parameter	Lee et al. (1983)* COV (%)	Lacasse and Nadim (1996)* and Lamb (1974)* COV (%)	Duncan (2000) COV (%)
Unit weight (γ)	1 - 10	5 - 10	3 - 7
Undrained shear strength (s_u)	20 - 50	5 - 20	13 - 40

*Taken from Baecher and Christian (2005)

Table 6-2: COV for common field measurements

Test	Soil type	Baecher and Christian (2005) COV (%)	Duncan (2000) COV (%)
Standard Penetration Test (SPT)	Sand and Clay	25 - 50	15 - 45
Cone Penetration Test (CPT)	q_t q_c Clay q_c Sand	<20 20 - 40 20 - 60	MCPT 15 - 37 ECPT 5 - 15
Vane shear test (VST)	Clay	10 - 40	10 - 20

Table 6-3: Uncertainty estimates for five common in-situ tests (Kulhawy and Trautmann 1996)

Test	Coefficient of Variation, COV (%)				
	Equipment	Procedure	Random (noise)	Total*	Range+
Standard Penetration Test (SPT)	5 - 75	5 - 75	12 - 15	14 - 100	15 - 45
Mechanical Cone Penetration Test (MCPT)	5	10 - 15	10 - 15	15 - 22	15 - 25
Electric Cone Penetration Test (ECPT)	3	5	5 - 10	8 - 22	5 - 15
Vane Shear Test (VST)	5	8	10	14	10 - 20
Dilatometer Test (DMT)	5	5	8	11	5 - 15
Pressuremeter Test (PMT)	5	12	10	16	10 - 20
Self-boring Pressuremeter Test (SBPMT)	8	15	8	19	15 - 25

*COV (Total) = $[COV(equipment)+COV(procedure)+COV(random)]^{0.5}$
+Range represent probable magnitudes of field test measurement error

Table 6-4: Guidelines for COV of undrained shear strength based on three common in-situ tests (Huber 2013)

Base Test	s_u COV(%)
Standard Penetration Test (SPT)	40 – 60
Cone Penetration Test (CPT)	15 – 50
Vane shear test (VST)	30 – 40

Based on the statistical information presented on soil parameters and testing, the following COV were selected for use in the reliability analysis:

1) For the unit weight a COV = 10% will be used. In general, geotechnical engineers can estimate this parameter reasonable well.
2) For the undrained shear strength, considering blow-count values are used directly without correct them, and the substantial variability observed in recommendations from different sources (see section 2.1) a COV = 60% will be used.

The statistical information included in this report suggest that, when possible, CPT or VST should be used instead of an SPT. A reduction in the uncertainty will have a significant effect on the final recommended factor of safety.

Chapter 7

RELIABILITY ANALYSIS

The reliability analysis consists in defining a performance function (also called limit state function) that represent the margin of safety, which intuitively is the difference between the resistance *(R)* and the load effect *(Q)*

$$g = R - Q \tag{7.1}$$

in some applications, it is preferred to understand the safety as the ratio resistance-to-load effect, and the limit function is written as

$$g = \frac{R}{Q} - 1 \tag{7.2}$$

in both cases, a negative value of the function *g* means failure (or unsatisfactory performance). *R* and *Q* are random variables, which means they are uncertain, so is *g*. Let continue with the first form presented of *g*, the second form will help the reader to understand Appendix E. The mean (μ) and standard deviation (σ) of *g* relates to the statistics of *R* and *Q* as follows:

$$\mu_g = \mu_R - \mu_Q \tag{7.3}$$

$$\sigma_g^2 = \sigma_R^2 + \sigma_Q^2 - 2\rho_{RQ}\sigma_R\sigma_Q \tag{7.4}$$

where ρ_{RQ} is the correlation between *R* and *Q*. ρ_{RQ} is 1.0 if the variables are fully correlated and 0 if they are independent.

The performance of a given design is measured in terms of the reliability index, β. Which is defined as a function of the probability of failure, P_F

$$\beta = -\Phi^{-1}\left(P_F\right) \tag{7.5}$$

where, Φ^{-1} is the inverse standard normal distribution function. When P_F is normally distributed, and *R* and *Q* are independent, the reliability index can also be expressed as

$$\beta = \frac{\mu_g}{\sigma_g} = \frac{\mu_R - \mu_Q}{\sqrt{\sigma_R^2 + \sigma_Q^2}} \tag{7.6}$$

In this study, since the problem can be represented by two random variables, *Q* (wind load effect) and *R* (torsional resistance), the reliability index is calculated from the closed-form solution. *Q* and *R* are assumed lognormal and independent based on the literature reviewed and performed simulations, respectively. Therefore, the mean and standard deviation of *Q* and *R* are given as shown bellow. For the load effect random variable, *Q*

$$\sigma_{\ln Q}^2 = \ln\left(V_Q^2 + 1\right) \tag{7.7}$$

$$\mu_{\ln Q} = \ln(\mu_Q) - \frac{1}{2}\sigma_{\ln Q}^2 \tag{7.8}$$

for the resistance random variable, *R*

$$\sigma_{\ln R}^2 = \ln\left(V_R^2 + 1\right) \tag{7.9}$$

$$\mu_{\ln R} = \ln(\mu_R) - \frac{1}{2}\sigma_{\ln R}^2 \tag{7.10}$$

then, the reliability index can be expressed as

$$\beta = \frac{\mu_{\ln R} - \mu_{\ln Q}}{\sqrt{\sigma_{\ln R}^2 + \sigma_{\ln Q}^2}} \tag{7.11}$$

7.1 Resistance Model

According Nowak and Collins (2013) the load carrying capacity (the torsional resistance of a drilled shaft) is a function of material characteristics (soil properties), the cross section (shaft diameter) and the dimensions (embedment length). Although in design, these quantities are considered as deterministic, in reality, there is some uncertainty associated with each of them. Therefore, the resistance (*R*) is a random variable.

The possible sources of causes of uncertainty in resistance can be put into three categories: material (M) is the uncertainty in the soil strength properties (unit weight, cohesion); fabrication (F) is uncertainty in the overall dimensions of the drilled shaft (diameter and length); and analysis (P) which is uncertainty resulting from approximate methods of analysis.

Since information on the variability of the resistance of drilled shafts is not available, it is necessary to develop resistance models using available material data (soil data) and numerical simulation. Each category is quantified separately and then combined by assuming that the resistance can be considered as the product of the nominal resistance and three parameters. Each parameter account for one of the described sources of uncertainty

$$R = R_n MFP \tag{7.12}$$

therefore, the bias factor and coefficient of variation can be approximated as follows

$$\lambda_R = \lambda_M \lambda_F \lambda_P \tag{7.13}$$

$$COV_R = \sqrt{COV_M^2 + COV_F^2 + COV_P^2} \tag{7.14}$$

First, the material uncertainty is quantified by using Monte Carlo simulation based on the variability of the corresponding geotechnical parameters. The variability of the relevant parameters was selected in Chapter 6, section 6.2. Results of the simulation for different soil conditions are summarized in Tables 7-1 and 7-2. Details of the simulations are provided in Appendix B. Soil parameters were selected from ALDOT recommendations (see Appendix C).

Table 7-1: Monte Carlo simulation results for several clay conditions

Soil description	Mean soil parameters		Statistics		
	γ (kN/m^3)	s_u (kPa)	λ_M	COV_M	Lower tail distribution
Soft and extremely soft clay	16.5	12	1.00	0.59	Lognormal
Medium to moderately hard	18.1	36	1.00	0.60	Lognormal
Stiff weathered	18.8	72	1.00	0.56	Lognormal
Medium hard to hard, very stiff	19.6	144	0.93	0.57	Lognormal
Moderately hard to hard, hard	20.4	192	0.97	0.54	Lognormal

Table 7-2: Monte Carlo simulation results for several sand conditions

Soil description	Mean soil parameters		Statistics		
	γ (kN/m^3)	N_{spt} (blowcount)	λ_M	COV_M	Lower tail distribution
Loose and very loose sand	17.3	5	0.72	0.12	Lognormal
Medium sand	18.8	20	1.21	0.42	Lognormal
Dense and very dense sand	20.4	40	1.65	0.31	Lognormal

Second, the uncertainty in fabrication is expected to be low. Recommended values for bias factor and coefficient of variation of fabrication factor for reinforced concrete elements varies from 0.92 to 1.10 and 0.025 to 0.040, respectively. It was decided to perform the analysis with $\lambda_F = 1.005$ and $COV_F = 0.040$, based on (Nowak and Collins 2013).

Finally, the professional factor is quantified by comparing predictions and experimental results. Those values are obtained from Chapter 4, section 4.2.3. For α method $\lambda_P = 1.18$ and $COV_P = 0.19$, while the β method will be associated with $\lambda_P = 1.09$ and $COV_P = 0.03$.

Resistance model statistics are obtained by interpreting the material statistics presented in Tables 7-1 and 7-2, including fabrication, and analysis factors. The corresponding statistical parameters for each resistance model are shown in Table 7-3. Both methods will be modeled as lognormally distributed.

Table 7-3: Statistical parameter for resistance model

Method	Stat	Material	Fabrication	Analysis	Resistance Model
α Method	λ	0.98	1.005	1.18	1.16
	COV	0.58	0.040	0.19	0.61
β Method	λ	1.10	1.005	1.09	1.20
	COV	0.28	0.040	0.03	0.28

7.2 Wind Load Model

The load effect in a structure due to wind is a function of many parameters such as the wind speed, wind direction, geometry of the structure, local topography, and so on. The basic wind speeds in ASCE/SEI 7-10 are based on the 3-s gust wind speed map. The non-hurricane wind speed based on peak gust data collected at 485 weather stations where at least 5 years of data were available (J. A. Peterka 1992; Jon A. Peterka and Shahid 1998). For non- hurricane regions, measured gust data were assembled from a number of stations in state-sized areas to decreased sampling error, and the assembled data were fit using a Fisher-Tippett type I extreme value distribution. The hurricane wind speeds in the United States Gulf and Atlantic coast are based on the results of a Monte Carlo simulation model described in Vickery and Wadhera (2003), Vickery et al. (2009a), Vickery et al. (2009b) and Vickery et al. (2009c)

Although, *Alabama Standard Specifications* (ALDOT 2014) establish that all structures shall be designed in accordance with the requirements given in the AASHTO (2009), and the Appendix C is commonly used to determine the wind load. ALDOT plans to update their practice to the LRFD wind load. Therefore, this reliability analysis is done considering the LRFD specification of wind load. AASHTO (2015) required that wind load shall be based on the pressure of the wind acting horizontally on the supports, signs, luminaries, traffic signs, and other attachments computed in accordance with a series wind speed maps, using the appropriate mean recurrence interval (MRI) basic wind speed. The selection of the MRI accounts for the consequences of failure. A typical support could fall across the travelway during a failure creating a hazard for travelers (MRI = 700 yrs). The owner, in this case ALDOT, should specify the ADT and risk category (or directly the MRI). All supports that could cross a lifeline travelway are assigned a high-risk category to consider the consequences of failure (MRI = 1700yrs). Supports that cannot cross the travelway are assigned a low risk and 300 yrs MRI. For service limit states AASHTO (2015) requires the use of an MRI of 10 yrs.

The wind pressure is computed using the following formula,

$$P_z = 0.00256 K_z K_d G V^2 C_d \text{ (psf)} \qquad (7.15)$$

where V is the basic wind speed (mph); K_z is a height and exposure factor; K_d is the directionality factor; G is the gust effect factor; and C_d is the drag coefficient. All the parameters are random variables. The CDFs for the random variables and their recommended statistics are summarized in Table 7-4. Although the probability distributions for V are available, the probability distribution of the wind load (or load effect) is the one of interest for structural reliability calculations. The distribution of wind load is not necessarily type I since the wind pressure is proportional to V^2 instead of V. The wind load effect is commonly assumed as lognormal (Puckett et al. 2014).

Table 7-4: Statistics for wind load parameters (Ellingwood 1981)

Parameter	Mean/nominal	COV	CDF
Exposure factor, K_z	1.0	0.16	Normal
Gust factor, G	1.0	0.11	Normal
Pressure coefficient, C_p	1.0	0.12	Normal

Peak gust wind speeds for the coastal segments were obtained from Puckett et al. (2014). Those are reported in Table 7-5.

Table 7-5: Statistics for wind speed (Puckett et al. 2014)

Mean Recurrence Interval (MRI)	V_{MRI} (mph)	$\lambda_{MRI} = \mu_{MRI} / V_{MRI}$	COV_{MRI}
300 yrs	105 - 170	0.80	0.130
700 yrs	115 - 180	0.80	0.125
1700 yrs	120 - 200	0.80	0.115

Monte Carlo simulations were performed in order to obtain the statistical parameters of the wind load (of wind load effects). However, this led to unreasonable results. Therefore, without a better alternative, the COV for V^2 was assumed as the same that V, while the bias factor for V^2 is the bias factor of V squared. So, now bias factor and COV for the Q distribution can be expressed as

$$\begin{aligned}\lambda_Q &= \lambda_{K_z}\lambda_G\lambda_{C_p}\lambda_{V^2} \\ &= 1.0\cdot 1.0\cdot 1.0\cdot 0.80^2 = 0.64\end{aligned} \tag{7.16}$$

$$\begin{aligned}COV_Q &= \sqrt{COV_{K_z}^2 + COV_G^2 + COV_{C_p}^2 + COV_{V^2}^2} \\ &= \sqrt{0.16^2 + 0.11^2 + 0.12^2 + 0.13^2} = 0.26\end{aligned} \tag{7.17}$$

these statistical parameters are valid for all MRI. The owner should make the decision on the load level considered, but the variability associated with the load will not change.

7.3 Target Reliability Index

The building process in all kinds of projects involves planning, design, manufacturing, transportation, construction, operation/maintenance and demolition. Four major parties can be recognized: the owner/investor, the user, the designer and the contractor. All four parties' desire is to obtain a safe and reliable structure (or geotechnical system for these effects). In addition, the owner's particular interest is also to reduce the costs and maximize profit. Safety and cost are closely related, as the safety level increases the cost also increases. Therefore, the challenge is to define an acceptable level of safety that meets the implicit requirement assigned by the society to protect human life, avoid economic losses and prevent service disruptions, while at the same time keeping the cost in reasonable ranges that allows for infrastructure and economic development. This is a multidisciplinary task. It involves structural safety analysis, economic analysis, and even political decisions (Nowak and Collins 2013).

The acceptable safety margin must be established up front, in order to calibrate load and resistance factors, or in this case, a global factor of safety.

7.3.1 Usual Practice in Safety Management

In geotechnical systems, it is commonly accepted to define the safety margin by specifying a global safety factor. A global factor of safety (FS) approach is relatively simple to use and generally has worked well for many years (Phoon, Kulhawy, and Grigoriu 2003). Through experience, conventions have developed with regard to what values of a factor of safety are suitable for various situations. For example, the U.S. Army Corps of Engineers and many other agencies use FS = 1.5 for the long-term stability of slopes. Most geotechnical engineers use FS = 2.5 to 3.0 for bearing capacity, and the same range of values for safety against erosion and piping (Duncan 2000). Factors of safety between 2.0 and 3.0 are typically considered to be adequate in conventional foundation design (Focht and O'Neill 1985; Phoon, Kulhawy, and Grigoriu 2003). Recommended factors of safety in the FHWA (2001) for different geotechnical designs are listed below:

1) Slope Stability, $1.3 \leq FS \leq 1.5$
2) Foundation Bearing Capacity, $2.0 \leq FS \leq 3.0$
3) Foundation Sliding, $FS \geq 1.5$
4) Foundation Overturning, $FS \geq 2.0$

Factors of safety currently used by other DOTs in torsional design range from 1.0 to 1.5, while ALDOT requires a factor of safety of 2.0.

When designing a foundation or retaining wall, overturning failure is associated with a larger factor of safety than sliding failure, this is explained by the failure consequences. The

torsional failure of a drilled shaft can be seen as similar to a sliding failure in a retaining wall. After the wall slides, a decrease in the earth pressure would be observed, and consequently, the sliding movement would stop. Normally, sliding does not constitute a catastrophic failure. Similarly, during a heavy windstorm that may cause significant twisting in a drilled shaft due to torsion, after the rotation occurs, the wind effect would be reduced, and the twisting would stop.

7.3.2 Probability-based Approach

The same factor of safety can imply a very different safety margin in different cases. A more rational and convenient way to express a safety margin is in terms of a target reliability index (it could also be expressed as a target probability of failure/success).

Reliability index, reliability, and probability of failure references are needed to make a decision on the target level of safety, or target reliability index. Table 7-6 provides the relationship among those concepts.

Table 7-6: Reliability index, reliability, and probability of failure (Nowak 1999)

Reliability Index β	Reliability $S = 1 - P_F$	Probability of failure P_F
0.0	0.500	0.500×10^{0}
0.5	0.691	0.309×10^{0}
1.0	0.841	0.159×10^{0}
1.5	0.933 2	0.668×10^{-1}
2.0	0.977 2	0.228×10^{-1}
2.5	0.993 79	0.621×10^{-2}
3.0	0.998 65	0.135×10^{-2}
3.5	0.999 767	0.233×10^{-3}
4.0	0.999 968 3	0.317×10^{-4}
4.5	0.999 996 60	0.340×10^{-5}
5.0	0.999 999 713	0.287×10^{-6}
5.5	0.999 999 981 0	0.190×10^{-7}
6.0	0.999 999 999 013	0.987×10^{-9}
6.5	0.999 999 999 959 8	0.402×10^{-10}
7.0	0.999 999 999 998 72	0.128×10^{-11}
7.5	0.999 999 999 999 968 1	0.319×10^{-13}
8.0	0.999 999 999 999 999 389	0.611×10^{-15}

Use of this probabilistic approach can be found in the calibration of the ACI-318 Building Code Requirements for Structural Concrete, AASHTO LRFD Bridge Design Specifications and AASHTO LRFD Specifications for structural supports for highway signs, luminaries, and traffic signals, among others.

Although the term “probability of failure” is used extensively in reliability analysis, it needs to be understood that not all failures are disastrous or life-threatening. Some failures are better described as an unsatisfactory performance, i.e., exceed a deflection limit, excessive cracking, excessive vibration, sliding of a retaining wall, exceed a differential settlement threshold. A torsional failure of a drilled shaft actually means excessive twist under torsional loading, which would affect

the functionality of the supported traffic sign. Drivers may not be able to read the information in the sign or see the color of a traffic light. It would not block the highway or hit the traffic as an overturning failure would. Although in design, the torsional load is obtained from an ultimate wind load, the failure is better described as a service failure. Also, in an extreme windstorm event, no traffic should be using the roads, then even a combined type failure does not represent a life-threatening situation. Another point to take into consideration is that ALDOT is not willing to repair excessive rotations after a heavy windstorm.

The next section gathers examples of reliability indices used in the calibration of codes for structural design and instances related to geotechnical engineering. The aim is to provide guidance before selecting a reasonable target reliability index.

7.3.3 Experiences on Reliability-based Design

Representative values of target reliability index (β_T) commonly accepted are β_T approximately 3.5 for strength failure and β_T approximately 2.0 for serviceability failure (Hart 1982). In ACI 318 calibration, reported in Nowak and Szerszen (2003) and Szerszen and Nowak (2003), the target reliability indices for the ultimate limit state were selected equal to 3.5 for beams, 2.5 for slabs and 4.0 for columns. Because of the fact that failure of a column can be more brittle compared to a beam in pure flexure, this failure characteristic is taken into consideration by selecting a higher target reliability index. In AASHTO LRFD Calibration (Nowak 1999), reliability indices were calculated for a wide spectrum of bridges designed according to the AASHTO (1989) as a reference. Thus, the target reliability index for the ultimate limit state for girder bridges was taken as 3.5.

For the particular case of traffic signals and luminaries, NCHRP report 796 outlines the calibration of AASHTO LRFD Specifications for structural supports for highway signs, luminaires and traffic signals (Puckett et al. 2014). The load and resistance factors were calibrated to provide a reliability index of approximately 3.0 for 300-yr MRI, 3 to 3.5 for 700-yr MRI and 3.5 to 4.0 for 1700-yr MRI for main members. In general, the foundation systems that are supporting superstructures should have a consistent β_T.

AASHTO (2015) establish that the MRI should account for the consequences of failure and assign the responsibility to specify the average daily traffic (ADT) and risk category to the owner. Table 7-7 is recommended for selecting the appropriate MRI for wind speed. As a point of comparison, design of roadside sign support is based on a 10 yrs MRI.

Table 7-7: Mean recurrence interval for wind speed as a function of the risk category and the average daily traffic (AASHTO 2015)

	Risk Category		
Traffic Volume	**Typical**	**High**	**Low**
ADT ≤ 100	300	1700	300
100 ≤ ADT ≤ 1000	700	1700	300
1000 ≤ ADT ≤ 10,000	700	1700	300
ADT ≥ 10,000	1700	1700	300

Typical : Failure could cross travelway
High : Support failure could stop a lifeline travelway
Low : Support failure could not cross travelway

Phoon, Kulhawy, and Grigoriu (2003) explain that the reliability indices for most geotechnical components and systems lie between 1.0 and 5.0 (see Table 7-8). A target reliability index of 3.0 is widely used in probabilistic stability analysis of geotechnical structures (Kim and Salgado 2009).

Table 7-8: Relationship between reliability index (β) and probability of failure (p_f) from US Army Corps of Engineers 1997 (Phoon, Kulhawy, and Grigoriu 2003)

Reliability index β	Probability of failure $p_f = \Phi(-\beta)$	Expected performance level
1.0	0.16	Hazardous
1.5	0.07	Unsatisfactory
2.0	0.023	Poor
2.5	0.006	Below average
3.0	0.001	Above average
4.0	0.00003	Good
5.0	0.0000003	High

Note: $\Phi(\cdot)$ = standard normal probability distribution.

Target reliability indices associated with conventional design practices in geotechnical engineering of various types of foundation elements have been determined by Barker et al. (1991), i.e., 3.0-3.5 for spread footing and 2.5-3.0 for drilled shafts. Due to the redundancy of pile groups, AASHTO and FHWA, in agreement with Barker et al. (1991), recommend β_T from 2.0 to 2.5 for a single pile in a group of piles (Michael McVay et al. 2002).

Based on an annual probability of failure and consequence of failure, Phoon (2003) delimit the currently accepted theoretical probability of failure for foundations is between 0.01% and 0.1% (or β between 3.1 and 3.7). Nevertheless, for projects with low consequence of failure or short duration a lower target reliability index may be justifiable.

The axial capacity of driven piles has been studied by several authors. Different values of β have been reported. Meyerhof (1970) suggested the reliability index should lie between 3.0 and 3.6. Tang et al. (1990) reported that β for offshore piles ranges from 1.4 to 3.0. A reliability index of

2.5 was obtained for Meyerhof's SPT method when using a factor of safety 3.5 (FHWA, 2001). Values of reliability indices for other commonly used methods (e.g., α, β, λ, and CPT) of predicting the axial resistance of driven piles were calculated and were found to be between about 1.5 and 3.0 (Barker et al., 1991).

In FHWA manual (2001), different values of target reliability indices were used in the development of load and resistance factors for mechanically stabilized earth retaining walls, considering different levels of importance (β_T = 2.0, 2.5, 3.0, and 3.5).

The target reliability indices for circular tunnel designed according to the tunnel manual report FHWA-NHI-10-034 (2009) are 4.75, 3.5 and 5.0 for flexure, shear, and compression ultimate limit states, respectively (Ghasemi 2017; Nowak and Ghasemi 2014).

An extensive reliability study of relevant design experience related to foundations for transmission line structures was carried out by Phoon, Kulhawy, and Grigoriu (1995). The findings showed that an average target reliability index between 2.9 and 3.2 is applicable for a variety of common loading modes (Table 7-9). Adjusting for empirical rates of failure and the lower bound target reliability indices from the structural design of transmission lines, Phoon et al. (2003) recommended a target reliability index of 3.2 for foundations for transmissions line structures (spread footing and drilled shafts).

Table 7-9: Reliability indices implicit in existing foundation designs for transmission line structures (Phoon, Kulhawy, and Grigoriu 1995)

Foundation	Loading mode	Type of analysis	Range of β	Average β
Spread footing	Uplift	Undrained	2.6–3.7	3.15
		Drained	2.3–3.5	2.90
Drilled shaft	Uplift	Undrained	2.8–3.6	3.20
		Drained	2.4–3.6	3.00
	Compression	Undrained	2.7–3.6	3.20
		Drained	2.4–3.5	3.00
	Lateral-moment	Undrained	2.2–3.6	2.90
		Drained	2.5–3.5	3.00

Other examples of reliability indices can be found in the assessment of existing structures. ISO 31822 (2012) and the Dutch standard (NEN 8700 2009) indicate target reliability levels for ultimate limit states for different consequences of failure (see Table 7-10).

Table 7-10: Reliability indices recommended for assessment of existing structures for a reference period of 50 yrs

Failure consequences	ISO 13822 (2012)	NEN 8700 (2009)
Small	2.3	1.8
Some	3.1	
Moderate	3.8	2.5
High	4.3	3.3

For service limit states, ISO 13822 (2012) recommends target reliability index of 0.0 for reversible failure and 1.5 irreversible failure. Accordingly, Ghasemi and Nowak (2016) found the intended reliability index of steel girders in bridges concerning deflection criteria (SLS) is close to 0.10.

7.3.4 Analyzing a Similar Case: Sliding Failure of a Retaining Wall

The reliability indices of a sliding failure were calculated for retaining walls with cohesive and cohesionless backfill soil, separately. A typical factor of safety of 1.50 was applied in the design procedure. Details of the reliability indices calculations are provided in Appendix E.

The reliability indices obtained were β approximately 1.0 - 1.1 for cohesive soil (p_f = 0.159 - 0.136), and β approximately 2.1 - 2.2 for cohesionless soil (p_f = 0.018 - 0.014). The obtained results are a clear example of that the same factor of safety can imply different safety margins. In this case, the difference is one order of magnitude in the probability of failure.

7.3.5 Selecting a Target Reliability Index

As a conclusion from the reviewed usual practice related to safety in structural and geotechnical engineering, the following can be said:

1) A common approach when probabilistic methods are applied to structural or geotechnical design is to calibrate the factors so the results, on average, are in agreement with existing practice. Since the current practice for designing drilled shafts is consider overly-conservative, this approach is not very helpful in this research. However, comparing with similar geotechnical designs is relevant.
2) Phoon et al. (2003) recommended a target reliability index of 3.2 for foundations for transmissions line structures. Consequences of failure of transmission lines and traffic signals can be compared in order to define the target reliability for the ultimate limit state.
3) In general, the foundation system should have the same reliability index that the structure that is supporting. Thus, considering the work done by Puckett et al. (2014) the reliability index should be at least 3.5, for the ultimate limit state.

4) A torsional failure is not a life-threatening type of failure; therefore, the ultimate limit state is not included in this research. A torsional failure is better described as an unsatisfactory performance. Hence, the target reliability index for torsional design should be lower than those described in points 2) and 3).
5) Considering the recommendation of ISO 13822 (2012), a reliability index close to 1.5 should be used since the failure could be characterized as a service limit state with irreversible failure, such as the case of a drilled shaft excessive rotation.
6) Because of the similarities in failure consequences, the reliability index should be similar to the one used for sliding design of a retaining wall ($1.0 \leq \beta \leq 2.1$).

Therefore, a reasonable range for target reliability index for designing drilled shafts against torsion could be $1.5 \leq \beta_T \leq 2.0$. This range will be later modified, after consideration for ALDOT feedback.

7.4 Calibration of Factor of Safety

Recalling the limit state function, *g*

$$g = R - Q \tag{7.1}$$

for an Allowable Stress Design philosophy, all the uncertainties are lumped into a factor of safety, FS. Let's say the nominal value of the load effect, Q_n, is known. Thus, the nominal value of the resistance would be specified as $R_n = FS\,Q_n$. The mean and the standard deviation for the distributions can be calculated as follows

$$\mu_Q = \lambda_Q Q_n \tag{7.18}$$

$$\sigma_Q = COV_Q \mu_Q = COV_Q \lambda_Q Q_n \tag{7.19}$$

$$\mu_R = \lambda_R R_n = \lambda_R FS\,Q_n \tag{7.20}$$

$$\sigma_R = COV_R \mu_R = COV_R \lambda_R FS\,Q_n \tag{7.21}$$

recalling Equation (7.11) for reliability index, and writing it as a function of the equivalent normal statistical parameters we obtain:

$$\beta = \frac{\ln\left(\frac{\mu_R}{\mu_Q}\sqrt{\frac{1+COV_Q^2}{1+COV_R^2}}\right)}{\sqrt{\ln\left[\left(1+COV_Q^2\right)\left(1+COV_R^2\right)\right]}} \tag{7.22}$$

replacing the mean value for (7.18) and (7.20) in (7.22)

$$\beta = \frac{\ln\left(\frac{\lambda_R FS\, Q_n}{\lambda_Q Q_n}\sqrt{\frac{1+COV_Q^2}{1+COV_R^2}}\right)}{\sqrt{\ln\left[\left(1+COV_Q^2\right)\left(1+COV_R^2\right)\right]}}$$

canceling Q_n, we find Equation (7.23)

$$\beta = \frac{\ln\left(FS\frac{\lambda_R}{\lambda_Q}\sqrt{\frac{1+COV_Q^2}{1+COV_R^2}}\right)}{\sqrt{\ln\left[\left(1+COV_Q^2\right)\left(1+COV_R^2\right)\right]}} \tag{7.23}$$

this last expression depends only on the factor of safety, FS, and known statistical information. For our purpose, an expression to obtain FS based on a selected reliability index (β_T) is useful:

$$FS = e^{\beta_T\sqrt{\ln\left[\left(1+COV_Q^2\right)\left(1+COV_R^2\right)\right]} - \ln\left(\frac{\lambda_R}{\lambda_Q}\sqrt{\frac{1+COV_Q^2}{1+COV_R^2}}\right)} \tag{7.24}$$

Figure 7-1 shows the required factor of safety to obtain a specified target reliability index. Rounded results are presented tabulated for relevant target reliability indices in Table 7-11.

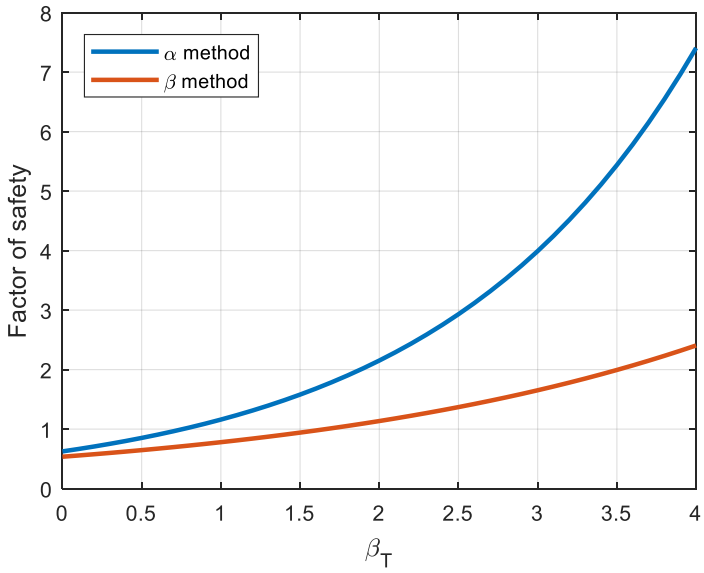

Figure 7-1: Required factor of safety vs. target reliability index

Table 7-11: Calibration of factors of safety

Target Reliability Index β_T	**FS required for α method FS_α (CLAY)**	**FS required for β method FS_β (SAND)**
1.0	1.15	0.80
1.5	**1.60**	**0.95**
2.0	**2.15**	**1.15**
2.5	2.90	1.40
3.0	4.00	1.65
3.5	5.45	2.00

Considering the target reliability index in the range 1.50 to 2.0, a factor of safety of 1.10 is appropriated for soil strength that can be considered as fully drained (sand). However, it is too low if the strength of the soil corresponds to an undrained condition (clay). A factor of safety of 1.30 is more than needed for cohesionless soils, but it is still low for a cohesive soil. A factor of safety of 1.60 is too high for sand, while meets the minimum value of the selected range for reliability index.

The final decision on the safety margin would be made by the owner. Nonetheless, this research suggests aiming for a reliability index between 1.5 and 2.0. These reliability indices correspond to probability of failure of 0.0228 to 0.0668, when the design wind pressure acts on the sign. That would a factor of safety of 1.0 to 1.15 for sands, and a factor of safety of 1.60 to 2.15 for clays.

This research team considers the following factors of safety for torsionally loaded drilled shafts as reasonable to use: a factor of safety of 1.10 for cohesionless soils when the β method is used for calculating the torsional resistance; and a factor of safety of 1.60 for cohesive soils when the α method is used for calculating the torsional resistance.

7.5 A Recommendation for Layered Soils

The goal of this section is to recommend the factor of safety for when the soil consists of layers of different soil types (or strengths) for a target reliability index in the range of 1.5 to 2.0.

First, let us define the torsional resistance contributed by the cohesive (clay) layers calculated using the α method as T_α, and the contribution of the cohesionless (sand) layers calculated using the β method as T_β. Then, the ratio sand-to-clay contribution can be calculated as

$$r_{\beta/\alpha} = \frac{T_\beta}{T_\alpha} \tag{7.25}$$

The reliability indices for ratios of sand-to-clay contributions in the range 0.01 to 100 were calculated using Monte Carlo simulation for various factors of safety (see Figure 7-2).

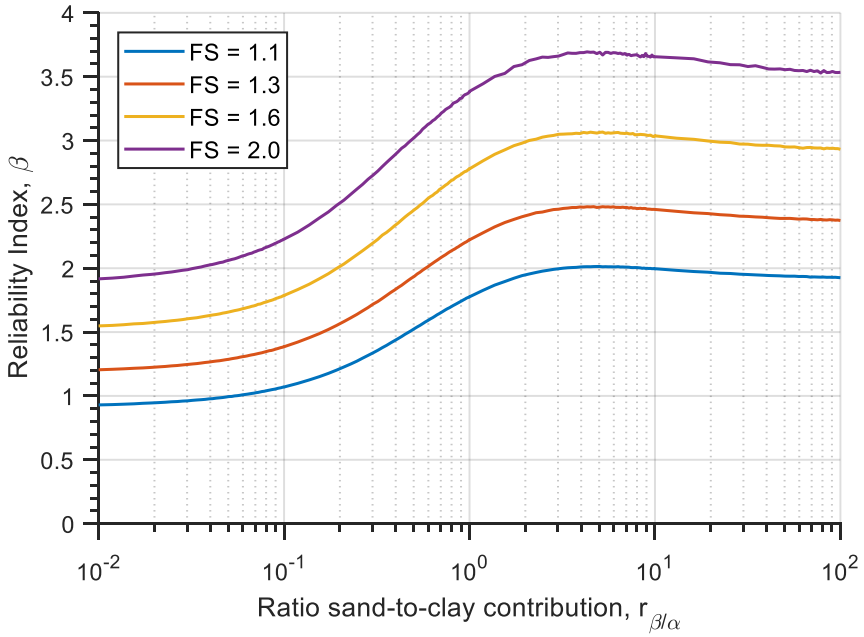

Figure 7-2: Reliability index vs. contribution ratio for various factors of safety

It seems reasonable to define a FS in a piecewise form. A factor of safety of 1.60 when the resistance is dominated by the clay contribution, and a factor of safety of 1.10 when the contribution of the sand layers dominate. See definition of piecewise factor of safety in Equation (7.26).

$$FS_{piecewise} = \begin{cases} 1.60 & if\ r_{\beta/\alpha} = \dfrac{T_\beta}{T_\alpha} < 1.0 \\ 1.10 & otherwise \end{cases} \tag{7.26}$$

The reliability indices obtained for different sand-to-clay contribution ratios are plotted in Figure 7-3, and for comparison purposes, reliability indices from the previous calculations with a factor of safety of 1.30 and 2.0 are also included.

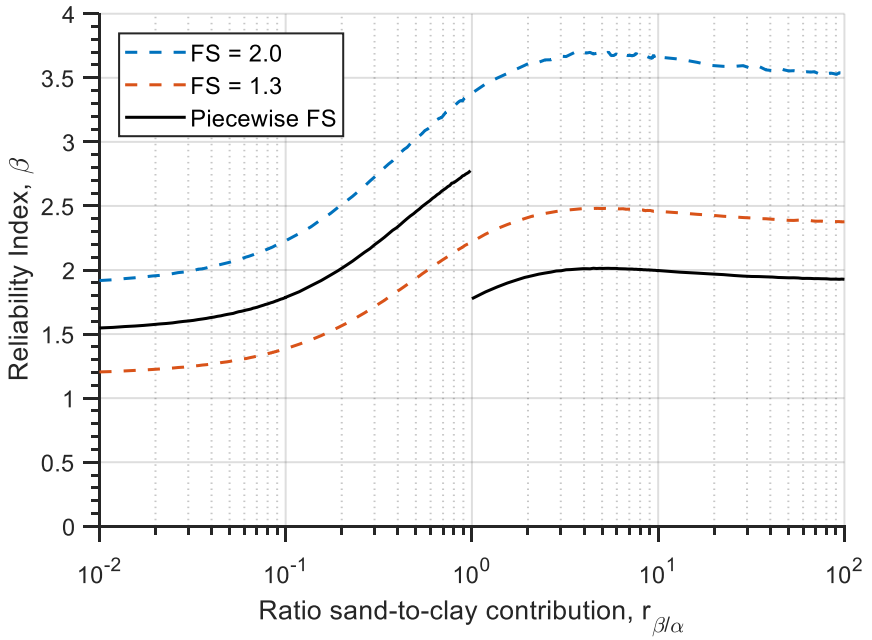

Figure 7-3: Comparison of reliability indices obtained from different factor of safety alternatives for layered soils

Figure 7-3 shows that a factor of safety of 1.30 results in reliability indices that range from 1.20 to 2.50. Factor of safety equal to 1.30 gives reliability indices below 1.50 for low values of $r_{\beta/\alpha}$ (clay dominated).

The piecewise definition of factor of safety for layered soils leads to reliability indices within the range of 1.5 to 2.0 in almost the whole domain, except for $0.2 \leq r_{\beta/\alpha} \leq 1.0$ where it provides conservative designs. This piecewise definition of the factor of safety is recommended for designing drilled shaft foundations for torsional loading when failure for this limit state is considered irreversible.

7.6 Input and Feedback from ALDOT

Providing safety in systems such as the foundations considered here has an economic cost. So, it is important that owners make a decision regarding the appropriate factor of safety that considers both the costs of being overly conservative and the consequences of failure. To this end, two meetings were held between the research team and ALDOT engineers. The first meeting was at an early stage of the project, and the level of risk that ALDOT is willing to accept was discussed qualitatively, as well as, the feasibility of repairing mast arm supports in case of a torsional failure. At that early stage, the goal was that there was no desire to risk torsional failure even during a hurricane. Also, the research team was asked whether FS = 1.10 or FS = 1.30 would be appropriate. ALDOT had already determined that using those factors of safety would eliminate the need for wings or complex foundations from ongoing construction projects.

The second meeting with ALDOT engineers was held after a draft of the project report was submitted to the ALDOT. Hence, the group involved in the discussion was familiar with the considerations made throughout the assessment, and the assumptions used for selecting the target reliability index. For instance: 1) if a torsional failure occurs, it will happen without traffic on the roads. 2) The only time when a failed (in torsion) drilled shaft could be dangerous for drivers is during the post-storm period. In the immediate post-storm period traffic is coming back to regular use, and the affected traffic signals or traffic lights are not functioning correctly. 3) Large rotations of the foundations are improbable during a single storm event because of the very long duration of wind from a single direction that would be required. And, 4) A torsional failure of a drilled shaft foundation is irreversible.

At the second meeting, different alternatives to adjust signal heads if the drilled shaft foundations rotate were discussed by ALDOT engineers. They described the possibilities of carrying out adjustments or modification if needed, so the failed traffic signals (foundation rotation) can keep performing their functions. Consequently, a torsional failure of the foundation should not be considered fully irreversibly. The discussion led to a modification of the target reliability index. The target reliability index range selected initially having in mind the consequences of an irreversible type failure ($1.5 \leq \beta_T \leq 2.0$), was modified to $1.2 \leq \beta_T \leq 2.0$. The new lower bound of the range is smaller than the ISO 13822 recommendation, yet higher than the expected reliability of retaining walls with cohesive back-soil for sliding failure.

In clay soils, a factor of safety of 1.30 is large enough to achieve a reliability index of 1.20. A target reliability index of 1.20 implies about a 10% probability of failure. Therefore, if the design wind speed occurs, 10% of the signs subjected to that full design wind could experience a torsional failure. This level of risk was considered tolerable by ALDOT engineers that attended the meeting. Also, the geotechnical engineers in the meeting expressed their opinion that a factor of safety of 1.30 in clays might still be more conservative than expected. The factor of safety of 1.10

recommended for sand was well received. All agreed in that the β method and the geotechnical properties inferred from an SPT provide enough conservatism when dealing with sand soils.

The final recommendation for the factor of safety is provided in equation (7.27),

$$FS_{piecewise} = \begin{cases} 1.30 & if\ r_{\beta/\alpha} = \dfrac{T_\beta}{T_\alpha} < 1.0 \\ 1.10 & otherwise \end{cases} \tag{7.27}$$

where T_β is the torsional resistance provided by all the cohesionless layers in the soil profile; and T_α is the torsional resistance provided by all the cohesive layers in the soil profile;

Figure 7-4 shows the reliability indices obtained with the application of this recommendation, and for comparison purposes, the reliability indices from the application of FS = 2.0 (current practice) and FS = 1.3 are also included.

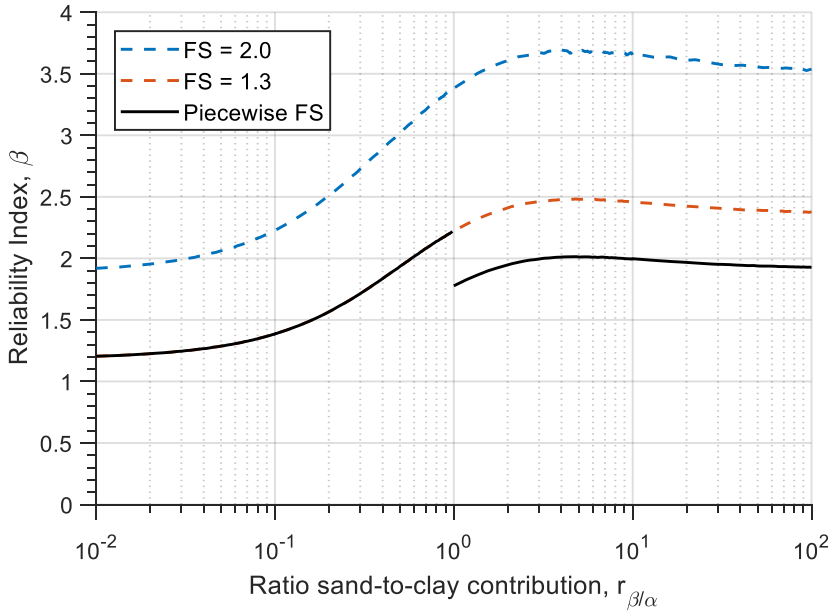

Figure 7-4: Comparison of reliability indices obtained from recommended factors of safety for layered soils, current ALDOT practice, and constant FS = 1.30

A summary with the final recommendations of this research is presented in Table 7-12,

Table 7-12: Recommended factor of safety against torsion for use with α and β methods

Soil condition	Recommended factor of safety
Uniform layer of cohesive soil	1.30
Uniform layer of cohesionless soil	1.10
Layered soils with $T_\beta < T_\alpha$ (torsional resistance dominated by cohesive layers)	1.30
Layered soils with $T_\beta \geq T_\alpha$ (torsional resistance dominated by cohesionless layers)	1.10

where T_β is the torsional resistance provided by all the cohesionless layers in the soil profile; and T_α is the torsional resistance provided by all the cohesive layers in the soil profile.

Chapter 8

CONCLUSIONS AND SUGGESTED RESEARCH

8.1 Conclusions

Drilled shaft foundations are commonly selected by public transportation agencies to support mast-arm traffic sign and signal pole structures. *Alabama Standard Specifications* (ALDOT 2018) requires the foundation design be sufficient to provide a minimum factor of safety of 2.0 against overturning and torsion induced displacements. The requirement related to torsional displacement has resulted in the increased size of drilled shaft foundations and in some cases the need for wings on the foundations to provide the specified resistance to torsion. The design for overturning is performed by imposing a displacement limit of 0.5 in. at the ground level when design wind load acts. Soil properties for performing those designs are provided by ALDOT based on uncorrected standard penetration test. Although drilled shafts are widely used, there is not a standard to helps engineers to design for torsional loading. Furthermore, the resistance mechanism against torsional loads is not well understood, and the existing design methods have been validated against only limited experimental data. There is a need for experimental information regarding the torsional behavior of drilled shafts, primarily to investigate how the torsional load is transferred from the shaft to the soil, torque-rotation response, and lateral-torsion interaction. This would allow researchers to improve current methods of predicting torsional capacity, making the design of torsionally loaded shafts more rational and accurate, and allowing for proper management of safety margin. Numerical research on the topic is also recommended.

For ALDOT projects, the torsional resistance of a drilled shaft is approximated based on the skin friction approach (α and β methods). This study reviewed several methods for calculating the torsional resistance of drilled shafts along with the available test data. Cohesive, cohesionless, and layered soils were included in the analysis. It is not clear which is the best method to predict the torsional capacity of drilled shafts. None of the available methods were found to accurately predict the distribution of the shear stress along the length of the shafts. The α and β, and CDOT methods were able to predict the torsional resistance reasonably well. The α and β methods are well known for their use to determine the axial capacity of piles, and consequently that approach was followed and recommended to design against torsion.

The interaction between torque and overturning resistance is not currently considered in analysis or design. The possibility of including the interaction in this research project was dismissed by ALDOT authorities because of lack of definitive research on that matter. Nevertheless, the influence of torque on the overturning capacity of short piles was studied using finite element analysis to contribute to the understanding of the phenomenon. The response under an

eccentrically applied lateral load of a mast-arm assembly supported by a short drilled shaft was simulated using ABAQUS/Standard (Hibbitt, Karlsson, and Sorensen 2001). Two loading conditions and five eccentricities were considered. The results of the analyses suggest that the torsional resistance is enhanced when combined loading is applied. The eccentricity of the lateral loads decreases the overturning resistance in sand. No significant reduction in the overturning resistance was observed for the clay soil. The lateral-torsional failure mode was observed in some of the models. This failure mode is characterized by an initial torsional failure followed by overturning failure at a very large angle of rotation that is probably not realistic for a single storm event. There is not enough evidence to incorporate this phenomenon in the ALDOT design provisions, and more research in this area is highly recommended.

Wind provisions from Appendix C in AASHTO (2009) are currently used by ALDOT designers and consultants. These provisions were compared to the methods for calculating wind pressure in AASHTO (2009) and AASHTO (2015). Significant differences were found in the design wind pressure. Guidance to help engineers in the transition from the former wind provision to the current one could be beneficial.

The torsional failure of a drilled shaft foundation was initially considered as a service limit state with irreversible consequences which do not represent a life-threat nor significant economic losses. ALDOT input indicated that the consequences of torsional displacement of the foundations are not truly irreversible. A range of target reliability index for drilled shaft foundations supporting traffic signs was selected based on literature and comparison to other design codes and practices with consideration for the qualitative input from ALDOT. A reliability analysis was performed, which showed that a factor of safety of 2.0 is unnecessarily high, especially when the soil strength comes from fully drained loading behavior (cohesionless soil). The final decision on the safety margin will be made by ALDOT. This research indicates that a factor of safety of 1.10 for sands, and a factor of safety of 1.30 for clays are large enough to obtain a reliability index within the range 1.2 to 2.0, which is considered adequate for this kind of structure and the consequences of failure that can be expected. When the soil conditions correspond to a layered mixed soil, and the contribution of the sand layers is less than the contribution of the clay layers, then use a factor of safety of 1.30 (clay dominated). A factor of safety of 1.10 is recommended for sand and layered soils where the sand contribution dominates the torsional resistance. Lower factor of safety can be justified if more in-situ or lab tests are performed to narrow down the uncertainties in the geotechnical parameters. A summary of the recommended factor of safety are provided in Table 7-12.

8.2 Suggested Research

The torsional design of drilled shaft foundations was assessed in this research project. The margin of safety for torsion was studied and selected by means of a target reliability index range. In today's practice, there are two alternatives for designing drilled shaft foundations for overturning loading allowed by ALDOT: Brom's method and p-y analysis. The margin of safety associated with those design procedures is unknown. It is recommended that a study similar to the one presented in this report be performed to analyze the reliability obtained from the use of these typical design methods.

In general, the failure of a drilled shaft support does not represent a life-threatening condition, even in the unlikely event of overturning failure or combined overturning-torsional failure occurs during a severe windstorm, because no traffic should be using the roads in such weather. Nevertheless, the after storm condition of the signals may represent some hazard for drivers.

A torsional failure is an excessive rotation of the shaft foundation, which could imply that the drivers are not able to read the sign or see the color of a traffic signal. A common response of drivers, in that case, is to decrease the speed while approaching the signal. Therefore, the selection of a target reliability index range consistent with a serviceability limit state is justified. In contrast, an overturning type failure could have much more severe consequences. For traffic signals with long arms, small displacements or tilting angles would cause the traffic signals to interfere with the traffic on the road. The clearance is often overestimated by the naked eye, and this could end in an accident that is hazardous for drivers and eventually for pedestrians. Long arms traffic signals are used in wide roads; those are in general important and busy. Thus, careful attention is needed for these structures. It is recommended that overturning failure be considered as an ultimate limit state and aim for a reliability index according to the risk category defined in AASHTO (2015), similar to those reported in Puckett et al. (2014).

The issue of the coupled action of torsion and overturning was reviewed, the existing research was described, and finite element modeling was performed. Nevertheless, more research is needed in this area for understanding the phenomenon of lateral-torsional interaction. A design procedure that considers the coupled action would be beneficial when the torsional load controls the drilled shaft size, and it would help for better quantification of the safety when overturning loading controls.

REFERENCES

AASHTO. 1994. *Standard Specifications for Structural Supports for Highway Signs, Luminaires and Traffic Signals*. 3rd ed. Washington, DC: American Association of State Highway and Transportation Officials.

———. 2009. *Standard Specifications for Structural Supports for Highway Signs, Luminaires and Traffic Signals*. 5th ed. Washington, DC: American Association of State Highway and Transportation Officials.

———. 2012. *LRFD Bridge Design Specifications*. Washington DC: American Association of State Highway Transportation Officials.

———. 2015. *LRFD Specifications for Structural Supports for Highway Signs, Luminaires and Traffic Signals*. 1st ed. Washington, DC: American Association of State Highway and Transportation Officials.

ABAQUS. 2010. "Abaqus Analysis User's Manual (6.10)." 2010. https://www.sharcnet.ca/Software/Abaqus610/Documentation/docs/v6.10/books/usb/default.htm?startat=pt05ch20s03abm29.html#usb-mat-cdruckerprager.

ACI Committee. 2014. "Building Code Requirements for Structural Concrete:(ACI 318-99); and Commentary (ACI 318-14). American Concrete Institute." 2014.

Aguilar, V, C Sandoval, Jose M. Adam, J Garzón-Roca, and G Valdebenito. 2016. "Prediction of the Shear Strength of Reinforced Masonry Walls Using a Large Experimental Database and Artificial Neural Networks." *Structure and Infrastructure Engineering* 12 (12): 1661–1674.

ALDOT. 2002. *Standard Specifications for Highway Construction*. Montgomery, AL: Alabama Department of Transportation.

———. 2006. *Standard Specifications for Highway Construction*. Montgomery, AL: Alabama Department of Transportation.

———. 2008. *Standard Specifications for Highway Construction*. Montgomery, AL: Alabama Department of Transportation.

———. 2012. *Standard Specifications for Highway Construction*. Montgomery, AL: Alabama Department of Transportation.

———. 2013. "Special Provision No. 12-0737. Structures for Traffic Control Devices and Highway Lighting." Alabama Department of Transportation. Obsolete.

———. 2014. "Special Provision No. 12-0737(2). Structures for Traffic Control Devices and Highway Lighting." Alabama Department of Transportation.

———. 2018. *Standard Specifications for Highway Construcction*. 2018th ed. Montgomery: Alabama Department of Transportation.

Baecher, Gregory B., and John T. Christian. 2005. *Reliability and Statistics in Geotechnical Engineering*. John Wiley & Sons.

Barker, Richard M., J. M. Duncan, K. B. Rojiani, P. S. K. Ooi, C. K. Tan, and S. G. Kim. 1991. "Manuals for the Design of Bridge Foundations: Shallow Foundations; Driven Piles; Retaining Walls and Abutments; Drilled Shafts; Estimating Tolerable Movements; Load Factor Design Specifications; and Commentary."

Basack, Sudip, and Sankhasubhra Sen. 2014. "Numerical Solution of Single Piles Subjected to Pure Torsion." *Journal of Geotechnical and Geoenvironmental Engineering* 140 (1): 74–90.

Bowles, L. E. 1996. *Foundation Analysis and Design*. McGraw-hill.

Broms, Bengt B. 1964a. "Lateral Resistance of Pile in Cohesionless Soils." *Journal of the Soil Mechanics and Foundations Division* 90 (3): 123–58.

———. 1964b. "Lateral Resistance of Piles in Cohesive Soils." *Journal of the Soil Mechanics and Foundations Division* 90 (2): 27–64.

Brown, Dan A., John P. Turner, and Raymond J. Castelli. 2010. *Drilled Shafts: Construction Procedures and LRFD Design Methods*. US Department of Transportation, Federal Highway Administration.

Chen, S. L., L. G. Kong, and Li Min Zhang. 2016. "Analysis of Pile Groups Subjected to Torsional Loading." *Computers and Geotechnics* 71: 115–123.

Chow, Yean K. 1985. “Torsional Response of Piles in Nonhomogeneous Soil.” *Journal of Geotechnical Engineering* 111 (7): 942–947.
Das, Braja M. 2010. *Principles of Foundation Engineering*. 7th ed. Cengage learning.
Doherty, J. P., and A. J. Deeks. 2003. “Elastic Response of Circular Footings Embedded in a Non-Homogeneous Half-Space.” *Géotechnique* 53 (8): 703–714.
Duncan, J. Michael. 2000. “Factors of Safety and Reliability in Geotechnical Engineering.” *Journal of Geotechnical and Geoenvironmental Engineering* 126 (4): 307–316.
Ellingwood, Bruce. 1981. “Wind and Snow Load Statistics for Probabilistic Design.” *Journal of the Structural Division* 107 (7): 1345–1350.
FDOT. 2012. “FDOT Modifications to Standard Specifications for Structural Supports for Highway Signs, Luminaires and Traffic Signals (LTS-5).” FDOT Structures manual.
———. 2016. *Drilled Shaft Foundation for Sign & Signal Structures* (version 2.0.5). MathCAD. FDOT. http://www.fdot.gov/structures/proglib.shtm.
———. 2017. “FDOT Modifications to LRFD Specifications for Structural Supports for Highway Signs, Luminaires and Traffic Signals (LRFDLTS-1).” FDOT Structures manual.
FHWA. 2001. “Load and Resistance Factor Design for Highway Bridge Substructures.” Publication No. FHWA HI-98-032. Federal Highway Administration. US Department of Transportation.
Focht, J. A., and M. W. O’Neill. 1985. “Piles and Other Deep Foundations.” In *Publication of: Balkema (AA)*. San Francisco.
Georgiadis, Michael. 1987. “Interaction between Torsional and Axial Pile Responses.” *International Journal for Numerical and Analytical Methods in Geomechanics* 11 (6): 645–650.
Georgiadis, Michael, and Sofia Saflekou. 1990. “Piles under Axial and Torsional Loads.” *Computers and Geotechnics* 9 (4): 291–305.
Ghasemi, S. Hooman. 2017. “Load Resistant Factor Calibration for Tunnel.” In . Korea.
Ghasemi, Seyed Hooman, and Andrzej S. Nowak. 2016. “Reliability Analysis for Serviceability Limit State of Bridges Concerning Deflection Criteria.” *Structural Engineering International* 26 (2): 168–175.
Guo, Wei Dong, Y. K. Chow, and Mark F. Randolph. 2007. “Torsional Piles in Two-Layered Nonhomogeneous Soil.” *International Journal of Geomechanics* 7 (6): 410–422.
Guo, Wei Dong, and Mark F. Randolph. 1996. “Torsional Piles in Non-Homogeneous Media.” *Computers and Geotechnics* 19 (4): 265–287.
Hache, R. A. G., and A. J. Valsangkar. 1988. “Torsional Resistance of Single Pile in Layered Soil.” *Journal of Geotechnical Engineering* 114 (2): 216–220.
Hart, Gary C. 1982. *Uncertainty Analysis, Loads, and Safety in Structural Engineering*. Prentice Hall.
Helwany, Sam. 2007. *Applied Soil Mechanics with ABAQUS Applications*. John Wiley & Sons.
Herrera, Rodrigo. 2001. “Determine Optimum Depths of Drilled Shafts Subjected to Combined Torsion and Lateral Loads Using the Centrifuge.” Master’s thesis, University of Florida, Gainesville, Fla.
Hibbitt, Karlsson, and Sorensen. 2001. *ABAQUS/Standard User’s Manual*. Vol. 1. Hibbitt, Karlsson & Sorensen.
Hu, Zhihong. 2003. “Determining the Optimum Depth of Drilled Shafts Subject to Combined Torsion and Lateral Loads in Saturated Sand from Centrifuge Testing.” University of Florida Gainesville, FL, USA. http://purl.fcla.edu/fcla/etd/UFE0002722.
Hu, Zhihong, Michael McVay, David Bloomquist, Rodrigo Herrera, and Peter Lai. 2006. “Influence of Torque on Lateral Capacity of Drilled Shafts in Sands.” *Journal of Geotechnical and Geoenvironmental Engineering* 132 (4): 456–464.
Huber, Maximilian. 2013. *Soil Variability and Its Consequences in Geotechnical Engineering*. Inst. f. Geotechnik.
ISO 13822, CSN. 2012. “Bases for Design of Structures-Assessment of Existing Structures.” *CEN Brussels*.
Jae H. Chung. 2017. “FB-MultiPier Manual.” Florida Bridge Software Institute. 2017. https://bsi.ce.ufl.edu/downloads/files/FB-MultiPier/Demo/13BUQ6/FB-MultiPier_Help_Manual.pdf.

Kim, Dongwook, and Rodrigo Salgado. 2009. “Limit States and Load and Resistance Design of Slopes and Retaining Structures.”
Kramer, Steven L. 1996. “Geotechnical Earthquake Engineering Prentice Hall.” *New York*.
Kulhawy, Fred H., and Paul W. Mayne. 1990. “Manual on Estimating Soil Properties for Foundation Design.” Electric Power Research Inst., Palo Alto, CA (USA); Cornell Univ., Ithaca, NY (USA). Geotechnical Engineering Group.
Kulhawy, Fred H., and Charles H. Trautmann. 1996. “Estimation of In-Situ Test Uncertainty.” In *Uncertainty in the Geologic Environment: From Theory to Practice*, 269–286. ASCE.
Li, Qiang, Armin W. Stuedlein, and Andre R. Barbosa. 2017. “Torsional Load Transfer of Drilled Shaft Foundations.” *Journal of Geotechnical and Geoenvironmental Engineering* 143 (8): 04017036. https://doi.org/10.1061/(ASCE)GT.1943-5606.0001701.
McVay, M., R. Herrera, and Z. Hu. 2003. “Determine Optimum Depths of Drilled Shafts Subject to Combined Torsion and Lateral Loads Using Centrifuge Testing (BC-354, RPWO No. 9).” *Final Report to Florida Department of Transportation, Tallahassee, Fla*.
McVay, Michael, Bjorn Birgisson, Thai Nguygen, and Ching Kuo. 2002. “Uncertainty in Load and Resistance Factor Design Phi Factors for Driven Prestressed Concrete Piles.” *Transportation Research Record: Journal of the Transportation Research Board*, no. 1808: 99–107.
NEN 8700. 2009. “Grondslagen van de Beoordeling van de Constructieve Veiligheid van Een Bestaand Bouwwerk. Nederlands Normalisatie Instituut.”
Nowak, Andrzej S. 1999. “Calibration of LRFD Bridge Design Code.”
Nowak, Andrzej S., and Kevin R. Collins. 2013. *Reliability of Structures*. Second. CRC Press.
Nowak, Andrzej S., and S. Hooman Ghasemi. 2014. “Load and Resistance Factors Calibration for the Tunnels.”
Nowak, Andrzej S., and Maria M. Szerszen. 2003. “Calibration of Design Code for Buildings (ACI 318) Part I: Statistical Models for Resistance.” *Ann Arbor* 1001: 48109–2125.
Nusairat, Jamal, Robert Y. Liang, Rick Engel, Dennis Hanneman, Naser Abu-Hejleh, and Ke Yang. 2004. “Drilled Shaft Design for Sound Barrier Walls, Signs, and Signals.” *Rep. No. CDOT-DTD-R-2004* 8.
O’Neill, M. W., and L. C. Reese. 1999. “Drilled Shafts: Construction Procedures and Design.” Report FHWA-IF-99-025, Federal Highway Administration, McLean, Virginia.
Peck, Ralph Brazelton, Walter Edmund Hanson, and Thomas Hampton Thornburn. 1974. *Foundation Engineering*. Vol. 10. Wiley New York.
Peterka, J. A. 1992. “Improved Extreme Wind Prediction for the United States.” *Journal of Wind Engineering and Industrial Aerodynamics* 41 (1–3): 533–541.
Peterka, Jon A., and Sohban Shahid. 1998. “Design Gust Wind Speeds in the United States.” *Journal of Structural Engineering* 124 (2): 207–214.
Phoon, Kok-Kwang, F. H. Kulhawy, and M. D. Grigoriu. 1995. “Reliability-Based Design of Foundations for Transmission Line Structures.” *Rep. TR* 105000.
Phoon, Kok-Kwang, Fred H. Kulhawy, and Mircea D. Grigoriu. 2003. “Development of a Reliability-Based Design Framework for Transmission Line Structure Foundations.” *Journal of Geotechnical and Geoenvironmental Engineering* 129 (9): 798–806.
Poulos, Harry George. 1975. “Torsional Response of Piles.” *J. Geotech. Eng. Div.* 10 (101): 1019–35.
Puckett, Jay A., Michael G. Garlich, Andrzej Nowak, and Michael Barker. 2014. *Development and Calibration of AASHTO LRFD Specifications for Structural Supports for Highway Signs, Luminaires, and Traffic Signals*. NCHRP National Cooperative Highway Research Program Report 796. Washington, DC: Transportation Research Board of the National Academies.
Puzley, D. Carl. 2011. “Light Tower, Traffic Signal, Sign Structure Foundation Design. Memo 11.1 Shaft Overturning and Torsion Analysis.” All Geotechnical Manual User Memorandum. Illinois Department of Transportation.
Randolph, Mark Felton. 1981. “Piles Subjected to Torsion.” *Journal of the Geotechnical Engineering Division* 107 (8): 1095–1111.
Reese, L. C., S. T. Wang, W. M. Isenhower, J. A. Arrellaga, and J. Hendrix. 2004. “User’s Manual of LPILE plus 5.0 for Windows.” *Ensoft Inc., Austin, TX*.

Robertson, P. K., and K. L. Cabal. 2010. “Estimating Soil Unit Weight from CPT.” In *2nd International Symposium on Cone Penetration Testing*, 2–40.
Şahin, Abdurrahman. 2011. “Mathematical Models and Solution Algorithms for Computational Design of RC Piles under Structural Effects.” *Applied Mathematical Modelling* 35 (7): 3611–3638.
Stuedlein, Armin W., Andre R. Barbosa, and Qiang Li. 2016. “Evaluation of Torsional Load Transfer for Drilled Shaft Foundations.” https://trid.trb.org/view.aspx?id=1407802.
Szerszen, Maria M., and Andrzej S. Nowak. 2003. “Calibration of Design Code for Buildings (ACI 318) Part 2: Reliability Analysis and Resistance Factors.” *Ann Arbor* 1001: 48109–2125.
Tawfiq, Kamal. 2000. “Drilled Shaft under Torsional Loading Conditions.” https://trid.trb.org/view.aspx?id=655455.
Thiyyakkandi, Sudheesh, Michael McVay, Peter Lai, and Rodrigo Herrera. 2016. “Full-Scale Coupled Torsion and Lateral Response of Mast Arm Drilled Shaft Foundations.” *Canadian Geotechnical Journal* 53 (12): 1928–38. https://doi.org/10.1139/cgj-2016-0241.
Vickery, P. J., and D. Wadhera. 2003. “Wind Speed Maps for the Caribbean for Application with the Wind Load Provisions of ASCE 7.” *Appliied Research Associates*, 7–2875.
Vickery, Peter J., Dhiraj Wadhera, Jon Galsworthy, Jon A. Peterka, Peter A. Irwin, and Lawrence A. Griffis. 2009. “Ultimate Wind Load Design Gust Wind Speeds in the United States for Use in ASCE-7.” *Journal of Structural Engineering* 136 (5): 613–625.
Vickery, Peter J., Dhiraj Wadhera, Mark D. Powell, and Yingzhao Chen. 2009. “A Hurricane Boundary Layer and Wind Field Model for Use in Engineering Applications.” *Journal of Applied Meteorology and Climatology* 48 (2): 381–405.
Vickery, Peter J., Dhiraj Wadhera, Lawrence A. Twisdale Jr, and Francis M. Lavelle. 2009. “US Hurricane Wind Speed Risk and Uncertainty.” *Journal of Structural Engineering* 135 (3): 301–320.
Wood, David Muir. 2003. *Geotechnical Modelling*. Vol. 1. CRC Press.
Zhang, L. M., and L. G. Kong. 2006. “Centrifuge Modeling of Torsional Response of Piles in Sand.” *Canadian Geotechnical Journal* 43 (5): 500–515.
Zhang, Lianyang. 2010. “Nonlinear Analysis of Torsionally Loaded Piles in a Two-Layer Soil Profile.” *International Journal of Geomechanics* 10 (2): 65–73.

Appendix A:

DETAILS OF CHAPTER 4

Data from Poulos (1975) and Li et al. (2017), and predictions from Li et al. (2017) were used to perform the statistical analysis of the α-method. Table A-1 presents source, test ID, dimensions of the tested specimen, the measured torque at failure, the predicted resistance using α-method and the measured-to-predicted ratio. Average, standard deviation and coefficient of variation were calculated excluding outliers.

Table A-1: α-method data for statistical analysis

Source	**Test ID**	**D**	**L**	**L/D**	$T_{measured}$	T_{α}	$T_{measured}/T_{\alpha}$
		(mm)	*(mm)*		*(Nm)*	*(Nm)*	
Poulos (1975)	1A	25.4	254	10	2.75	2.30	1.20
	1B	12.7	203	16	0.56	0.50	1.12
	2A	25.4	254	10	3.53	4.00	0.88
	+2B	38.1	229	6	3.81	6.12	0.62
	3A	25.4	254	10	2.27	3.24	0.70
	3B	12.7	203	16	0.77	0.62	1.24
	4A	12.7	203	16	0.98	0.77	1.27
	4B	12.7	305	24	1.06	0.85	1.25
	5A	12.7	203	16	1.10	0.97	1.13
	5B	12.7	305	24	1.36	1.29	1.05
	6A	25.4	502	20	1.96	1.91	1.03
	6B	19.1	527	28	1.35	1.09	1.24
	7A	25.4	502	20	4.73	4.78	0.99
	7B	19.1	527	28	2.49	2.91	0.86
	8A	25.4	502	20	8.41	7.55	1.11
	8B	19.1	527	28	4.89	4.31	1.14
	9A	12.7	305	24	0.97	0.63	1.54
	10A	19.1	298	16	1.23	1.03	1.19
	11A	12.7	305	24	1.11	0.79	1.41
	11B	12.7	305	24	0.87	0.62	1.40
	12A	19.1	298	16	4.45	3.52	1.26
Li (2017)	*TDSFB	900	4,000	4	1.85	1.39	1.33
						AVG =	**1.16**
*Torque divided by 10^5						**STD =**	**0.20**
+Outlier						**COV =**	**0.17**

Data and predictions from Hu (2003) were used to perform the statistical analysis of the β-method. Table A-2 presents test ID, soil properties and dimensions of the tested specimen, the measured shear at failure, the predicted shear stress using β-method and the measured-to-predicted ratio. Average, standard deviation and coefficient of variation were calculated excluding outliers.

Table A-2: β-method data for statistical analysis

ID test	Soil properties			Geometry				Measured	Predicted with beta method	Measured/Predicted
	Dr (%)	γ (pcf)	ϕ (deg.)	Pole height (m)	Shaft length (m)	Diameter (m)	ecc. (m)	L/D	Shear stress (psi)	Shear stress (psi)	
BS1	69	124.5	38.0	6.1	7.63	1.525	4.42	5	6.68	5.46	1.22
BS2	69	124.5	38.0	6.1	7.63	1.525	4.42	5	6.68	5.46	1.22
BS3	34	120.5	33.6	6.1	7.63	1.525	4.42	5	5.46	5.11	1.07
BS4	34	120.5	33.6	6.1	7.63	1.525	4.42	5	5.46	5.11	1.07
BS5	69	124.5	38.0	6.1	7.63	1.525	5.86	5	5.72	5.46	1.05
BS6	69	124.5	38.0	6.1	7.63	1.525	5.86	5	5.72	5.46	1.05
BS7	34	120.5	33.6	6.1	7.63	1.525	5.86	5	6.63	5.11	1.30
BS8	34	120.5	33.6	6.1	7.63	1.525	5.86	5	6.63	5.11	1.30
BS9	69	124.5	38.0	6.1	10.68	1.525	4.42	7	7.67	6.74	1.14
BS10	69	124.5	38.0	6.1	10.68	1.525	4.42	7	7.67	6.74	1.14
BS13	69	124.5	38.0	6.1	10.68	1.525	5.86	7	6.90	6.74	1.02
BS14	69	124.5	38.0	6.1	10.68	1.525	5.86	7	6.90	6.74	1.02
BS15	34	120.5	33.6	6.1	10.68	1.525	5.86	7	7.06	6.31	1.12
BS16	34	120.5	33.6	6.1	10.68	1.525	5.86	7	7.06	6.31	1.12
+KB3	69	124.5	38.0	6.1	7.63	1.525	5.86	5	8.4	5.46	1.54
KB4	34	120.5	33.6	6.1	7.63	1.525	5.86	5	6.57	5.11	1.29
+KB5	69	124.5	38.0	6.1	10.68	1.525	5.86	7	10.16	6.74	1.51
+KB6	69	124.5	38.0	6.1	10.68	1.525	4.42	7	10.16	6.74	1.51
KB7	34	120.5	33.6	6.1	10.68	1.525	4.42	7	7.31	6.31	1.16
KB9	34	120.5	33.6	6.1	10.68	1.525	5.86	7	6.88	6.31	1.09
KB10	34	120.5	33.6	6.1	10.68	1.525	5.86	7	6.88	6.31	1.09
+Outlier										**AVG =**	**1.14**
										STD =	**0.09**
										COV =	**0.08**

Data from several sources and the authors' predictions using $\alpha\beta$, CDOT, FDOT, FL7 and FL SDO methods were used to assess the accuracy of the method under analysis. Table A-2 presents test ID related to the original source, the measured torque at failure, the predicted resistance and the measured-to-predicted ratio for each of the methods.

Table A-3: Accuracy of selected methods

Test	Measured	Predictions					Measured-to-predicted ratio				
ID	T_m	$\alpha\beta$	CDOT	FDOT	FL D7	FL SDO	$\alpha\beta$	CDOT	FDOT	FL D7	FL SDO
TS1	95	90	107	25	63	94	1.06	0.89	3.86	1.51	1.01
TS2	285	258	277	389	108	165	1.10	1.03	0.73	2.64	1.72
TS3	232	220	260	351	128	171	1.05	0.89	0.66	1.81	1.35
TH2	569	704	526	908	183	171	0.81	1.08	0.63	3.11	3.33
TDS	251	209	327	422	144	144	1.20	0.77	0.60	1.74	1.75
						AVG =	**1.04**	**0.93**	**1.30**	**2.16**	**1.83**
						STD =	**0.14**	**0.12**	**1.44**	**0.68**	**0.89**
						COV =	**0.14**	**0.13**	**1.11**	**0.31**	**0.48**

NOTE:
Torque measured in KN-m
TS1, TS2, and TS3 from Thiyyakkandi et al. (2016)
TH2 from Tawfiq (2000)
TDS from Li et al. (2017)

Appendix B:

MONTE CARLO SIMULATIONS

The material uncertainty in the resistance model was quantified by using Monte Carlo simulation based on the variability of the identified geotechnical parameters. A simulation was run for each of the soil range used for ALDOT to recommend soil properties. Results are shown in term of the histogram, CDF in normal probability paper, and CDF in lognormal probability paper. When necessary, an auxiliary distribution was used to approximate the lower tail. The simulated scenarios are plotted as blue crosses, the line fitting to the full distribution is shown in black dashed line. Lower tail fitting is shown in color magenta. The reader should notice that a normal distribution looks like a straight line in normal probability paper, so does a lognormal distribution in a lognormal probability paper.

B1. MC simulations for α-method

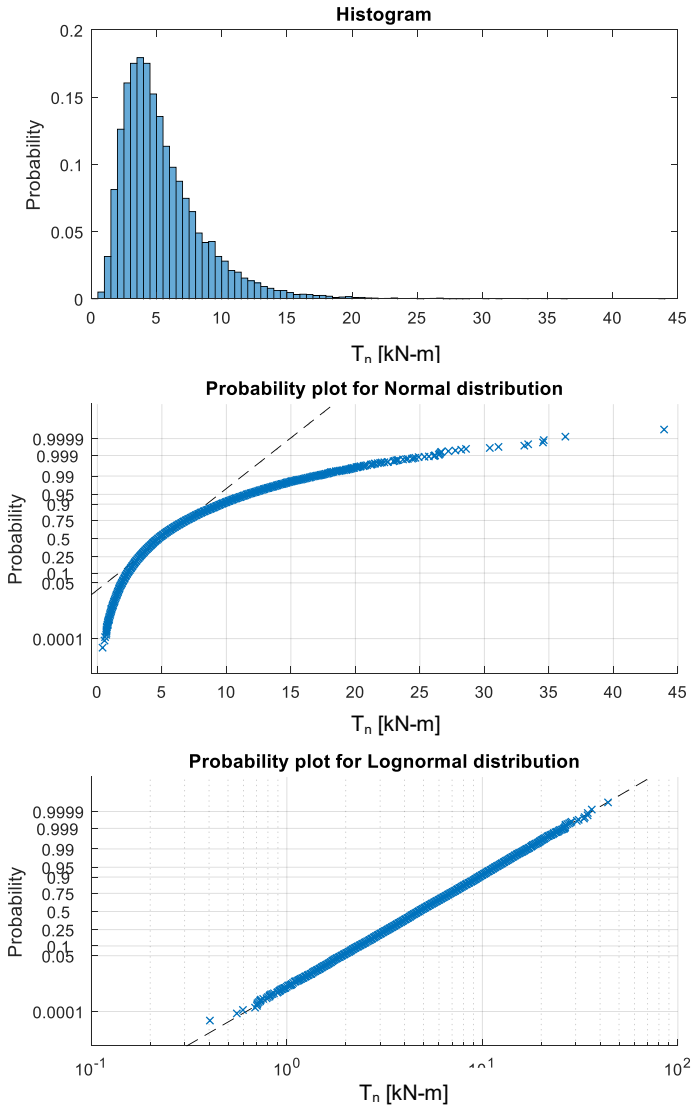

Figure B-1: Soft and extremely soft clay. γ=16.5 kN/m^3 s_u=12 kPa. Lognormal λ=1.00 COV=0.59

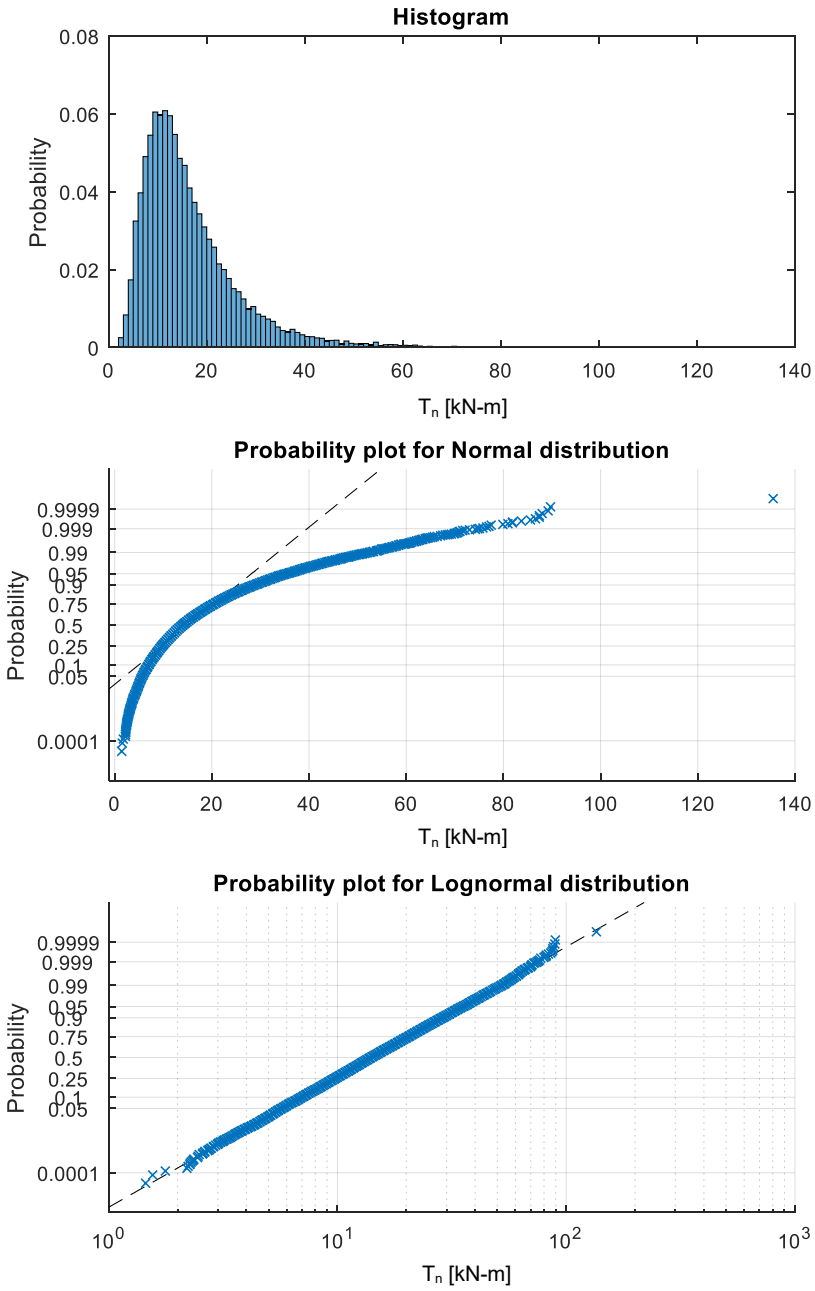

Figure B-2: Medium to moderately hard clay. γ=18.1 kN/m^3 s_u=36 kPa. Lognormal λ=1.00 COV=0.60

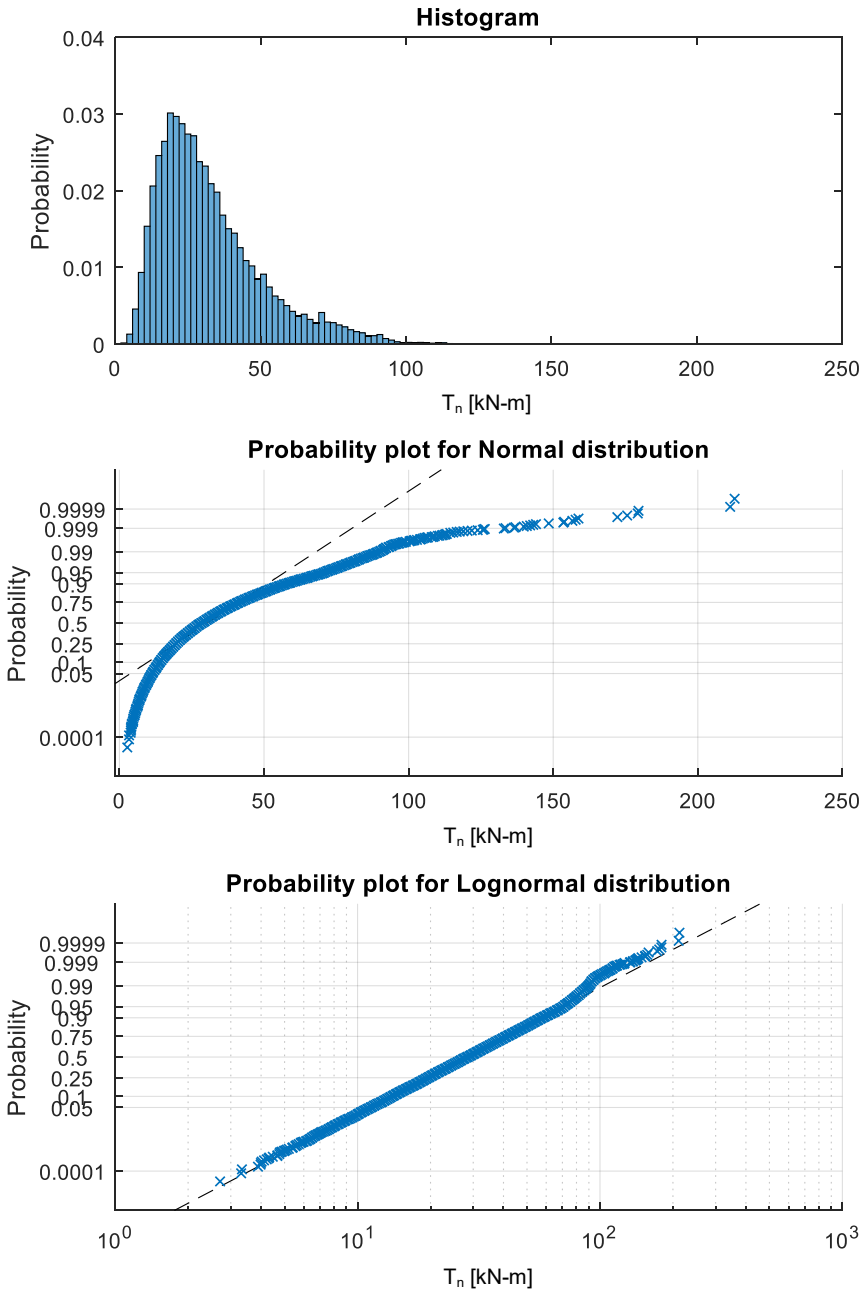

Figure B-3: Stiff weathered clay. γ=18.8 kN/m^3 s_u=72 kPa. Lognormal λ=1.00 COV=0.56

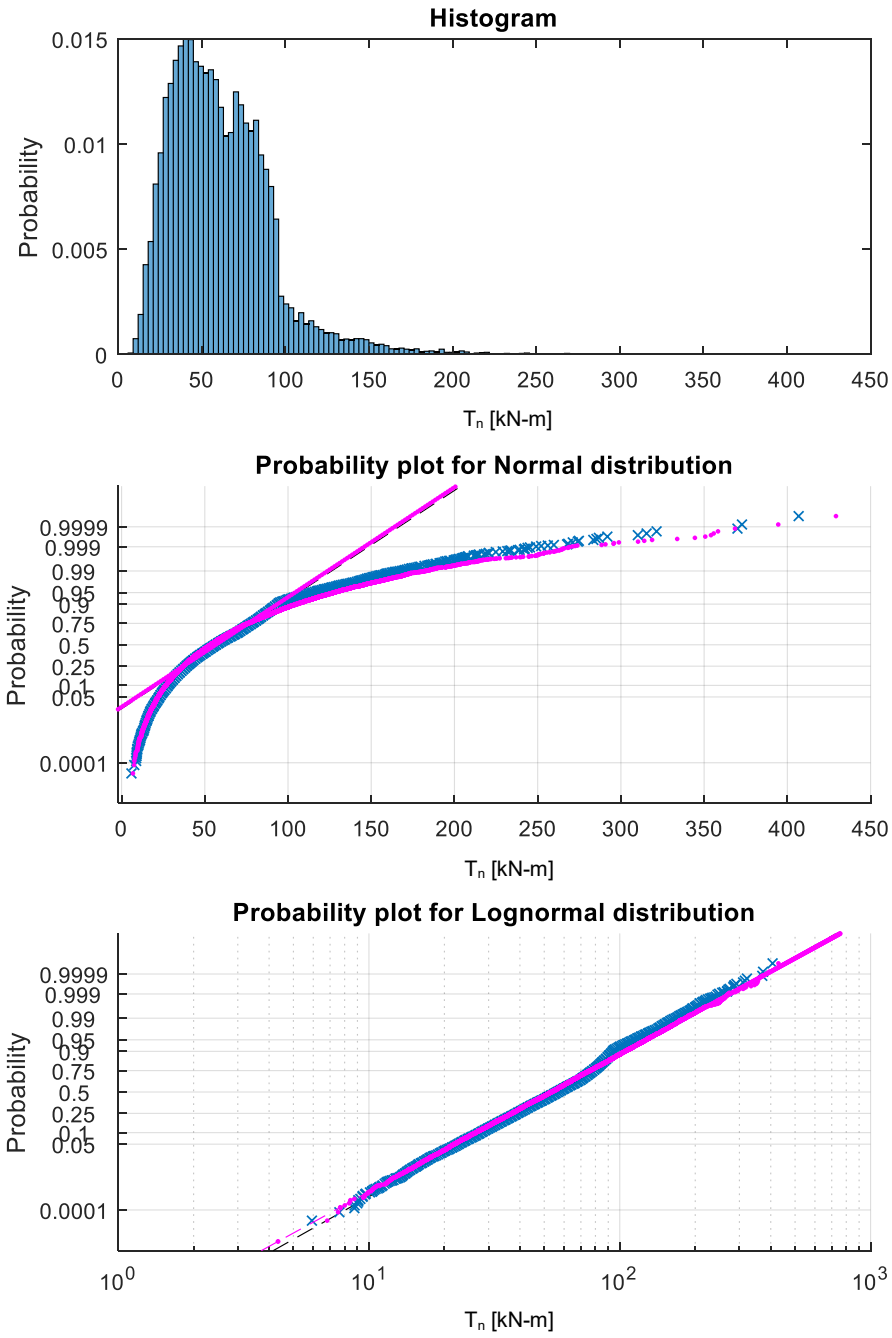

Figure B-4: Medium hard to hard and very stiff clay. γ=19.6 kN/m^3 s_u=144 kPa. Lognormal λ=0.93 COV=0.57

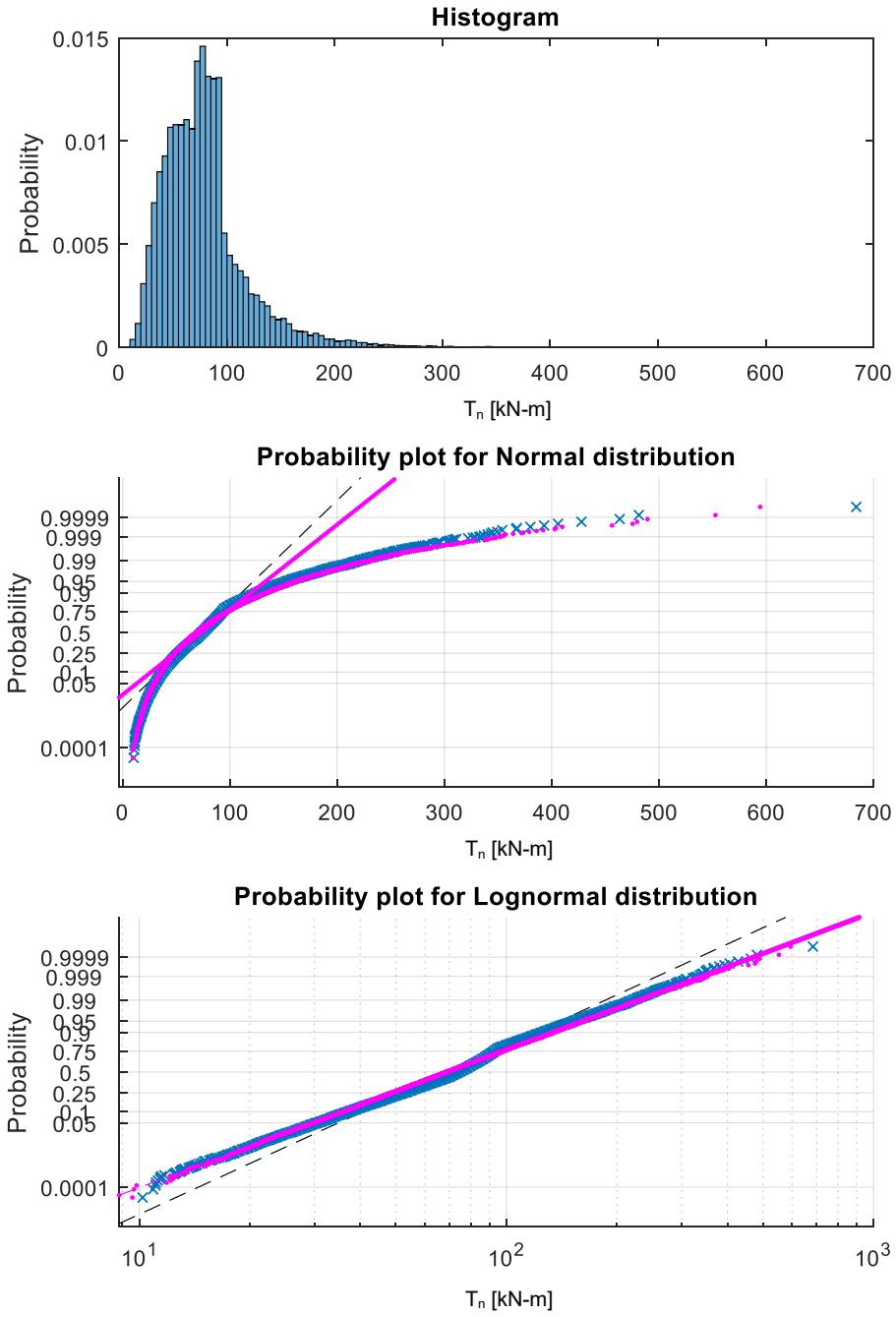

Figure B-5: Moderately hard to hard and hard clay. γ=20.4 kN/m^3 s_u=192 kPa. Lognormal λ=0.97 COV=0.54

B2. MC simulations for β-method

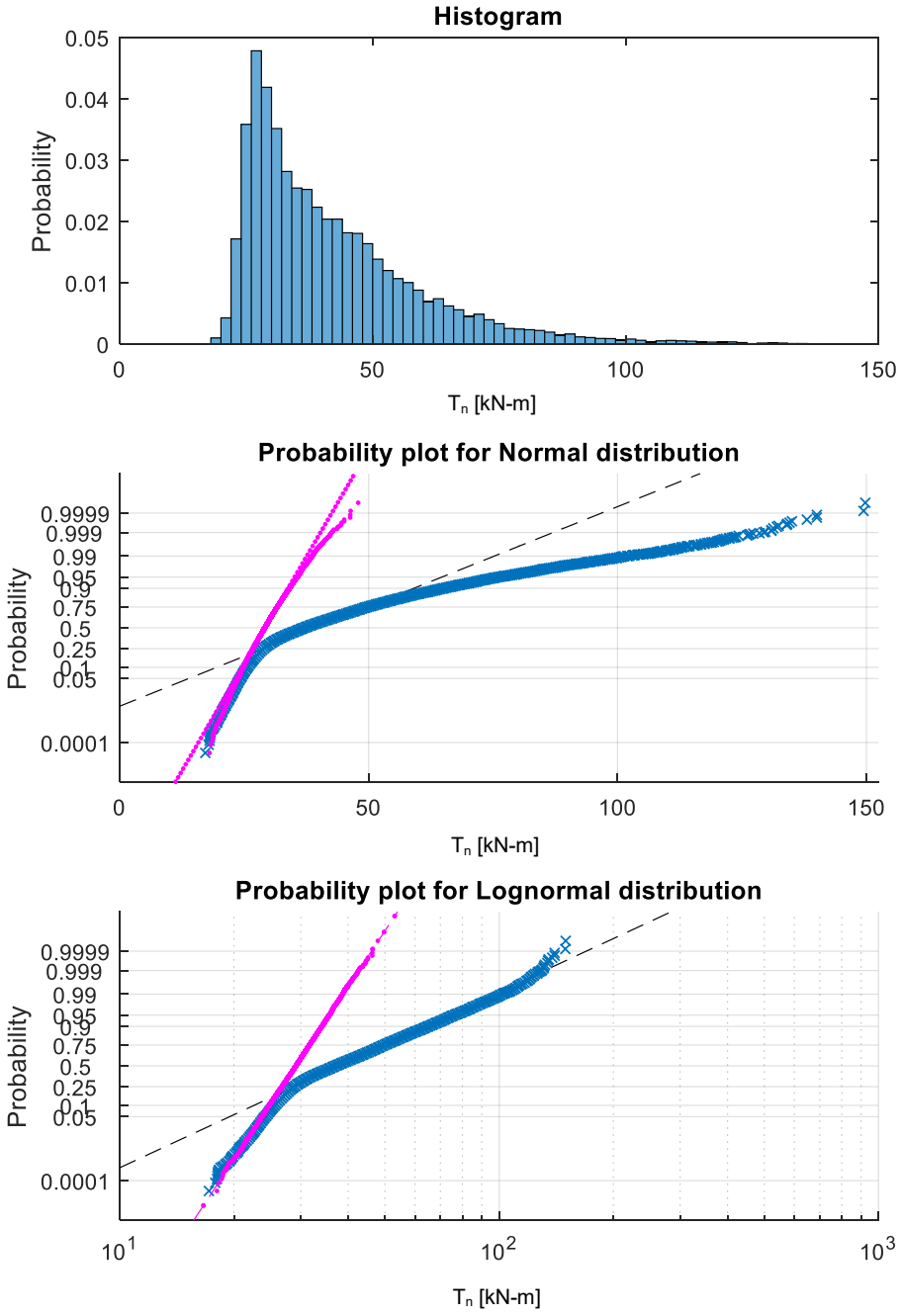

Figure B-6: Loose and very loose sand. γ=17.3 kN/m^3 N_{spt}=5. Lognormal λ=0.72 COV=0.12

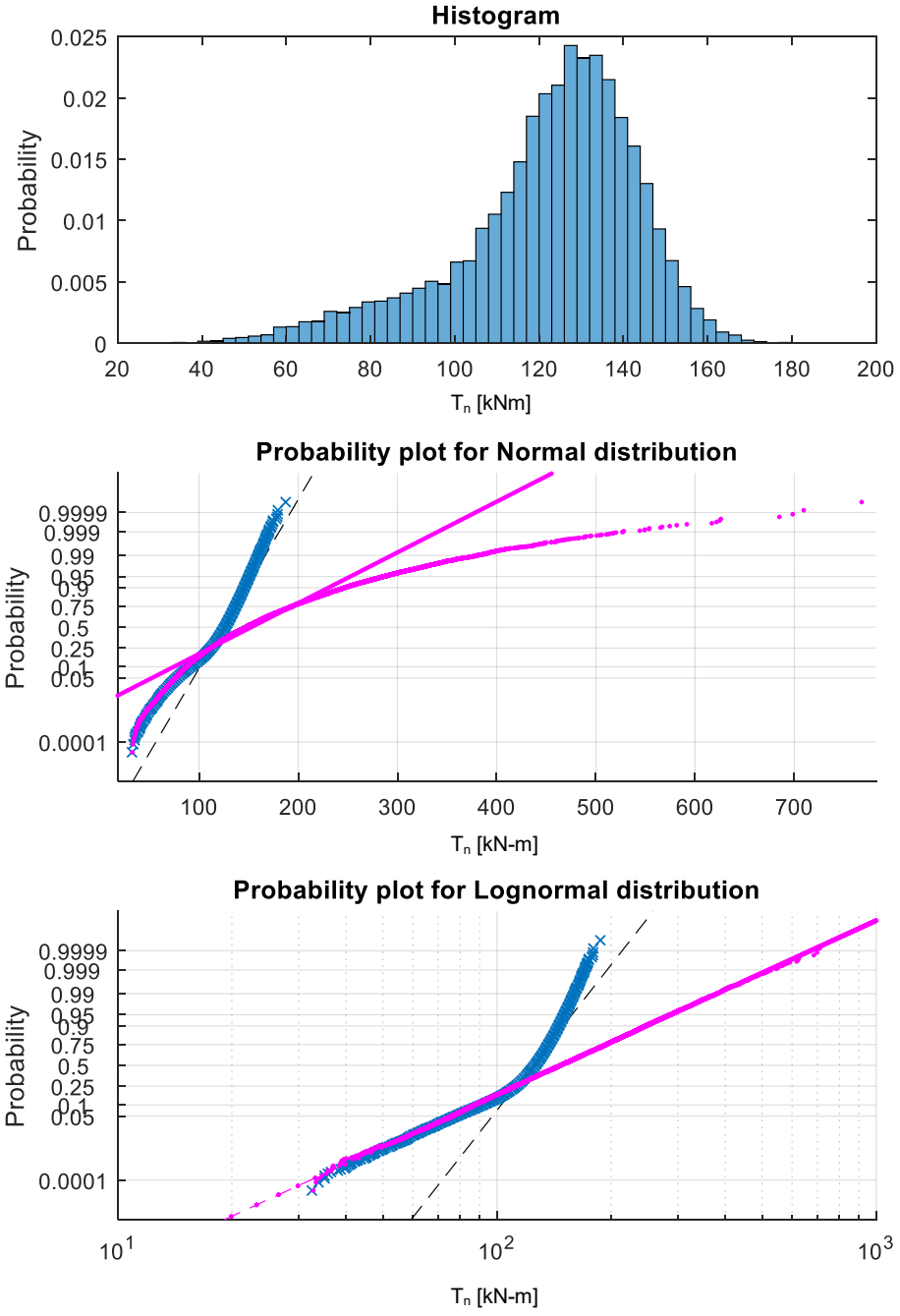

Figure B-7: Medium sand. γ=18.8 kN/m^3 N_{spt}=20. Lognormal λ=1.21 COV=0.42

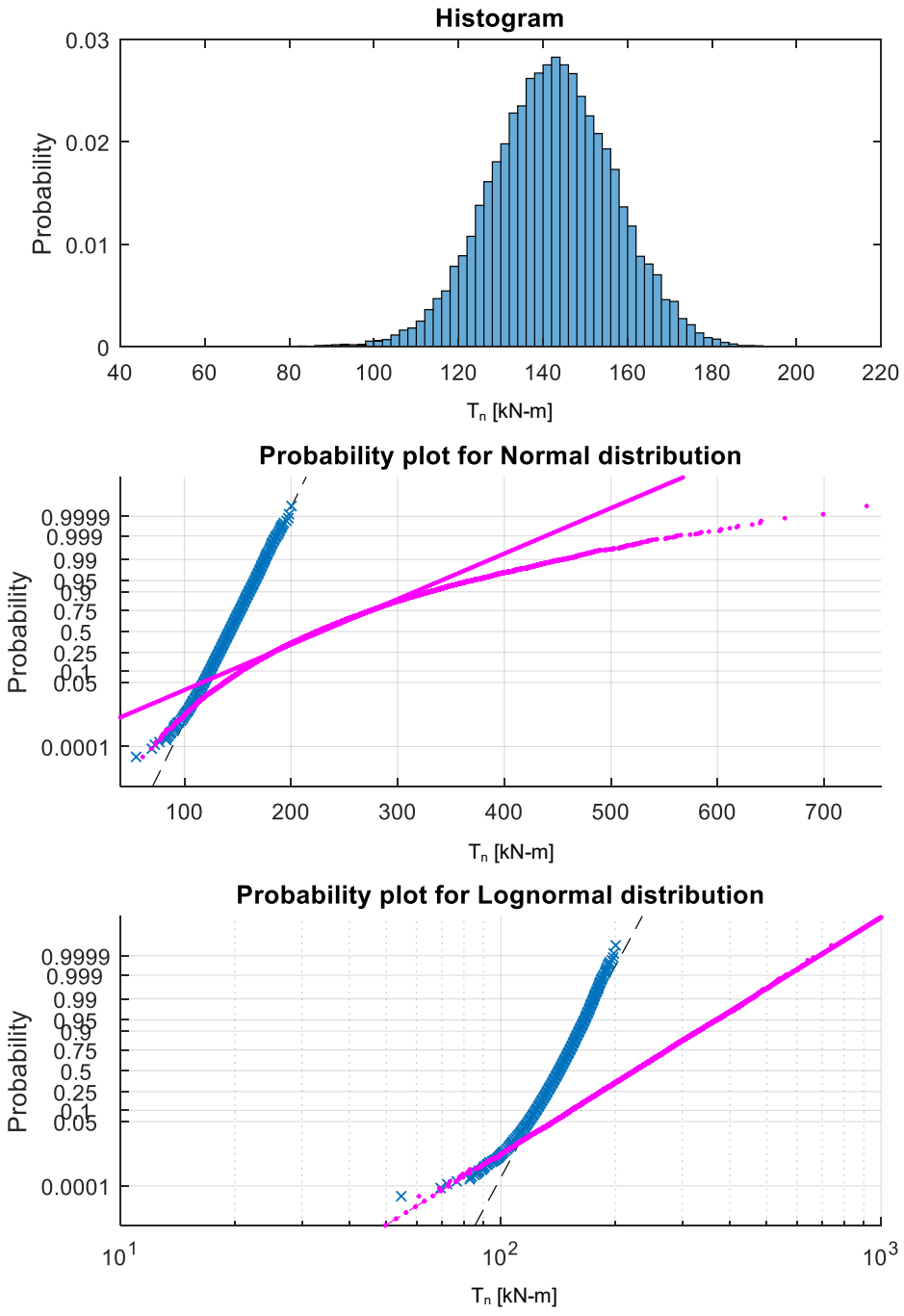

Figure B-8: Dense to very dense sand. γ=20.4 kN/m^3 N_{spt}=40. Lognormal λ=1.65 COV=0.31

Appendix C:

ALDOT GEOTECHNICAL PARAMETERS RECOMMENDATION

Table C-1: Soil parameters recommended by ALDOT (U.S. customary units)

Relative Density	Description	N value		Undrained Shear Str.		k_s (static) (lbs/ in^3)	k_c (cyclic) (lbs/in^3)	E_{50}	Φ	γ_d (pcf)
		blowcount		psf	psi					
MSO, SO, SOM, VSO, XSO	Medium Soft , Soft , Soft to Medium , Extremely Soft	0	4	250	1.736	30	-	0.02	0	105
MC, SOMH	Medium, Soft to Moderately Hard	4	8	750	5.208	100	-	0.01	0	115
ST, W	Stiff, Weathered	8	15	1500	10.417	500	200	0.007	0	120
MEH, VST	Medium Hard to Hard, Very Stiff	15	30	3000	20.833	1000	400	0.005	0	125
H, MH, MHH	Hard, Moderately Hard, Moderately Hard to Hard	30	50	4000	27.778	2000	800	0.004	0	130
R	Rock	-	-	6000	41.667	2000	800	0.004	45	140
LO, VLO	Loose Sand, Very Loose Sand	0	10	0	0	25	25	0	30	110
MS	Medium Sand	10	30	0	0	90	90	0	35	120
D, VD	Dense Sand, Very Dense Sand	30	50	0	0	225	225	0	40	130
LO_H2O	Loose Sand (Under Water Table)	0	10	0	0	20	20	0	30	110
M_H2O	Medium Sand (Under Water Table)	10	30	0	0	60	60	0	35	120
D_H2O	Dense Sand (Under Water Table)	30	50	0	0	125	125	0	40	130

Table C-2: Soil parameters recommended by ALDOT (SI units)

Relative Density	Description	N value		Undrained Shear Str.	k_s (static) (kN/m^3)	k_c (cyclic) (kN/m^3)	E_{50}	Φ	γ_d (kN/m^3)
		blowcount		kPa					
MSO, SO, SOM, VSO, XSO	Medium Soft , Soft , Soft to Medium , Extremely Soft	0	4	12	8143	-	0.02	0	16.5
MC, SOMH	Medium, Soft to Moderately Hard	4	8	36	27145	-	0.01	0	18.1
ST, W	Stiff, Weathered	8	15	72	135724	54289	0.007	0	18.8
MEH, VST	Medium Hard to Hard, Very Stiff	15	30	144	271447	108579	0.005	0	19.6
H, MH, MHH	Hard, Moderately Hard, Moderately Hard to Hard	30	50	192	542894	217158	0.004	0	20.4
R	Rock	-	-	287	542894	217158	0.004	45	22.0
LO, VLO	Loose Sand, Very Loose Sand	0	10	0	6786	6786	0	30	17.3
MS	Medium Sand	10	30	0	24430	24430	0	35	18.8
D, VD	Dense Sand, Very Dense Sand	30	50	0	61076	61076	0	40	20.4
LO_H2O	Loose Sand (Under Water Table)	0	10	0	5429	5429	0	30	17.3
M_H2O	Medium Sand (Under Water Table)	10	30	0	16287	16287	0	35	18.8
D_H2O	Dense Sand (Under Water Table)	30	50	0	33931	33931	0	40	20.4

Appendix D:

WIND PRESSURE CALCULATIONS

This appendix presents calculation details for the comparison made in chapter 3 about different specifications or method to determine the wind pressure acting on a traffic sign.

Wind pressure for a traffic signal, h=18 ft, exposure category C, 25-yr service life
Location: **Mobile, AL**

1. AASHTO (2009)

Basic wind speed for MRI = 50 yrs

$V_{50} := 110 \quad mph$

Factors associated to the design assumptions

$K_z := .882 \qquad G := 1.14 \quad C_d := 1.20 \quad I_r := 0.77$

Wind design pressure

$P_z := 0.00256 K_z \cdot G \cdot (V_{50})^2 \cdot I_r \cdot C_d \cdot psf = 28.779 psf$

$P_{zmin} := 0.00256 K_z \cdot G \cdot (100)^2 \cdot 0.87 \cdot C_d \cdot psf = 26.873 psf$

2. AASHTO (2009) - Appendix C

Fastest mile wind speed specify by ALDOT (2018)

$V_{fm} := 100 \quad mph$

Factors associated to the design assumptions

$C_d := 1.2 \qquad C_h := 1.0$

Wind design pressure

$P_z := 0.00256 (1.3 V_{fm})^2 \cdot C_d \cdot C_h \cdot psf = 51.917 psf$

3. AASHTO (2015)

Basic wind speed for several MRI

$V_{10} := 81 \ mph \qquad V_{300} := 142 \ mph \qquad V_{700} := 154 \ mph \qquad V_{1700} := 163 \ mph$

Factors associated to the design assumptions

$K_z := 0.878 \qquad K_d := .85 \qquad G := 1.14 \qquad C_d := 1.20$

Wind design pressure for different MRI

$P_{z10} := 0.00256 K_z K_d \cdot G \cdot (V_{10})^2 \cdot C_d \cdot psf = 17.148 psf$

$P_{z300} := 0.00256 K_z K_d \cdot G (V_{300})^2 \cdot C_d \cdot psf = 52.701 psf$

$P_{z700} := 0.00256 K_z K_d \cdot G (V_{700})^2 \cdot C_d \cdot psf = 61.984 psf$

$P_{z1700} := 0.00256 K_z \cdot K_d \cdot G \cdot (V_{1700})^2 \cdot C_d \cdot psf = 69.441 \cdot psf$

Wind pressure for a traffic signal, h=18 ft, exposure category C, 25-yr service life
Location: **Montgomery, AL**

1. AASHTO (2009)

Basic wind speed for MRI = 50 yrs

$V_{50} := 90 \quad mph$

Factors associated to the design assumptions

$K_z := .882 \qquad G := 1.14 \quad C_d := 1.20 \quad I_r := 0.87$

Wind design pressure

$P_z := 0.0025 K_z G (V_{50})^2 \cdot I_r \cdot C_d \cdot psf = 21.767 psf$

2. AASHTO (2009) - Appendix C

Fastest mile wind speed specify by ALDOT (2018)

$V_{fm} := 80 \quad mph$

Factors associated to the design assumptions

$C_{dv} := 1.2 \qquad C_h := 1.0$

Wind design pressure

$P_{zv} := 0.0025 (1.3 V_{fm})^2 \cdot C_d \cdot C_h \cdot psf = 33.227 psf$

3. AASHTO (2015)

Basic wind speed for several MRI

$V_{10} := 76 \, mph \qquad V_{300} := 106 \, mph \qquad V_{700} := 116 \, mph \qquad V_{1700} := 120 \, mph$

Factors associated to the design assumptions

$K_z := 0.878 \qquad K_d := .85 \qquad G := 1.14 \qquad C_{dv} := 1.20$

Wind design pressure for different MRI

$P_{z10} := 0.0025 K_z K_d G (V_{10})^2 \cdot C_d \cdot psf = 15.096 psf$

$P_{z300} := 0.0025 K_z K_d G (V_{300})^2 \cdot C_d \cdot psf = 29.366 psf$

$P_{z700} := 0.0025 K_z K_d G (V_{700})^2 \cdot C_d \cdot psf = 35.169 psf$

$P_{z1700} := 0.0025 K_z K_d G (V_{1700})^2 \cdot C_d \cdot psf = 37.636 psf$

Appendix E:

RELIABILITY OF THE SLIDING FAILURE OF A RETAINING WALL

Let approximate the implicit reliability index of typical retaining wall designs against a sliding failure. Only material uncertainties will be considered in this approximate analysis. A more precise calculation would require consideration of analysis and fabrication uncertainties, as well.

If the wall is seated in a cohesionless soil layer, the design condition is typically written as:

$$FS = \frac{N\mu}{E_h} \geq 1.5$$

where,

N = normal force on base (wall and soil weight),

μ = friction coefficient on the base, typically calculated as the tangent of base interface angle

E_h = horizontal earth pressure force on a vertical plane through the heel of wall

on the other hand, if the wall is seated on a cohesive soil layer:

$$FS = \frac{2xs_u}{E_h} \geq 1.5$$

where,

s_u = undrained shear strength of the clay

x = reduced effective footing width (see Meyerhof's method 1953)

E_h = horizontal earth pressure force on a vertical plane through the heel of wall

the horizontal earth pressure can be computed as follows:

$$E_h = \frac{1}{2} K_a \gamma h^2$$

where,

γ = soil unit weight

h = wall height

K_a = active earth pressure coefficient

In both cases, the performance function is defined in a ratio form

$$g = \frac{R}{Q} - 1$$

Equivalently, it can be express as:

$$g = R - Q$$

where,

R = Resistance can be taken as:

$N\mu$ if cohesionless soil

$2xs_u$ if cohesive soil

Q = Load effect, in this case, the horizontal force due to active earth pressure

Load model

Let consider statistics reported by FHWA (2001) for earth pressure coefficient (λ=1.0 and COV=0.15) and data from Duncan (2000) for soil unit weight (λ=1.0 and COV=0.05).

$$\lambda_Q = 1.0 \quad COV_Q = \sqrt{0.15^2 + 0.05^2} = 0.16$$

Resistance model

For cohesionless soil

N is the sum of concrete and soil self-weight, using Nowak and Collins (2013) statistical data bias and COV can be considered λ=1.05 and COV=0.10. The friction coefficient μ was associated with a COV=0.10 in FHWA (2001). Therefore,

$$\lambda_R = 1.05 \quad COV_R = \sqrt{0.10^2 + 0.10^2} = 0.14$$

For cohesive soil

The stats of the resistance model will be controlled by the undrained shear resistance: $\lambda_R = 1.0$ $COV_R = 0.30$, medium values reported in Duncan (2000).

Reliability indices calculation

Considering a nominal value of load $Q_n = 1.0$, by using a factor of safety 1.50 the nominal resistance value would be $R_n = 1.50$. Mean, and standard deviation can now be calculated,

Load effect: $\mu_Q = \lambda_Q Q_n = 1.0 \Rightarrow \sigma_Q = COV_Q \mu_Q = (0.16)(1.0) = 0.16$

Cohesionless: $\mu_R = \lambda_R R_n = (1.05)(1.50) = 1.58 \Rightarrow \sigma_R = COV_R \mu_R = (0.14)(1.58) = 0.22$

Cohesive: $\mu_R = \lambda_R R_n = (1.0)(1.50) = 1.50 \Rightarrow \sigma_R = COV_R \mu_R = (0.30)(1.50) = 0.45$

If *R* and *Q* are assumed normally distributed independent, the reliability index can be calculated as indicated in equation (7.6)

Thus,

$\beta \approx 2.1$ for cohesionless soil ($p_f = 0.018$)

$\beta \approx 1.0$ for cohesive soil ($p_f = 0.159$)

If *R* and *Q* are assumed lognormally distributed independent, the reliability can be calculated according to equation (7.11)

Thus,

$\beta \approx 2.2$ for cohesionless soil ($p_f = 0.014$)

$\beta \approx 1.1$ for cohesive soil ($p_f = 0.136$)

These results are a clear example of the same factor of safety (FS=1.5) implies a different safety margin. In this case, the difference is one order of magnitude in the probability of failure.